My Adventures in Microfluidics: Exploration of Novel Modes for Sized-Based DNA Separation

A DISSERTATION
SUBMITTED TO THE FACULTY OF THE GRADUATE SCHOOL
OF THE UNIVERSITY OF MINNESOTA
BY

Joel Daniel Pierson Thomas

IN PARTIAL FULFILLMENT OF THE REQUIREMENTS
FOR THE DEGREE OF
DOCTOR OF PHILOSOPHY

Kevin D. Dorfman and David J. Norris

June, 2014

Acknowledgements

I would like to thank my advisers, Kevin Dorfman and David Norris, for all their advise and guidance while I was here. I would also like to thank the Dorfman group. There were many discussions had within the group, both at meetings and impromptu, that greatly helped me during my time here. Special mention goes to Scott King and Doug Tree.

I would like to thank my family and friends who helped keep me sane when things were not working. Their support and encouragement is a major reason I was able to get this far.

Financial support for my research was provided by The David and Lucile Packard Foundation and the National institute of Health (R01-HG005216 and R21-GM103409). The fabrication work presented here was performed in the Minnesota Nano Center at the University of Minnesota, which receives partial support from NSF through the NNIN program. The characterization work shown here was carried out in the Characterization Facility, University of Minnesota, a member of the NSF-funded Materials Research Facilities Network (www.mrfn.org) via the MRSEC program.

Abstract

DNA separation is ubiquitous in biological research. The common technique for performing these separations, gel electrophoresis, leaves much to be desired. The separations are slow, taking hours to separate. There can also be huge variations in quality between gels, due to the randomness of the gel. Gels are limited to DNA smaller than about 15 kbp, unless pulsed fields are used that take even longer to separate. Performing these separations in microfluidic devices overcomes some of these problems. Two common geometries used to separate DNA are the slit-well geometry and the post array geometry. Using the understanding gained using these geometries, researchers have been able to create continuous separation devices.

We have tested novel operations modes, initially predicted by theory and simulations, within these well understood geometries. We achieved bi-directional migration using an asymmetric pulsed electric field in the slit well geometry. This created a non-clogging DNA filter. We achieved improved separation in a hexagonal post array by rotating the array. We were able to separate DNA in a shorter array, 4 mm, and at a higher electric field, 50 V/cm, than seen before. We also tried to create a continuous DNA separation device using proximity field nano-patterning, but were ultimately unsuccessful.

While the work done to develop microfluidic DNA separation devices by a multitude of researchers ultimately did not change how DNA separations are performed in biology labs, the advances and insights gained from those performing the work led to great advancements in DNA manipulation techniques, including genomic and sequencing techniques. In fact, a genomic technique called DNA barcoding, which is performed by stretching DNA in very small channels, or nanochannels, would not have been possible without the initial microfluidic work in DNA separation techniques.

Contents

List of Tables

List of Figures

Explanation of Author Contribution

Some of the research presented here has already been published in peer reviewed journals. Many of the journal articles have multiple authors listed, so I would like to briefly explain my contribution to the reasearch.

Parts of chapter 2 appear in sections 6.1.2 and 6.6 of K. D. Dorfman, S. B. King, D. W. Olson, J. D. P. Thomas, and D. R. Tree. Beyond gel electrophoresis: Microfluidic separations, fluorescence burst analysis, and DNA stretching. *Chem. Rev.*, **113**(4):2584-2667, 2012. I wrote both of those sections in the review article.

Chapter 3 is based on J. D. P. Thomas, M. N. Joswiak, D. W. Olson, S.-G. Park, and K. D. Dorfman. Ratchet Nanofiltration of DNA. *Lab Chip,* **13**:3741, 2013. This work was performing experiment in a nanofilter array using a pulsed field to achieve bi-directional migration of DNA. I performed all the experiments and data analysis for the published data.

Chapter 4 may appear as J. D. P. Thomas and K. D. Dorfman. Tilted post arrays for separating long DNA. *Biomicrofluidics.* [Submitted]. This work was peforming long DNA separation in a rotated post array such that the DNA is no longer driven down the lattice vector of the array. This was used to achieve improved separation performance when compared to a normal post array. I designed and fabricated the separation device. I performed all the experiments and analysis.

Chapter 1

Introduction

Deoxyribonucleic acid (DNA) is the macromolecule that contains all the information needed for life. Since DNA plays such a central role, it is used in almost all fields of biology. Plant and animal breeding uses knowledge of genes, segments of DNA that encode for proteins, to improve organisms. DNA fingerprinting uses DNA fragments to identify pathogens, new medicinal products, or criminals. DNA fingerprinting works by comparing the sizes of the digested DNA fragments to existing libraries or known samples. DNA sequencing [1] has been central to the Human Genome Project and genomics in general. Biotechnology modifies organisms by directly inserting desired genes into the cell's genome. However, while the use of DNA is ubiquitous in biological research, researchers typically only look at specific desired fragments of the genome they are studying. To purify the specific desired fragment the DNA must be sorted and separated, usually based on size. Before we can understand how to separate DNA we need to understand the physics of a single molecule of double stranded DNA when it is freely suspended in a solution.

1.1 DNA in free solution

In nature, DNA is found in cells. In prokaryotic cells (bacteria) it is a loop of DNA called a plasmid and is found coiled up in the cell. In eukaryotic cells (animals, plants, and fungi) it is found in several supercoiled structures called chromosomes that are contained in the cell nucleus. The structure of the chromosomes is complex and not yet fully understood. In order to gain useful information from the DNA it first has to be extracted from the cell and then suspended in a solution, typically an ionic solution. Once in a solution the DNA can be manipulated in several ways. Before we discuss the manipulations possible, with a focus on separation based on size, we need to understand the physics of the molecule. For this we will briefly look towards theories developed in polymer physics to introduce some concepts that will aid in the discussion of separations. The discussion here is based on the text *Polymer Physics* by Rubinstein [2].

DNA is a stiff molecule. The persistence length of the molecule is around 50 nm, compared to persistence length of order 1 nm for common synthetic polymers. The persistence length is the length at which the bending energy is order k_BT, where $k_B = 1.381 \times 10^{-23}$ is the Boltzmann constant, and T is the temperature. A useful length related to the persistence length is the Kuhn length, which is twice the persistence length and is used as a representative length when describing a polymer chain. DNA is also a charged molecule, the phosphate groups on the backbone give it a net negative charge. Since it is also a polymer it is called a polyelectrolyte. If we were to assume a bare chain, DNA would have a charge of -2e, where e is the charge of an electron ($1.602 \times 10^{-19}C$), per monomer of the polymer, which is called a base pair (bp). However, the charge is actually around 0.6e per bp in a ionic solution due to Manning condensation [3], or the strong attachment of positive ions from solution that partially screens the charge below a critical amount such that the repulsion between monomers is not too strong. Another phenomenon that occurs in an ionic solution is that a charged double layer

forms around the polyelectrolyte or charged surface, shown in Fig. 1.1. The first layer being the Stern layer, which is a very thin layer, typically $<$ 1nm, of strong positive charge. The next layer is the diffuse Debye layer, which has a length, κ, that depends on the ionic strength,

$$\kappa^{-1} = \sqrt{\frac{\epsilon_0 \epsilon k_B T}{2e^2 I}} \ , \tag{1.1}$$

where $\epsilon_0 = 8.854 \times 10^{-12} F/m$ is the permittivity of free space, and ϵ is the permittivity of the solution. All of these, with the exception of ϵ, are constant and even ϵ is roughly the same in common biologically relevant solutions, but $I = 0.5 \sum_i z_i^2 c_i$, where z is the valence and c is the concentration of the ions present, can be varied to tune the Debye length. Within the Debye length the solution has a charge opposite that of the charged surface. Outside the Debye length the solution is neutral again. A typical Debye length in ionic solutions is usually between 1-10 nm.

We will now briefly discuss the size of a DNA molecule in an ionic aqueous solution, a typical solution used when manipulating DNA. We will first look at the DNA molecule as a number of segments. When saying segments, instead of monomer, we mean the number of Kuhn segments. In this definition the contour length, or the length of a stretched out polymer, is $L_c = Nb$, where b is the Kuhn length and N is the number of segments. Now that we have defined contour length we can talk about the radius of gyration, R_g, which is the characteristic size the molecule when in solution. For very short DNA, shorter than the Kuhn length, the radius of gyration is the same as the contour length, since the DNA is to short too bend much, so $R_g \sim L_c = Nb$. For short DNA, the DNA can be defined as an ideal chain and follows a random walk where $R_g \sim bN^{1/2}$. For long DNA, the DNA becomes able to cross itself and excluded volume effects become important, so the random walk model does not hold any more. Instead Flory theory must be used and $R_g \sim bN^{\nu}$, where $\nu \approx 0.6$. A model that well describes both the short and long DNA sizes is the wormlike chain model. There is currently

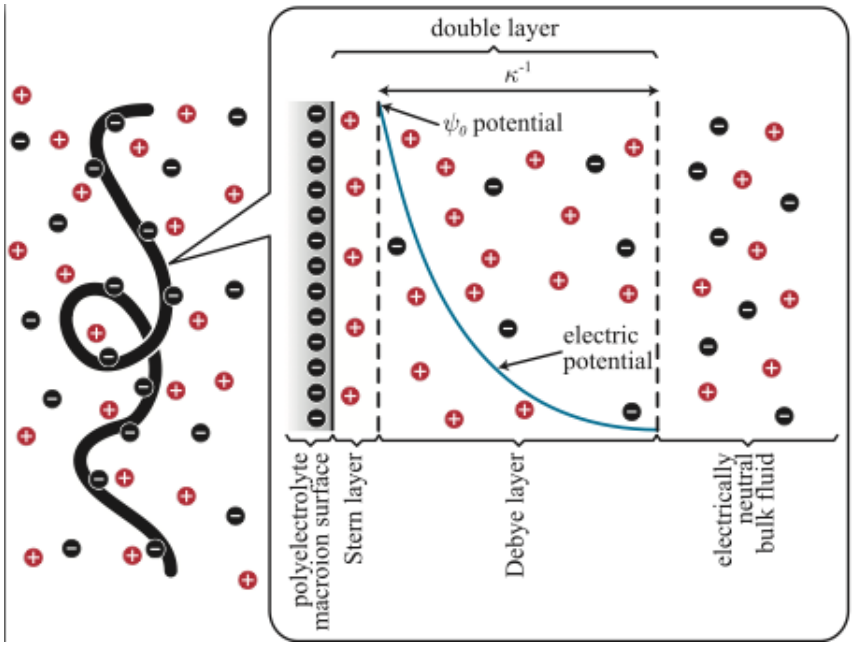

Figure 1.1: A schematic of the electric double layer that is established in an ion solution around a polyelectrolyte. In this case the surface is negatively charged, as is the case with DNA. This leads to the Stern layer and Debye layer being positively charged. This layer is also established on a charged surface as well. Reproduced from Ref. [4].

some debate as to the value of the exponent ν for the DNA currently being used as a standard for long DNA, λ DNA which is 48.5 kbp [5–7], but that is beyond the scope of this work.

1.2 DNA Separation

Almost all fields of biology utilize DNA fragments for research and usually the DNA needs to be sorted by size. The most common method is DNA electrophoresis with some sort of separation media, for example gel electrophoresis. Since DNA is a charged molecule, it will move when an electric field is applied to it. However, DNA electrophoretic mobility in free solution, in the absence of a separation matrix, is independent of size. This can be illustrated by using a local force balance. Care must be taken

when using this description as it only applies when the electric field is the only force acting on the molecule [8]. This is usually not the case, but this is still a worthwhile exercise and does model the behavior correctly. The basic idea behind the local force balance is that the frictional force balances the force applied by an electric field. The electric force, F_{el}, is given by

$$F_{el} = qNE \ , \tag{1.2}$$

where q is the electrophoretic charge, N is the number of segments, and E is the electric field. It is important to note that q is not the same as the charge along the backbone, but is actually an empirical value to get the correct physical behavior. The electric force is balanced by the frictional force, F_{fric}, given by

$$F_{fric} = fv \ , \tag{1.3}$$

where v is the velocity and f is the overall friction coefficient. Balancing the forces by setting Eq. 1.2 and 1.3 equal and solving for the electrophoretic mobility, $\mu = v/E$, we obtain the result

$$\mu_0 = \frac{qN}{f} \ . \tag{1.4}$$

Since this balance was performed under free solution conditions, the free solution mobility, μ_0, is presented. Typical DNA electrophoresis experiments are performed in solutions that are sufficiently ionic that the positively charged counter-ions in the solution effectively screen the negative charges on the DNA backbone. The friction from the flow of these counter-ions cancels out the size dependent mobility on the molecule, making it appear freely draining. For a freely draining coil, the friction follows the well-described Rouse model,

$$f = N\xi \ , \tag{1.5}$$

where ξ is the friction factor of each segment. Combining Eq. 1.4 and 1.5 leads to the result that electrophoretic mobility of DNA in free solution is independent of size [9],

$$\mu_0 = \frac{qN}{N\xi} = \frac{q}{\xi} \ . \tag{1.6}$$

Because electrophoretic mobility is independent of size in free solution, a separation matrix is required in order to obtain size-dependent separation. One of the most common separation matrices used for DNA separation is agarose gel. An agarose gel consists of a matrix of randomly cross-linked fibers with pores that range from about 200 to 500 nm depending on the concentration of the agarose used [10–13]. The movement of DNA through an agarose gel is described by four regimes. The first two are useful for separating DNA and having been named "the Ogston regime" and "the reptation regime without stretching" by Slater *et al.* [12]. The third regime is the entropic trapping regime, which occurs when the pore size is about the same as the characteristic size of the molecule. The fourth regime, which is not useful for separating DNA by size is called "the reptation regime with stretching" [12].

The first regime is the sieving regime and is based on the results of Ogston's development describing how hard spheres migrate though a random array of fibers [14]. Rodbard and Chrambach were able to extend Ogston's model to account for a flexible coiled polymer in different types of gel geometries [15] and were able to use the model to predict physical parameters of both the gel and the molecule [16]. The model is a linear relationship between the log of the mobility versus the gel concentration,

$$\ln \mu = -K_r C + \ln \mu_0 \ , \tag{1.7}$$

where K_r represents a retardation coefficient, C is the concentration of the gel, and μ_0 is the free solution mobility [17]. The retardation coefficient depends on the size of the molecule and is what accounts for size-based separation observed in this regime. For cylindrical fibers, the best geometry to describe agarose gels, the retardation coefficient

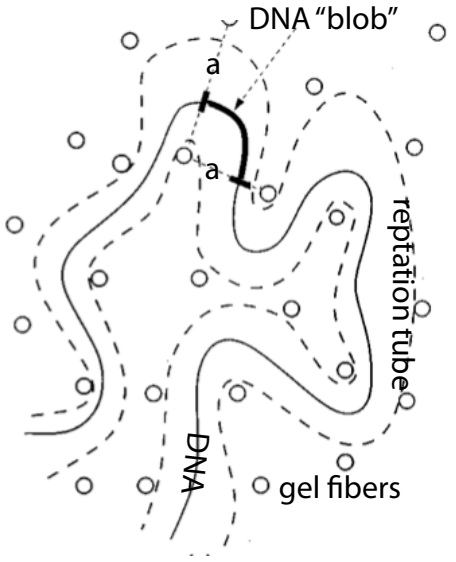

Figure 1.2: A representation of DNA traveling through a reptation tube in an agarose gel as explained in the biased reptation model. The dark line is the DNA molecule and the bold section is a single blob of DNA. The dashed line is the reptation tube with thickness a. The circles are gel fibers. The image was reproduced and modified from reference [13].

is given by [15]

$$K_r \sim (R + r)^2 \ . \tag{1.8}$$

In this equation, R is the characteristic size of the particle or molecule, usually the radius of gyration for DNA, and r is the radius of the gel fibers. While this model fits experimental data for pore sizes larger than the radius of gyration of the DNA molecule, it begins to break down as the pore sizes get smaller than the radius of gyration. This is because the DNA no longer travels as a random coil, but travels as a long stretched out polymer in order to squeeze into the small pores. The model also does not capture the loss of size-based separation observed for large molecules [12].

The shortcomings of the sieving model led to the development of a model for the

second regime [18, 19]. The model was based on the work done by de Gennes on how polymers move in polymer melts [20]. This model, known as the biased reptation model [12], describes the DNA chain as a series of Gaussian blobs of size a, moving through the pores in a tube of size a, as depicted in Fig. 1.2. Only the end segments leaving the end of the tube can sample different possible orientations, the rest of the chain is confined to the tube. The electric field adds a bias to the normal diffusion and causes the mobility to scale with the projection of the chain in the field direction, which leads to a size-based separation. Under low enough electric fields the tube takes on a random walk orientation, but at high electric fields the chain becomes oriented with the field and mobility becomes a function of the electric field, not size. The biased reptation model correctly predicted that the mobility scales inversely with the number of segments, $\mu \sim N^{-1}$, below N^*, a critical separation size of the DNA chain that depends on the electric field. However, its prediction that the mobility depends on the square of the electric field, $\mu \sim E^2$, for N larger than N^*, and that N^* depends on the square of the electric field, $N^* \sim E^2$, did not match with experiments or computer simulations [13]. Consequently, a new model was developed, the biased reptation with fluctuations model, which took into account the fluctuations of the DNA inside the tube. This model also predicted that the mobility scales inversely with the molecular weight, $\mu \sim N^{-1}$, for N less than N^*. However, the biased reptation with fluctuations model was able to correctly predict a linear dependence of mobility on the electric field, $\mu \sim E$, for N greater than N^* and a linear dependence of N^* on the electric field, $N^* \sim E$ [21–23]. This model has been confirmed to fit experimental data [24, 25], shown in Fig. 1.3, and agree with computer simulations [26].

The third regime is the entropic trapping regime. The relevant transport mechanism in entropic trapping involves hopping between cavities separated by an energy barrier associated with a temporary loss of configurational entropy [27–29]. This covers a

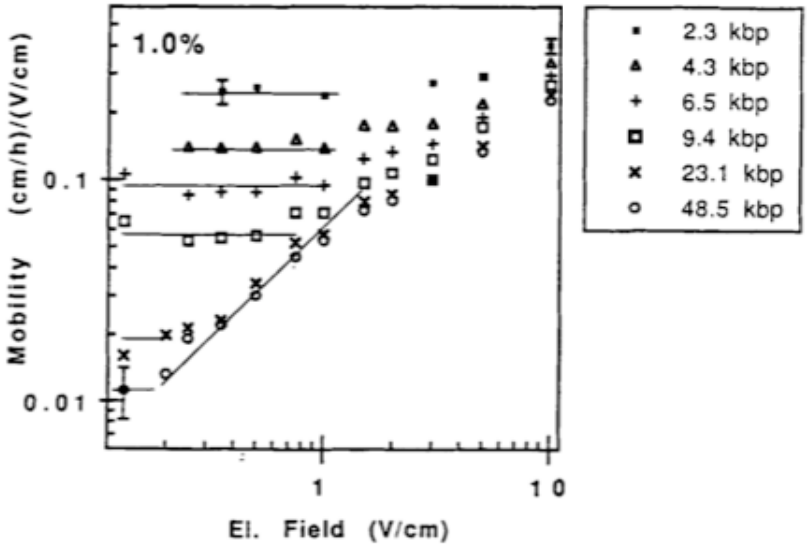

Figure 1.3: A plot of mobility as a function of electric field with a wide variety of DNA sizes. This plot shows the transition from biased reptation regime without stretching where mobility is not a function of electric field to the biased reptation with stretching regime where $\mu \sim E$. It also shows that $N^* \sim E$. These match the biased reptation with fluctuations model. The image was taken and modified from reference [24].

narrow range of molecular weights and the motion of the molecule is complicated. The details of this regime are beyond the scope of this work, but the regime has been well studied [28, 30].

The fourth regime, "the reptation regime with stretching", does not separate DNA based on size. The DNA completely orients with the electric fields and moves quickly though the gel in a size independent fashion. This occurs for either long DNA or for high electric fields. This transition happens at higher electric fields in less concentrated gels [24]. However, going lower than a 0.5% gel makes the gel very difficult to handle. A way to separate these long DNA in agarose gels is to use pulsed field gel electrophoresis. This uses two electric fields oriented either 180° or 120° from each other [31, 32]. The two operation modes work differently than normal gel electrophoresis, but both result

in sized based separation of long DNA based on the difference in the time it takes the DNA to reorient with the applied electric field.

Although theories are available that well describe DNA electrophoresis in a gel for a wide range of DNA fragment sizes, gel geometries, and electric field strengths, major practical limitations for agarose gels are still present. Agarose gels are made of randomly cross-linking polymers. This results in a non-uniformity of pore sizes between and within gels, which leads to reproducibility problems when separating DNA in gels. Additionally, there is a large amount of wasted space because the DNA cannot sample all the pores in the gel, which leads to areas in the gel that are not being used. Also, for pulsed field systems, which is the only way to separate long DNA, the separation can take on the order of days to complete [33]. Finally, Joule heating greatly limits the electric fields one can apply to the gels without them melting. So while these systems are currently the gold standard for both industrial and academic research there is great room from improvement.

1.3 DNA separation in microfluidic devices

Microfluidics has begun to address some of the issues present in agarose systems. There are even some commercially available microfluidic systems for certain operations. DNA separations in microfluidic systems require less reagents and time, with some systems being able to separate in seconds [34]. This is great for when there is very little sample, such as forensics where only trace amounts of DNA can be found. Microfluidic devices can be made with very specific sizes and geometries. This allows devices to be designed to look at separation mechanisms or to develop novel separation modes not possible in gels. The materials used are much more robust than gels, which allows for very sparse arrays. This allows for rapid separation of large DNA molecules, which are difficult to separate in gels. There are also continuous devices, which can match the throughput of

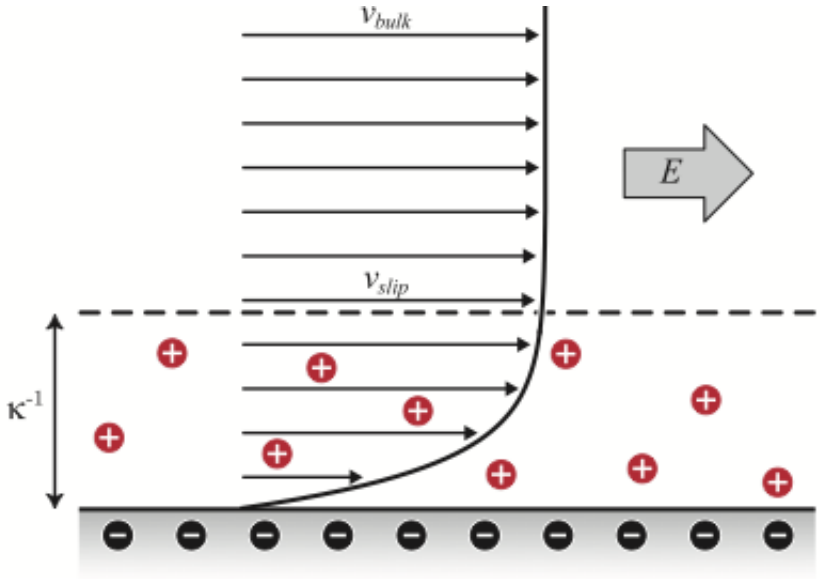

Figure 1.4: A schematic showing the electroomosis effect. A velocity profile is established in the Debye layer, with an interface velocity v_{slip}, caused by the electric field, causes a plug flow in the channel move at v_{bulk}. Figure obtained courtesy of Kevin Dorfman.

gels. These continuous devices will be discussed more in section 2.3. Another advantage of microfluidic separation devices is that they can be integrated into larger microfluidic device, sometime referred to micro total analytical systems. These larger systems are beginning to appear in the literature [35, 36] and seem to be the future for point of care needs, especially where large scale lab equipment is not available.

There are issues that do arise that are unique to microfluidic devices. One potentially large issue arises from the Debye layer that is established along the walls of these channels. Many microfluidic devices are made in glass or in silicon with an insulating silicon dioxide layer. Both of these materials have a negative charge and so the Debye layer has a positive charge. When an electric field is applied the ions in the Debye layer are affected and begin to move. This can cause a flow in the bulk due to the viscous forces. This effect is known as electroosmotic flow, shown schematically in Fig. 1.4.

While this effect can be used advantageously, for DNA electrophoresis in microfluidic devices it is generally a detriment. If there is too much roughness or non-uniformities along the wall this can lead to rotational flow, which causes band broadening [13]. Electroosmotic flow also opposes the DNA motion in these cases, so it can slow down the DNA resulting in a longer than expected separation. A method to reduce this effect is to increase the ionic strength of the buffer, reducing the Debye layer size. Another way is to use polymer brushes, either permanent or dynamically attached to the walls.

Besides separations there are many exciting frontiers in which microfluidics are being used. Direct sizing using stretching and fluorescence burst analysis may be a better way to assemble genomic maps to assist with DNA sequence assembly. This is done using nano-channels made such that only one molecule of DNA can fit into a channel [4]. While these other uses for microfluidics are very exciting we will focus on separation technologies in this work. First we will give an overview of the literature and present some geometries that have been developed and studied. These geometries are the slit-well geometry and the hexagonal post array. We will also discuss continuous devices, which was a major motivation for the work presented in chapter 5. Below is an outline of each chapter to be presented.

1.4 Dissertation Outline

- In chapter 1 we briefly introduced some of the physical parameters used to describe DNA and the meaning of those parameters. We then discussed DNA separations, including the models used to explain separation in agarose gels, the regimes seen in gels, and the condition under which these regimes are observed. Finally, we briefly discussed the advantages of using mircofluidics for DNA separations.

- Chapter 2 presents a review of some microfluidic devices used to separate DNA

based on size. The focus will be on the slit-well geometry and the post array geometry to give a background on the devices in which we performed the work presented. This will be followed by a look at continuous separation devices, as they were a major motivation for much of the unpublished work done presented in chapter 5.

- Chapter 3 presents the work we have done in the a slit-well geometry to create a temporal asymmetry ratchet in order to separate DNA by size. This resulted in bi-directional migration of the DNA, creating a non-clogging DNA filter. The work was done with small DNA, but could also be used for long DNA by changing the length scales in the geometry.

- Chapter 4 presents work done in a tilted post array geometry. By tilting the post array you break up the channels between the posts seen in the standard post array. This allows separations to be performed at higher electric fields, while still maintaining similar resolution. This resulted in a much faster separation and not requiring as much length to perform the separation.

- Chapter 5 discusses unpublished work done while trying to create a DNA separation matrix using proximity nano-patterning (PnP). This was in an attempt to create a more regular "artificial gel" that would allow for a more reproducible and better separation of smaller DNA, smaller than 15 kbp. The final aim of the project was to create a continuous separation device using the PnP separation matrix.

- Chapter 6 restates the important points and conclusion of each chapter. We then discuss what impact our work has had on the field of DNA separations in microfluidic devices. We then take a step back and discuss, in the author's opinion, major accomplishments of the field and where the field is heading in the future.

Chapter 2

Microfluidic DNA Separation Devices

Presented here is an in depth discussion of the background of a select number of separation geometries. These geometries will be the slit-well geometry and the post array geometry. We will also discuss continuous separation devices, which can be made with different separation geometries depending on what is needed. We have chosen to focus on the slit well and post array geometries because they were the geometries used to perform the studies presented in the following chapters. We take a look at continuous separation devices because it was a motivating factor and an overall goal for the unpublished work presented in chapter 5.

2.1 Slit-Well Geometry

We first turn our attention to how microfabricated devices enhance separations in the regimes of DNA electrophoresis covered in chaper 1, namely Ogston sieving and the entropic trapping regime. Recall that Ogston sieving refers to the case where the radius

of gyration of the DNA is smaller than the pore size, and the separation is due to the molecular weight dependence of the free volume available to the DNA as it migrates through the gel in the absence of substantial deformation [14, 15, 37]. In contrast, the entropic trapping regime refers to the case where the nominal pore size in the gel is commensurate with the radius of gyration of the DNA. One particular challenge for entropic trapping in gels is the variance in the pore sizes in the gel [38], which leads to a distribution in energy barriers during entropic trapping [39] and concomitant band broadening. One also experiences similar problems in the Ogston sieving regime of gel electrophoresis, since the local free volume available to the DNA in a heterogeneous gel fluctuates (in the Lagrangian sense, where we follow the particle) and thus leads to band broadening. Microfabricated devices should be able to minimize the latter issues, since we have already seen that it is straightforward to produce periodic sieving matrices by microfabrication.

The regimes of Ogston sieving and entropic trapping have been exploited primarily using the device designs illustrated in Fig. 2.1. When the device is used for separating long DNA, it is referred to as an entropic trap [40–43]. When the device is used for separating short DNA, it is referred to as a nanofilter [44–47]. In both cases, the device is an array of repeating thick and thin regions. The lateral patterning of the device is done by optical lithography, so the typical length of a thick or thin region is in the micron regime and the channel is around 25 μm wide. The thick regions are about 300 nm to 3 μm deep and the thin slits are usually between 20 and 90 nm, with smaller lengths scales prevalent for the nanofilter and the longer length scales prevalent for entropic trapping. Recently, the nanofilter geometry was turned on its side and called a "nanowall" array [48]. The latter device consists of 5 μm high and 215 μm long walls separated by a gap of 200 nm. The device contains 20 nanowall regions before the detector, where each wall region is separated by a 35 μm gap. The periodicity of

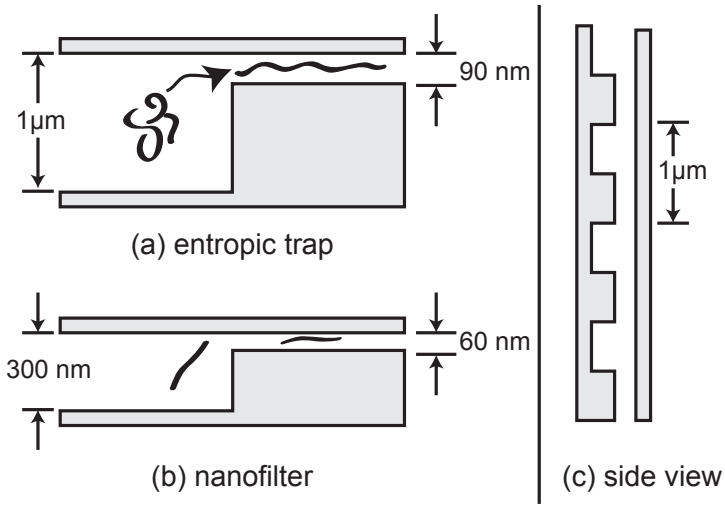

Figure 2.1: Slit-well motifs for exploiting (a) the entropic trapping regime using long DNA and (b) the Ogston sieving regime using short DNA. (c) The devices are patterned by two etching steps. As we see from the side view of the device (90° rotation of the other schematics), the optical lithography patterning of the devices leads to similar periodicities and channel sizes in both types of devices. The direction of the DNA motion is the same in panels (a) and (b).

the nanowall device is much larger than the schematic in 2.1, and features much fewer periods than the standard entropic trapping system [42].

The DNA can be driven though the array with an electric field [40–47] or by a pressure driven flow [49]. We will devote most of our time in this section to discuss the separations achieved in entropic trapping and nanofilter configurations. However, the slit-well motif [50] is not the only way to exploit the physics of these regimes. Thus, we will also devote some time to consider alternative designs that are amenable to soft lithography [51, 52] and a rather novel idea of using oil slugs to create entropic traps in large microchannels [53, 54].

The basis for separations using the system in Fig. 2.1a was the subject of considerable interest. The original device [40] consisted of alternating thick regions, about 1 μm deep, and thin regions, 90 nm deep, and was only used for observing single molecules

of long DNA as they moved through the traps under the influence of an electric field. Remarkably, the experiments revealed that the large molecules travel faster than the smaller molecules. This result was unexpected, since the configurational entropy lost by entering the slit should increase with molecular weight. The explanation [41] is that the larger molecules have a higher escape attempt frequency, which is more important than their larger free energy barrier [41, 42]. These experiments also spurred a great deal of theoretical work to understand the details of the process. We recently reviewed the theoretical literature elsewhere [50].

In the present work, we would like to focus on the applications of the entropic trapping device rather than the underlying physics. In addition to verifying that the single molecule dynamics in previous work [40, 41] indeed lead to a separation, the seminal experiments on entropic trap separations [42] introduced two practical innovations. The first innovation was the method for loading the DNA. Escaping an entropic trap requires overcoming the energy barrier in a thermally activated escape process. The electric field tilts the potential energy landscape, so the effective barrier height decreases with increasing electric field strength [41]. Indeed, for a sufficiently high electric field, there will be no trapping since the DNA can easily overcome the barrier when the favorable change in enthalpy caused by moving in the potential gradient dominates the entropic penalty for entering the slit. In contrast, at very low electric fields, the probability of jumping over the barrier by thermal energy is exponentially small. As a result, the DNA can be pressed against the first trap using a weak electric field. When the electric field is increased to the separation voltage, the DNA hop over the first barrier as a narrow injection band. While this type of injection was first proposed in the entropic trapping separation [42], it was critically important in the ultrafast separations of long DNA via pulsed field electrophoresis in a post array a few years later [34]. The second innovation was the multilane separation device illustrated in Fig. 2.2, which mimics the

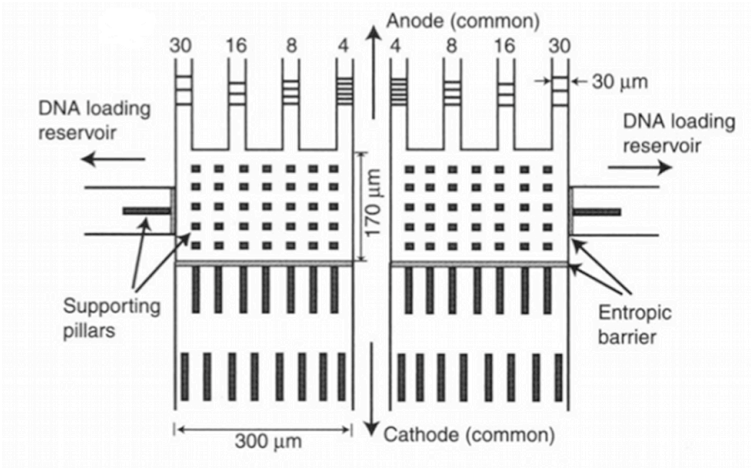

Figure 2.2: Schematic of the multilane separation device for entropic trapping. All eight channels are connected to a common anode and cathode. Each set of four arrays is connected to their own DNA loading zone. This allows for two different mixtures to be separated simultaneously, similar to a submarine gel electrophoresis setup. Reproduced from Ref. [42].

typical setup in gel electrophoresis. One of the challenges in the microfluidic separation devices is the calibration. The experimental data seen in microfluidic systems [4] always involved separating known sizes of DNA. These are the sensible experiments to validate the operation of a device. However, if we want to identify the size of unknown bands, we need to compare their speeds to a calibrated standard. One of the major (and rarely discussed) shortcomings in many microfluidic separation devices is the reproducibility of the absolute mobility. Since these devices have extremely high surface area to volume ratios and very small amounts of sample, the combination of experiment-to-experiment fluctuations in the surface properties and the relatively low signal-to-noise ratio makes an absolute calibration challenging in prototype devices. The device architecture in Fig. 2.2 minimizes these issues.

The key variables for the separation are the electric field strength and the pitch of the array [42, 43]. A smaller pitch leads to better separations since it can increase the

number of traps for a given length. However, the use of optical lithography limited the original pitch to 2 μm [42]. The current pitch limitation is just under 1 μm without using expensive and slow direct write lithography systems. Higher electric fields decrease the elution time, but lower the resolution since the barrier for escaping the trap is lowered. The resolution also decreased with DNA length. This requires longer DNA molecules to be run at lower field and for a longer time [43], analogous to gel electrophoresis. The entropic trap can resolve DNA in the hundreds of kilobase pair range in around 30 minutes, which is comparable to the performance in post arrays. The band capacity of the entropic trap appears to be superior to the post arrays, with almost complete baseline of a 5 kbp DNA ladder (7 bands) [42, 43].

In the standard entropic trapping device [40–43], illustrated schematically in Fig. 2.1, the deep region of the device has a volume that is large compared to the nominal volume R_g^3 of the DNA coil. As we show in Fig. 2.1, the DNA can thus coil freely in the deep region. If the length scales are decreased further, then the DNA will be deformed in both the slit and the well region. A device of this type [49] was named the "nanogroove array." Here, the well is only 150 nm deep and varies in width from 75 to 600 nm. The DNA in the well is in a de Gennes regime. The slits are 50 nm deep and the periodicity of the device is between 1 μm and 2.6 μm. For these experiments [49], the λ DNA, T4 DNA and 42.2 kbp circular DNA were animated by a pressure driven flow instead of an electric field. At low flow rates, the DNA falls into the 150 nm grooves and is extended along the width of the device in the de Gennes regime, but is not able to escape the groove. By increasing the flow velocity, the DNA will exit the groove and travel to the next groove in a "sidewinder" type motion. The sidewinder motion is independent of DNA size. Increasing the velocity further causes herniation into the slit, which leads to a "tumbleweed" conformation. The molecule can transition between the two states with the "tumbleweed" state being faster. Also, longer molecules are more likely to exhibit

the "tumbleweed" state so this leads to sized based separation [49]. At the very highest flow velocities, only the "tumbleweed" conformation is seen and separation no longer occurs. The transition between the two states is also different for linear and circular DNA, so this device can also separate DNA based on topology and not just size [49].

All the above studies [40–43, 49] used long DNA (greater than 5 kbp). The radii of gyration of these DNA are always on the order of or larger than the slit depth. The DNA must deform from their free solution configuration in order to escape the entropic trap, and the long molecules elute first due to an increased probability to escape the trap. Let us now consider the opposite limit where we work with relatively short DNA molecules in the 100 bp range. The persistence length of DNA is around 53 nm, corresponding to 300 bp per Kuhn length. Thus, these short DNA are expected to be fairly rigid molecules. When the depths of the slit and the well are decreased somewhat, as illustrated schematically in Fig. 2.1, the device becomes appropriate for separating short DNA in a manner akin to Ogston sieving [44, 45]. Small DNA fragments, 50 bp to 1600 bp, and slits between 55 and 80 nm were used to satisfy the requirements of the Ogston regime. In this regime, the smaller fragments eluted first. These are exactly the physics one would expect from the Ogston model, since the free volume available to the DNA in the slits decreases with molecular weight. While the model bears some similarities to Ogston sieving, it is probably more appropriate to think of the device as a one-dimensional chromatographic separation based on the partitioning between the slits and the wells [45, 55].

Note that such an equilibrium model is only valid for very weak electric fields where the DNA have sufficient time to sample their configurational space in the well and the slit via rotational diffusion. At higher electric fields, scaling analysis and simulations [56] predict that the device would operate in a band inverted mode, where the larger rod-like DNA would elute first. These predictions were eventually realized in experiments [47]

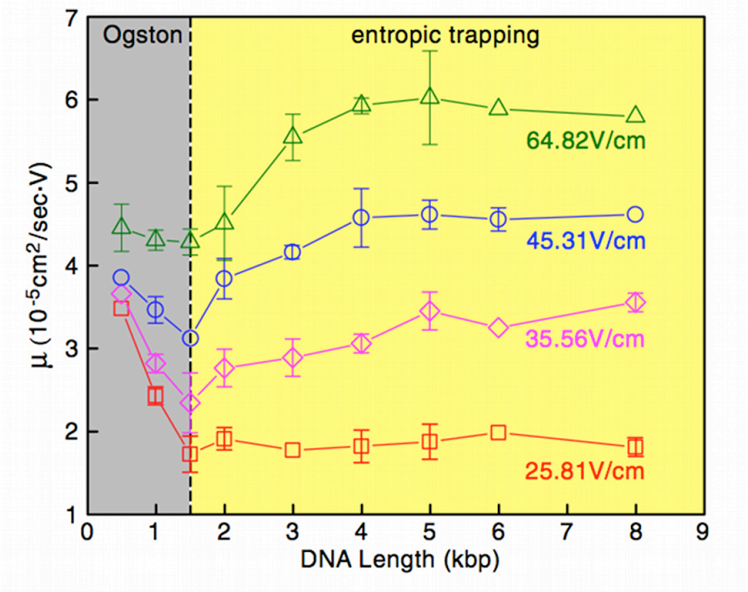

Figure 2.3: Mobility as a function of DNA length at several electric fields in the DNA nanofilter [45]. This figure illustrates the transition from the Ogston regime, where the mobility decreases with length, to the entropic trapping regime, where the mobility increases with molecular weight. Reproduced from Ref. [45].

using a fused silica device that could support the very high electric fields (circa 500 V/cm) required to reach the band inversion regime.

As we might expect, there is also a band inversion [45] that must occur as a function of molecular weight as the transport transitions between the Ogston regime, where the smaller DNA elute first, and entropic trapping regime, where the larger DNA elute first. Fig. 2.3 shows this transition from a decreasing to an increasing mobility as a function of DNA fragment size, independent of electric field [45]. The transition occurs when the radius of gyration is about the same size as the slit. In this case the slit was 73 nm and the radius of gyration for the DNA at the crossover point was 80 nm [45].

While steric interactions are sufficient to provide confinement, the slit size needs to be very small (tens of nanometers) to see a partitioning effect for small DNA. Recall from section 1.1 that any charged surface is associated with a Debye layer of counterions

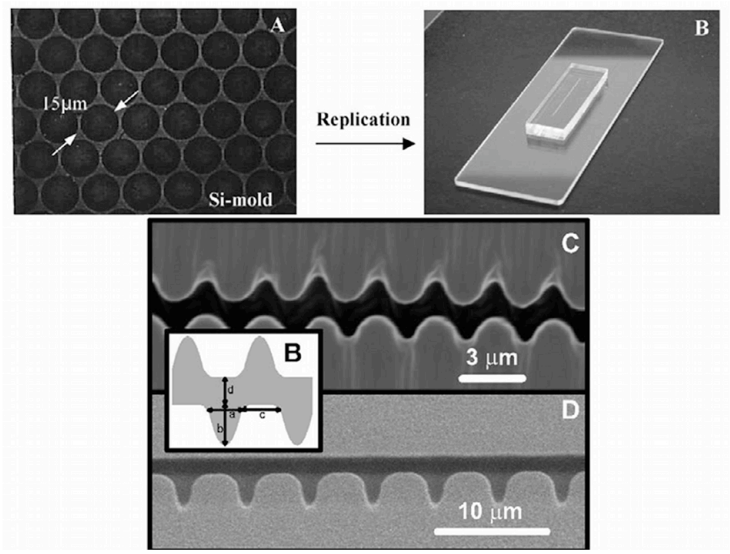

Figure 2.4: Images of the PDMS devices for entropic trapping. The top two images are a post array device [52], where (A) is an SEM of the silicon mold and (B) is a photograph of the final device. Reproduced from Ref. [52]. Copyright 2003 Elsevier Science B.V. The bottom panel are SEM images of structured channels, with the inset defining the dimensions of the structures. Reproduced from from Ref. [51].

whose characteristic length scale is given by Eq. (1.1). The devices we have considered thus far are fabricated in silicon, followed by thermal oxidation, or fabricated in fused silica. In either case, the surface adopts a negative charge in the basic pH buffers used for electrophoresis. As a result, the DNA is repelled from the surface by electrostatic interactions. Lowering the ionic strength increases the electrostatic repulsion between the DNA and the walls, leading to an increase in the size of the region where the double-layers overlap between the DNA and the walls. Since the nanofilter mode of the device operates through a standard chromatographic mechanism [45] based on the partitioning of the rigid, short DNA molecules between the slit and the well [55], the effect of the electrostatic interactions is equivalent to reducing the physical size of the slit. As we might expect, the selectivity and resolution are enhanced at low ionic strength [46].

The slit-well motif in Fig. 2.1 is not the only artificial gel that operates in the Ogston

sieving and entropic trapping regimes. Fig. 2.4 shows two particular examples fabricated in PDMS. Note that entropic trapping via thin slits is unlikely to be successful in a soft material like PDMS, since they would collapse. The upper panels of Fig. 2.4 show a post array with 15 μm posts with 1 μm spacing at the thinnest point [52]. These posts are much too large to be useful for the separations discussed later in section 2.2, since the post sizes are almost an order of magnitude larger than the DNA coil. For the same reason, this post array is not the same as the systems studied using the exactly solvable lattice models for DNA electrophoresis [57–64]. Rather, the device operates in an entropic trapping mode because the interstitial space between the post, where the DNA travels, has larger pockets connected by thin gaps, shown as the lighter grey area in Fig. 2.4. These gaps act as entropic traps. This device features a size based separation of molecules that have a radius of gyration on the order of the gap [52]. The lower panel of Fig. 2.4 shows a device with a uniform depth but wavelike structures along the walls [51]. One can think of this system as the slit-well motif turned on its side, albeit at a slightly larger length scale where the features are commensurate with the radius of gyration of the DNA rather than its persistence length. Two different systems are shown in Fig. 2.4, one with the wavelike structures on both walls and one with the wavelike structure on a single wall [51]. Videomicroscopy experiments [51] of T2 and λ DNA electrophoresis in these systems showed that the DNA interacts with and is stretched by the features on the wall. The interaction between the DNA and the wall was stronger for the longer DNA and this led to a smaller velocity when traveling through the channel [51]. Both of the devices in Fig. 2.4 have gaps that are about the size as the radius of gyration of the molecules they are separating, where the longer molecule has to squeeze a little more than the smaller one. So the larger molecule travels slower [51,52], as opposed to the case in the early entropic traps where the gap was much smaller than the radius of gyration and the larger molecules traveled faster [40].

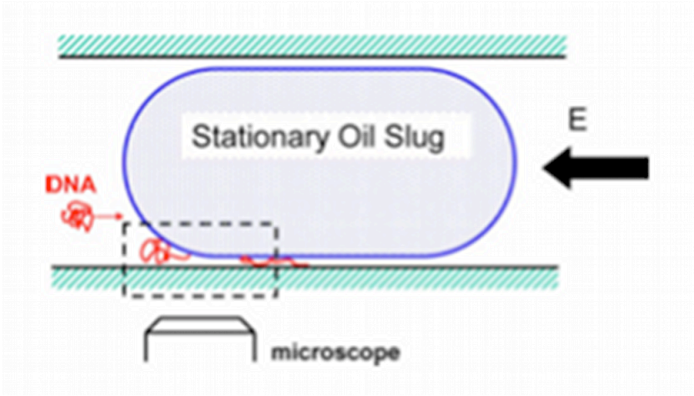

Figure 2.5: Schematic of the oil slug in the microchannel. The region between the wall of the channel and the oil slug creates a nanoslit. The interface between the channel and the nanoslit causes the DNA molecule to stretch. Reproduced from Ref. [53].

An alternate approach to entropic trapping is to use the thin film formed between an oil slug and the wall of a channel [53], shown in Fig. 2.5. This thin region produces a nanoslit and the transition from the large channel to the slit serves as an entropic trap. When the DNA is driven through the channel it encounters the slug and slowly stretches as the bulk of the coil slowly unravels to fit into the thin region. Once most of the molecule enters the thin area it quickly transverses the gap and exits due to the intensified electric field in the gap. While one should, in principle, be able to construct an entropic trapping device out of a series of oil slugs in a channel, this setup has only been used thus far to stretch DNA [53] to about 50% of its contour length [53]. The DNA can also be combed to the surface using a surfactant for the surface coating and high electric fields [54]. Both the stretching and combing were achieved in cheap and easy to fabricate PDMS channels at very tractable dimensions between 100 and 200 μm [53, 54].

Overall, the entropic trapping geometry seems quite promising, since the speed of the separation is comparable (but somewhat slower) than the other methods discussed

in a recent review article [4] and the band capacity seems very good. There are some minor technical challenges relative to the post arrays but they are easily overcome. For example, the device fabrication requires two etching steps to create the slit and the well, but the patterning is all done using conventional photolithography. Likewise, the injection method requires multiple field strengths, but this is easily implemented using a programmable power supply. The limiting issue is the band inversion as a function of electric field and molecular weight. Care needs to be taken when performing separations as the order of elution can be reversed if the molecule is about the same size as the slit size [45].

2.2 Post Arrays

One of the major limitations of agarose gel electrophoresis is that long DNA cannot be separated using a DC electric field. The gels can only be made so dilute before they can no longer support themselves and the electric field can only be turned down so low. Practically it is difficult to separate DNA species above 25 kbp in a DC field gel [24]. Pulsed field gel electrophoresis gave a way to separate longer DNA, but these separations can take many hours and maybe even days to complete. To solve this issue researchers turned to silicon processing techniques to make small separation devices out of silicon. Several post array devices are shown in Fig. 2.6. This allowed researchers to make arrays that could be used to separate long DNA in a large variety of post size, spacing, and material [65–77]. Researchers have also used other techniques to create post arrays, including magnetic beads [78–80] and nanowires [81, 82]. In addition to being able to rapidly separate long DNA, typically on the order of minutes, there are other advantages to using microfabricated devices, which were discussed in section 1.3.

In this section we will focus on the post arrays made of stationary obstacles, typically made in fused silica or silicon, as opposed to the nanowires or magnetic particles

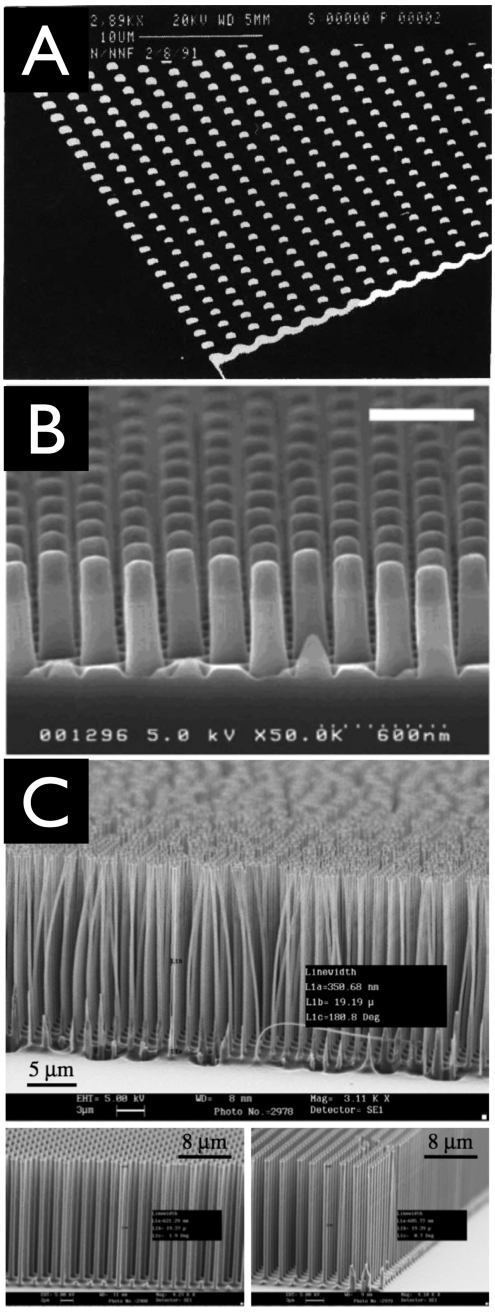

Figure 2.6: SEM images showing the progression of post arrays. (A) shows the first microfabricated post array device, reproduced from ref. [65]. (B) shows a side view of a post array, reproduced from ref. [66]. (C) shows an impressive device with very high aspect ratio posts, reproduced from ref. [67]. This compilation is reproduced from ref. [4].

mentioned above. The first post array was a post array made in silicon dioxide in 1992, Fig. 2.6A [65]. There have been many different post arrays since then. Some have been dense arrays with very thin posts. These are made by electric beam lithography and have array lengths of about 1 mm. These are typically called nanopost arrays, Fig. 2.6B and C [66–70, 83, 84]. Some have been sparse arrays made with photolithography. These typically have 1 μm posts with spacing larger than the size of the DNA they are separating. They also usually have arrays tens of mm long [34, 72, 73, 75, 76, 85]. Very similar to the sparse post arrays, there have been sparse post arrays with posts that are sub-micron sized using a technique called oxygen plasma thinning [74, 86]. Finally there are geometries that are variations on the standard post array. These include the disordered post array, created to study the effect of order on DNA sparation [76], and the nanofence array, created to take advantage of the relaxation time of λ DNA for more efficient separations [87].

Separation in the sparse post arrays happen by a single DNA molecule colliding with a post, stretching around the post, sliding off the post, and relaxing before colliding with another post. This occurs many times and results in a bulk size dependent mobility of the DNA. Whether the DNA will wrap around the post when it collides depends strongly on the impact parameter [81, 86, 89, 90], or how far the center of mass of the molecule is from the center of the post. There are a couple reasons the DNA would not wrap around the post: either the DNA molecule was too far to the side of the post and it glances off, or the DNA is too small to wrap around the post. If the DNA does not wrap around the post the collision does not hold up the molecule long enough for it to contribute to a separation. Once the DNA has collided it stretches out. An electric field of at least 10 V/cm is required to stretch the molecule sufficiently [89, 91]. When looking at isolated posts, or a sparse enough array, there are 4 types of collisions: U, J, X, and W type collisions [88, 92], shown in Fig. 2.7. If the posts are close enough, or

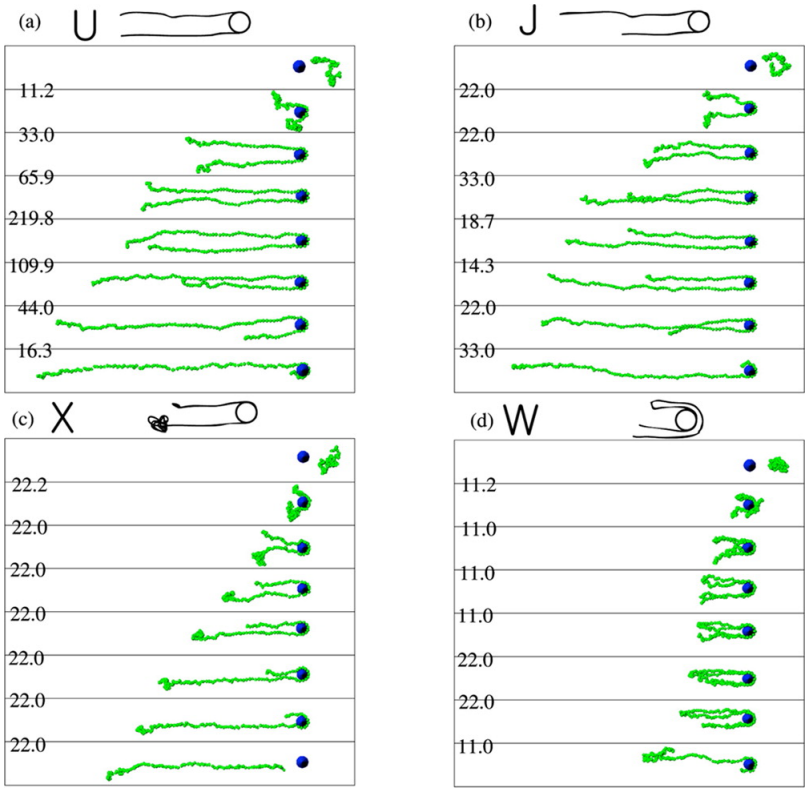

Figure 2.7: A schematic showing the four collision types for an isolated post. The U collision is when the DNA fully extends and is the same on both sides of the post. The J collision is when the DNA fully extends, but is longer on one side of the post. The X collision is when the DNA does not fully extend on one side. The W collision is when a hairpin folds over the post. This figure was reproduced from ref. [88].

the molecule long enough, for the DNA to interact with multiple posts there are many other types of collision that can happen [93]. Once the DNA molecule has wrapped around the post it begins to slide off the post in a rope over pulley type motion [85, 94]. This unhooking process is a deterministic process since the motion due to the electric field is much stronger than diffusive motion [95]. While the unhooking time seems like a good time to model the separation, it actually overestimates the amount of time it takes since the center of mass of the molecule is changing during the unhooking process. A better time to use is the hold up time, or the delay in the center of mass motion of

the molecule due to the collision [96]. This hold up time is size dependent [85, 94]. The DNA then relaxes and the process repeats. This is the unit operation for separation in a post array device.

Initial computer simulations in post arrays predicted that DNA would not separate in ordered post arrays and that some amount of disorder was necessary for separation. The prediction was that in a well ordered array the DNA would travel through the region, or channel, between the posts and would result in very few collisions and poor to no separation [97–99]. However, these models neglected the effect the insulating posts would have on the electric field, most notably the electric field bends around the insulating posts, shown in Fig. 2.8. This was an important effect and it was shown that DNA can be separated in sparse post arrays [72]. More careful work both experimentally and by simulations showed that there is a channeling effect, but only at high electric fields, or in very sparse arrays where the bending of the electric field was negligible compared the space between the posts [73]. Recently computer simulations showed that rotating the array, coined a tilted post array, breaks up these channels. This resulted in a better separation as the electric field was increase, instead of getting worse for normal post arrays [77].

To model the separation of DNA in a post array, researchers looked to the Scher-Lax continuous time random walk model (CTRW) [100]. Here we will only present a quick overview of the more recent developments in the model. For a more in depth look at the history of modeling this system, including pre-CTRW models, see reference [4]. The first CTRW model applied to the post array system assumed all collisions resulted in a fully extended chain, so U and J collisions only [80]. An improved model was then developed that took these incomplete extension collisions into account [99, 101]. These, however, did not calculate the collision probability or hold up time with enough accuracy. The most recent model that was develop seemed to have solved most of these issues. This

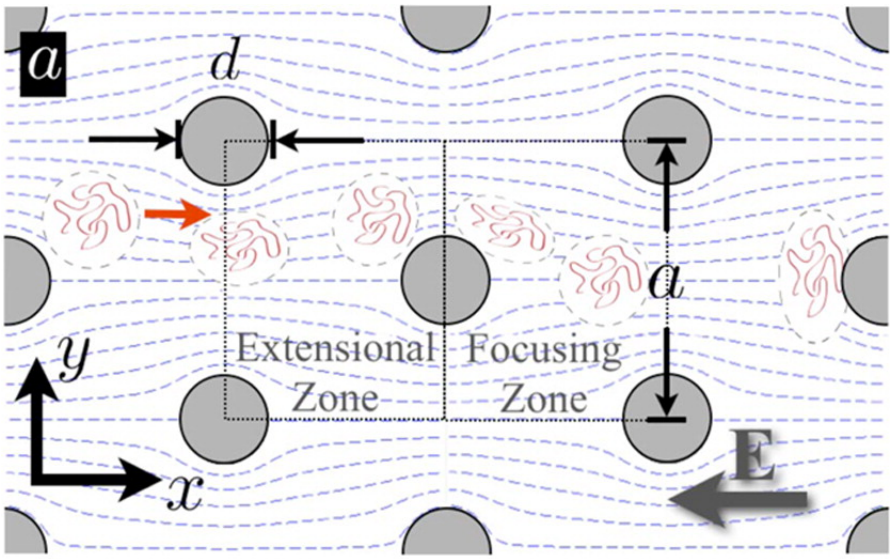

Figure 2.8: A schematic showing how the electric field interacts with the insulating posts. This pulls the DNA into the path of the posts and explains why DNA can be separated in ordered hexagonal post arrays. Reproduced from ref. [72].

model was compared to experimental results and was found to match very well [102].

Post array separation devices have drastically improved the separation time needed for separating long DNA. However, operating these devices usually requires a complex setup around the device. This may be a reason post arrays have not seen great success as a commercial product [4]. In the works referenced, the device typically separated 2 or 3 species of DNA. This speaks to the poor peak capacity of these devices, or the amount of DNA they can theoretically separation. Despite these issue, sparse hexagonal post arrays, with post about 1 μm in diameter, are relatively easy to fabricate. Because of this, posts seem to be the medium of choice for some continuous separation devices, in particular the DNA prism [103], which will be discussed in the next section. Post arrays have also found use in DNA stretching devices as a pre-stretching regions so hairpins do not form in the nanochannels [4]. So while alone post arrays may not be the next great thing, they have found their way into some of the newest DNA separation and

manipulation devices.

2.3 Continuous Separation Devices

The separation devices we have discussed so far all operate in a batch mode, analogous to gel electrophoresis and capillary electrophoresis. Batch separations are appropriate for analytical scale separations, where a small amount of DNA are analyzed to determine their molecular weight distribution. The small amount of sample certainly has some advantages, for example, when the sample is rare and only a small amount of material is available for the separation. In many cases, it is desirable to separate the DNA and collect the fractionated products, which is normally referred to as a preparative separation. At a laboratory scale, agarose gel electrophoresis is sufficient for preparative purposes, since fairly large amounts of DNA can be processed in a single run and the bands are readily extracted from the gel with a scalpel.

In principle, batch microfluidic separations could be run in a massively parallel fashion to process enough DNA for preparative purposes. However, there are several critical issues with such an approach. First, the number of channels required for the separation is enormous; if a single microfluidic injection analyzes a few nanoliters of fluid, we would need thousands of channels to reach the throughput of gel electrophoresis. Second, while the injection methods used are effective at creating a narrow injection band for an analytical separation, they waste a large amount of material in the loading process. In contrast, gel electrophoresis makes efficient use of most of the starting material. Third, collecting the bands from a batch separation is a challenging task. While there are several approaches appearing in the literature [104, 105], it is not obvious that the bands in a complicated and unknown mixture of DNA can be efficiently collected at the end of the microchannel.

If one desires a throughput appropriate for preparative separations, it is better to

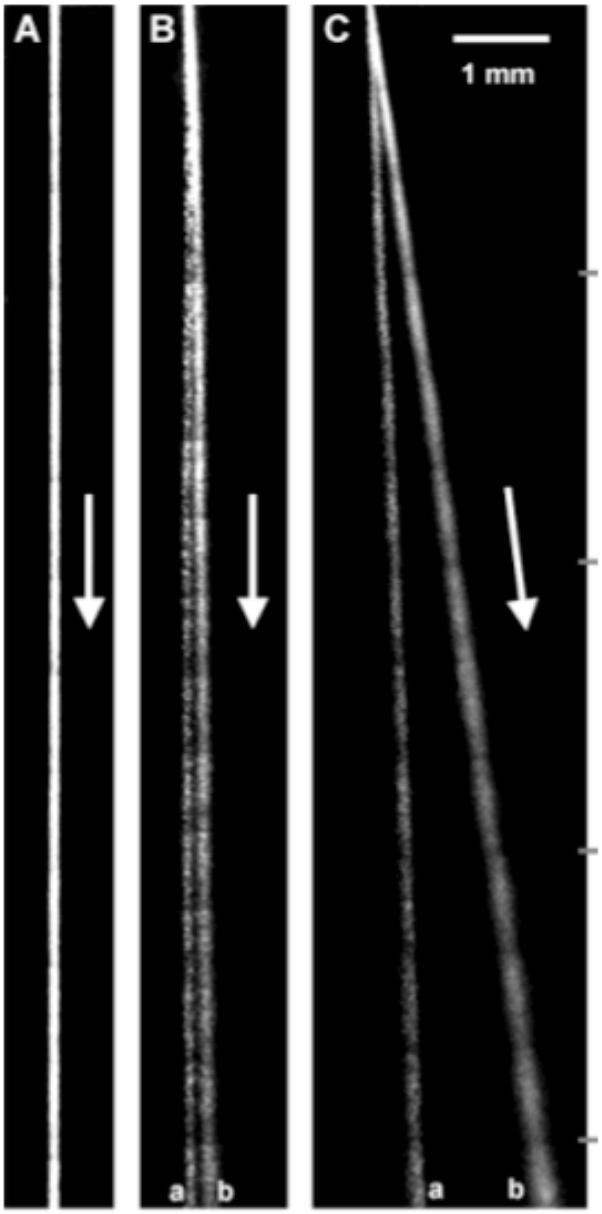

Figure 2.9: A separation of two different sized DNA molecules performed in a continuous separation device. The band with the larger defection angle is the smaller DNA. (A) No tilt, high speed. (B) No tilt, low speed. (C) Tilted, low speed. Species (a) is 164 kbp and species (b) is 48.5 kbp. Adapted from Ref. [106].

switch to a continuous separation process. As we will see in this section, continuous separations have been developed as extensions of some of the methods we discussed in sections 2.1 and 2.2, such as pulsed field electrophoresis in a post array [103, 107] and entropic traps/nanofilters [108, 109]. Other methods, such as ratchet based separations [106, 110–116] and deterministic lateral displacement [117], rely on physical principles that have not yet been covered in this work. The advantage of a continuous separation is easily seen in Fig. 2.9, which reproduces data from an optimized version of a tilted Brownian ratchet separation [106]. Different sized DNA fragments travel at different angles from the initial injection stream. By the end of the device the DNA has separated into different bands which can be shunted off into different channels for collection and further analysis. These devices can be run for hours and sometimes for days [103, 115], which allows for throughput that is currently impossible in batch microfluidic devices. Also, continuous devices simplify the injection procedure. All continuous devices need is a thin initial stream, which can be created by using a thin channel before the DNA enters the device as opposed to more complicated batch injection procedures required for most microfluidic separation devices [4]. These advantages make continuous separation devices ideal for integration into larger lab-on-a-chip type devices [35, 36] that require DNA (or protein) separations as one of the preparatory steps of the device.

One of the earliest working continuous separation devices was the DNA prism [103], seen in Fig. 2.10. The working principle behind the DNA prism is a clever extension of the pulsed field post array system [34]. In conventional pulsed field gel electrophoresis, the electric field strength remains constant but the direction of the electric field changes. As a result, DNA of different sizes move at different speeds but all of the DNA move in the same net direction [118]. As we can see in Fig. 2.10, the DNA prism operates using two different field directions *and* two different electric field strengths [103]. Following the standard practice in pulsed field gel electrophoresis, the fields are oriented at 120° from

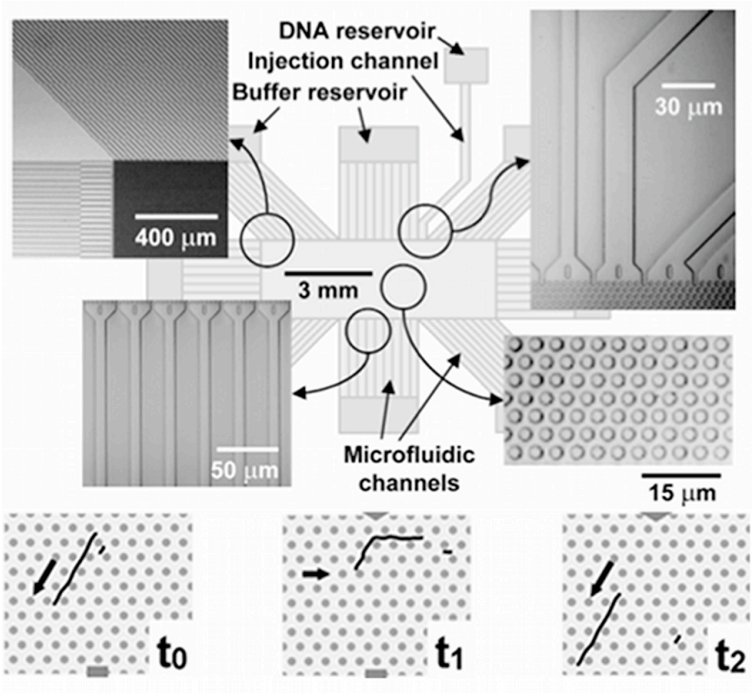

Figure 2.10: Top: Schematic of the DNA prism. The SEM images in the insets highlight different regions of the device. Bottom: Illustration of the separation mechanism. At t_0 both the long and short fragment travel in the strong field direction. At t_1 the field is switched to the weak field in a new direction. The long DNA molecule cannot get all the way around the corner, but the smaller molecule can. At t_2 the field is switched back to the strong field and the long DNA travel down the same channel while the shorter DNA is now in a new channel. Reproduced from Ref. [103].

each other. The DNA initially travels in the direction of the stronger field. The field is then switched to the weaker field direction. Since the electric field is not very strong, the longer DNA molecules are unable to reorient with the field. This means that on average the longer DNA travels in the direction of the stronger field. The shorter DNA molecules are able to reorient and travel in the new field direction until the stronger pulse is applied again. This means the shorter DNA tends to travel in the average field direction to varying degrees that depend on the DNA length. Note that the relevant parameter for the separation is the amount of time the DNA have to reorient when the

direction of the field changes. Thus, although the initial work used a square wave of different electric field strengths [103], one can effect the same separation by using long and short pulses of electric fields with the same magnitude.

The first DNA prism device [103] was constructed using photolithography as a 3 mm by 9 mm hexagonal array of posts. The post are 2 μm in diameter, spacing, and height. As we can see in Fig. 2.10, the array is surrounded by several bundles of microfluidic channels that lead to large buffer reservoirs. The channels serve two purposes. First, they create uniform and tunable electric fields within the large post array by the current injection method, where the high resistance channels act as current injectors [119]. Second, the microfluidic channels can also be used to selectively capture the separated DNA fragments. The location of these outlet channels can be designed so that the desired fragments can be collected for further analysis while the other fragments are sent to separate stream for separate analysis or to the waste. Note that the current injection method [119] is a robust way to apply the pulsed fields, but it still requires at least four, and up to eight, electrodes to work.

More recently, the DNA prism technology was recreated in colloidal crystals [107]. This device can be seen as a straightforward combination of the colloidal crystal separation device [120] and the DNA prism technology [116]. The major challenge is creating a large crack-free self assembled colloidal crystal, which benefits from the fact that the current injection microchannels also create more evaporation fronts for convective self assembly [107]. These later devices [107, 121, 122] also carefully considered the role of pore spacing and the frequency of the electric field. At very low and very high frequencies, there is no separation [107]. Neither result is particularly surprising in light of the regimes of pulsed field gel electrophoresis [4], since the low frequency regime minimizes the effect of the reorientation time (which is the origin of the separation [103]), and the high frequency regime does not provide sufficient time for any of the DNA to reorient.

Since one must get a separation in the DNA prism for some frequency range, there is a peak in the deflection angle at moderate frequencies between 1 and 30 Hz, with the exact location of the peak depending on the electric field [107] and vanishing when the colloids are very small [121]. In moderate sized colloids (330 nm and 900 nm), the optimal separation frequency is higher for higher fields, with the smaller colloids (330 nm) producing better separations than the larger (900 nm) colloids [107]. The mechanisms for the peak in deflection angle as a function of frequency was recently explored using simulations in post array prism [123]. Similar to what we saw in the discussion of post arrays [76] in section 2.2, the colloidal crystal separation benefits from having an ordered array of pore spacing [122]. The DNA prism has also been integrated into lab-on-a-chip devices for sample preparation [35, 36].

The entropic traps and nanofilters we saw in section 2.1 have also been integrated into a continuous separation format in the so-called anisotropic nanofilter array (ANA) [108, 109, 124] illustrated in Fig. 2.11. This device works by superimposing two perpendicular electric fields, using the current injection method to create the electric fields [119]. One field drives the DNA through a deep channel while the other field drives it towards a parallel deep channel. Separating the two deep channels is a narrow space that constitutes the entropic trap or nanofilter. As was the case in the batch devices we discussed in section 2.1, the probability of the DNA crossing through the thin gap depends on the size of the DNA, which leads to different sized fragments traveling at different angles [108]. If the thin slits act as entropic traps [40–43], then the larger DNA are most likely to cross through the trap and have a larger deflection angle. Conversely, if the thin slits act as nanofilters [44, 45], then the smaller DNA have a higher hopping frequency and thus a larger deflection angle.

There are two generic ways to create the anisotropic nanofilter array. Recall from section 2.1 that the entropic traps and nanofilters were originally fabricated using two

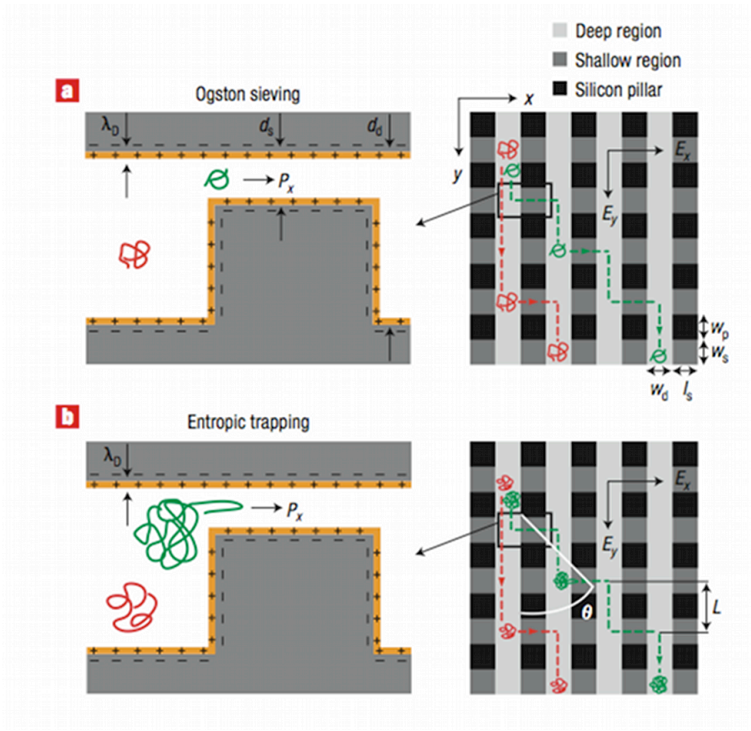

Figure 2.11: Schematic illustration of the anisotropic nanofilter array (ANA). (a) For the Ogston sieving regime, where the radius of gyration is smaller than the gap, the smaller molecule has a higher rate of crossing the gap. (b) For the entropic trapping regime, where the radius of gyration is larger than the gap, the larger molecule has a higher rate of crossing the gap. This image is for the planar ANA device, but the same idea holds for the vertical device. Adapted from Ref. [108].

etch steps to create a multiple-depth device, with the narrow slit having a thickness in the tens of nanometer range. In the planar device ANA device, the same strategy is employed in the continuous separation device, where the distance between the etched silicon and the glass ceiling creates the thin slit [108]. It is also possible to create an array of high aspect ratio pillars that span the channel height with very narrow gaps between them, where the gap between the pillars creates the thin slit (which is now turned on its side) [109]. The latter vertical device is much harder to fabricate, since it requires making highly anisotropic etches and backfilling to produce the narrow gap

[109]. However, the vertical device has a much higher throughput, 1000 nl/h [109], when compared to the 1 nl/h throughput for the planar device [108]. While the two devices have not been directly compared, the separation mechanisms are the same so their performance should be very similar, aside from the increased throughput for the vertical device. In applications, one should carefully consider the balance between throughput and cost of the fabrication.

The devices described so far (DNA prism and ANA) are continuous versions of the post arrays and entropic traps we saw in previous sections. Let us now consider ratchet methods, which permit continuous separations of DNA without using any of the physical principles seen in other batch microfluidic devices. We will focus our attention on ratchet systems rather than the emerging methods using deterministic lateral displacement [117], which seem to have found their niche in the separation of colloidal particles and cells [125–127] rather than their limited applications to DNA [117]. Brownian ratchets have a rich history in physics [128]. The idea behind a Brownian ratchet is to "rectify" the random Brownian motion in order to achieve directional transport. The rectification requires doing work on the particles, which for DNA usually occurs in the form of an electric field. There are two different ways to rectify the motion — a flashing ratchet, where the electric field changes in time, and a Brownian ratchet, where the geometry of the device produces the separation under a constant electric field.

The flashing ratchet [129] has been used to separate DNA by size [111, 113, 114]. In a flashing ratchet, an asymmetric potential field turns on and off periodically. When the potential is on, the DNA are localized at the minima of the potential field. When the field is turned off, the DNA travel randomly under Brownian motion. The typical choice of potential is a sawtooth. Since the potential is asymmetric in space, it is more likely that the DNA will diffuse to the "short" side of the sawtooth rather than the "long" side in the absence of the field. Thus, when the potential field turns back on,

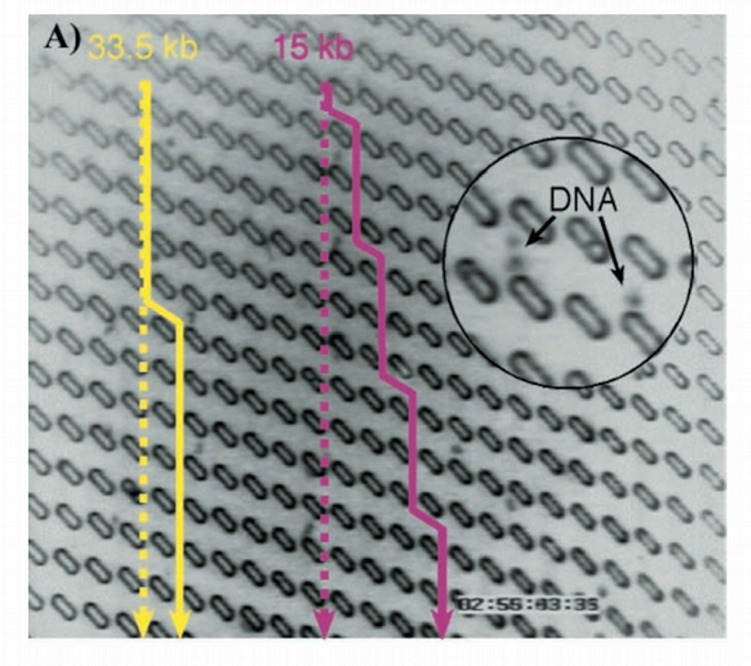

Figure 2.12: A image of the Brownian ratchet. For the molecule to travel from the gap it is in to the adjacent gap to the right, it needs to move from the gap to the start of the next tilted obstacle, about 1.5 μm. To move to the left gap the molecule needs to travel the entire distance of the obstacle, about 5 μm, or be shunted back to the gap it started at by the obstacle. It also has less time to diffuse left before colliding with the obstacle. Practically, no molecules travel to the left. Reproduced from Ref. [112].

the random motion is rectified into directional motion as the DNA fall into the local minima of the sawtooth potential field. In the context of DNA, the flashing sawtooth potential was created [111,113,114] using an interdigitated electrode array. As predicted by theory [129], the DNA travel up the array in a size dependent manner that depends on the frequency and duration of the on/off pulses [111, 113, 114].

It is sometimes preferable to try to use a passive post array over interdigitated electrodes, since the passive system simplifies the device operation. Theoretical analysis [130, 131] suggested that an array of obstacles tilted with respect to the electric field can separate DNA by size in a continuous manner. The experimental realization [112] of this

idea appears in Fig. 2.12. (Note that a similar principle was also realized using charged lipids moving in a patterned lipid bilayer [110].) The obstacles are arranged in such a way so that, as the DNA moves downward through the array, the diffusion path to the next channel on the right is shorter than to the left. Smaller molecules diffuse much quicker than larger molecules, so the smaller molecules are more likely to travel to the right, while the larger DNA molecules tend to travel in the field direction, as shown in Fig. 2.12. There are some questionable assumptions in the original theories [130, 131], in particular related to the neglect of the curved field lines caused by the insulating obstacles [50, 132, 133]. However, as the results for the optimized ratchet device in Fig. 2.9 show, one can certainly separate DNA by size using a Brownian ratchet.

The progress from the prototype in Fig. 2.12 to the optimal result in Fig. 2.9 was an interesting one, so it is worthwhile to recount the key steps along the way. The first device was a large array of asymmetric obstacles set at 45° from the applied field, created to test a theoretical idea that DNA molecules could be separated based on their size dependent diffusion [112]. Single molecule experiments [112], shown in Fig. 2.12, demonstrated that different sized molecules travelled at different angles. However, the original device [112] was not used for a separation since it was incapable of injecting a thin steam of the DNA [112]. The next step taken to improve the device was to add an injection port [115]. This second generation device featured a laser micromachined hole in the back of the device, usually 10-30 μm in diameter, that now allowed the device to be used for separations [115]. While the latter experiments did show that the separations occurred in the expected range [130] for the electric field strength, they revealed that the models [130,131] of the process did not accurately capture the separation due to the deflection of the electric field lines by the insulating obstacles and the finite size of the DNA. Realizing the optimal separations [106] required tilting the obstacles 18.4° from horizontal and tilting the entire array away from the vertical [116]. This second change

led to a smaller distance between the center of a channel and the distance needed to diffuse in order to be in the next channel, allowing for faster separations and ultimately producing the results seen in Fig. 2.9 [106].

Chapter 3

Ratchet Nanofiltration of DNA

This chapter is based on the publication:

J. D. P. Thomas, M. N. Joswiak, D. W. Olson, S.-G. Park, and K. D. Dorfman

Lab on a Chip, **13**, 3741 (2013).

3.1 Introduction

The DNA nanofilter [44], seen in Fig. 3.1, is one of a bevy of microfabricated devices used to enhance DNA separations or study the basic physics of DNA electrophoresis [4, 50]. Under a constant electric field, this device separates short DNA (less than approximately 1000 base pairs, bp) as a function of molecular weight. If the time scale for electrophoresis is slow compared to diffusion, the resulting near-equilibrium separation is analogous to standard chromatography [45]. Due to excluded volume interactions in the slit, the partition coefficient between the slit and the well is a function of the molecular weight of the DNA [55]. The shorter DNA have more degrees of freedom in the slit, whereupon they elute from the device first [44–46, 108, 134, 135]. Under a strong dc electric field, the physics of the DNA motion are less well understood [47, 56].

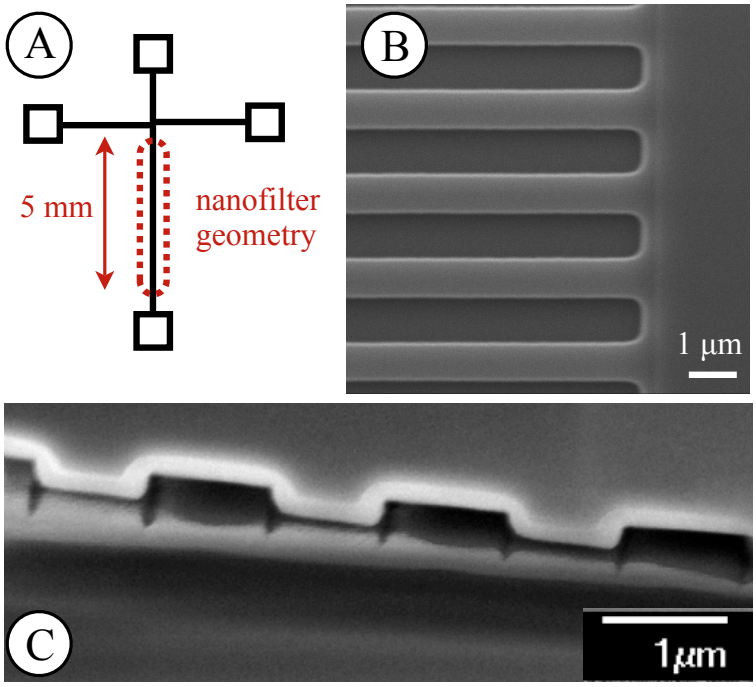

Figure 3.1: (A) Schematic of the shifted-T channel geometry including the 5 mm separation arm containing the nanofilter geometry. Voltages are applied via platinum electrodes in the reservoirs to control the electric fields. (B) Top-down scanning electron microscope image of the wells and slits comprising the nanofilter. The slit and well length are 1 μm and the DNA travels, on average, from the top to bottom in this figure. (C) A scanning electron microscope image of the cross section of the device. The top layer is the silicon, with the white film being the silicon dioxide layer. The bottom layer is the glass.

Importantly, for any constant value of the electric field, all of the DNA molecules move from the inlet to the outlet of the device. As a result, a nanofilter operating under a constant electric field does not actually filter the DNA in the conventional sense. Rather, it serves as a medium for separating the DNA as a function of their size.

We show here that, as predicted by theory [136, 137], the electric field in the nanofilter device can be tuned to operate as a temporal asymmetry ratchet [137] that only

allows those DNA smaller than a critical molecular weight to reach the end of the device. In doing so, we expand the practical functionality of the slit-well motif [50] from separations to actual filtration. Since the ratchet nanofilter described here provides a molecular weight cut-off without clogging like a traditional filter, it should become a useful component of the microfluidics toolbox. In addition to demonstrating experimentally the principle of ratchet nanofiltration, we also show that a temporal asymmetry ratchet that permits all of the DNA to elute from the device can enhance their separation when compared to a constant electric field separation.

3.2 Theory

Let us first recall the relevant theory for a temporal asymmetry ratchet [136, 137]. Denote the electrophoretic velocity of a DNA molecule of N base pairs by $v(N, E)$, where E is the magnitude of the electric field resulting from an imposed potential drop across the nanofilter. It will prove convenient to also define an electrophoretic mobility, $\mu \equiv v/E$. For a time t_1, we apply an electric field of strength E_1 from bottom-to-top in Fig. 3.1, such that the negatively charged DNA move from top-to-bottom. Subsequently, for a time t_2 we apply an electric field $E_2 \neq E_1$ from top-to-bottom. In both cases $i = (1, 2)$, the time is chosen such that the distance travelled by the DNA under the given electric field E_i is long compared to the nanofilter pitch. As a result, the corresponding velocity $v_i(N, E_i)$ is approximately the average velocity of the DNA under a constant electric field, ignoring the brief transience in the velocity when the electric field changes direction and magnitude. The net velocity of the DNA of size N from top-to-bottom in Fig. 3.1 is then

$$v_{net}(N) = \frac{v_1(N, E_1)t_1 - v_2(N, E_2)t_2}{(t_1 + t_2)} \ . \tag{3.1}$$

If the velocity is a linear function of the electric field, $v = \mu(N)E$, as is the case

for Ogston sieving in gel electrophoresis [13], then all of the DNA should move in the direction of the time-averaged electric field,

$$v_{net}(N) = \mu(N)\frac{(E_1 t_1 - E_2 t_2)}{(t_1 + t_2)} \ , \tag{3.2}$$

albeit at different speeds. However, if the velocity is a nonlinear function of electric field, Equation 3.1 allows for the possibility that DNA of different sizes may move in different directions. It is known from prior experimental work [45] that the DNA electrophoretic mobility in the nanofilter geometry is indeed a nonlinear function of the electric field, and that this function depends on molecular weight.

To achieve filtration in the conventional sense, where the smaller DNA pass through the filter and the larger DNA are retained, it is not sufficient to simply have a mobility $\mu = \mu(N, E)$ that depends on both the size of the DNA and the electric field. We also need be able to select values of E_i and t_i such that there exists a critical molecular weight N^* where $v_{net}(N < N^*) > 0$ and $v_{net}(N > N^*) < 0$. The requisite conditions for E_i and t_i are not always readily apparent, but they can be determined if we know the functional form of $\mu(N, E)$ under a steady electric field. For example, Tessier and Slater [137] found one such condition via simulations of DNA electrophoresis in the entropic trap array [42], which is a slit-well motif for separating long DNA. In the present circumstances, the semi-phenomenological model [45] used to describe DNA electrophoresis in the nanofilter array permits many monotonically decreasing functions of $v_{net}(N)$ for given values for E_i and t_i. To achieve filtration, we need to select one such set of values of for E_i and t_i such that the monotonic function $v_{net}(N)$ passes through zero at the desired value N^*.

In many cases of interest, the particular DNA in the mixture may not contain any species where $N \approx N^*$. In these circumstances, no DNA are entrained inside the filter; long DNA that enter the array are shuttled back to the inlet while the shorter DNA are allowed to pass through to the outlet. Even if the mixture contains a species with zero

net velocity under the temporal asymmetry ratchet, this species can easily be removed by applying a backward pulse after recovering the eluted products. As a result, a ratchet nanofilter performance does not decrease due to clogging, as is the case in traditional filtration.

3.3 Methods

We used projection photolithography and reactive ion etching to build the nanofilter device. We first spin-coated a 700 nm layer of SPR995-CM photoresist (Rohm and Haas) on a four-inch silicon wafer. This photoresist layer was exposed on a projection lithography stepper (Canon FPA 2500 i3) using a photomask that contains the fluid reservoirs and connecting channels (Fig. 3.1A), which have a width of 30 μm. After developing, we used a deep trench etching process (Plasma-Therm SLR 770) to etch the exposed portions of the wafer to a depth of 60 nm, as measured by profilometry. We then spin-coated a new layer of photoresist on the etched wafer and aligned a second mask to the features on the etched wafer. This second mask was identical to the first photomask except that it had 1 μm long stripes in the nanofilter geometry region that prevented exposure of the slit portion during photolithography. After exposure and development, we etched all exposed areas of the wafer to a depth of 320 nm, again confirmed by confocal microscopy and surface profilometry. The device then was cleaned using oxygen plasma followed by a piranha bath. We then deposited a 100 nm layer of low stress nitride on the whole wafer using low pressure chemical vapor deposition. We removed the nitride layer on the fluid reservoir portions of the device, and then used potassium hydroxide at 90°C for 6 hours to etch the reservoirs through the wafer. We immersed the wafer in phosphoric acid at 160°C for 12 hours to remove the nitride layer, and then grew a 200 nm oxide layer over the whole device in an oxygen environment at 1100°C for 2 hours. The dimensions of the device were then confirmed using confocal

and scanning electron microscopy. The images in Fig. 3.1 are all after the oxide layer has been added. A scanning electron microscope image of the final slit-well geometry is shown in Fig. 3.1B and a cross-section of the device is shown in Fig. 3.1C. After characterization, we anodically bonded (Karl Suss SB6) the oxidized silicon device to a 500 μm thick borofloat glass wafer and cut the device out of the wafer using a wafer saw (Disco DAD 2H/6T).

For the electrophoresis experiments, we filled the device with 5x TBE buffer (Sigma) at pH 8.1, supplemented with 0.07% (w/v) ascorbic acid, 0.07% (w/v) 40 kDa polyvinyl pyrrolidine, and 3% (v/v) β-mercaptoethanol (all from Sigma). Platinum electrodes attached to a high voltage power supply (LabSmith HVS-1500) fixed the electric potential at each fluid reservoir. We calculated the electric field in the nanofilter using Kirchoff's laws based on the fixed electric potential in each of the reservoirs, assuming the resistance of a given part of the device of length L is $R = \sigma L/A$, where A is the cross-sectional area available for ionic conduction and the resistivity σ is independent of position. For the slit-well portion of the device, we computed the resistance of this arm as resistors in series.

The device was mounted on a programmable stage and intensity data were collected from a photomultiplier tube (Hamamatsu H7422-04) mounted on an inverted microscope (Leica DMI-4000). During the experiments, the 40x microscope objective scanned the 5 mm nanofilter region of the device at a speed of 2.5 mm/s every 20 seconds and the data were collected at 1 kHz, resulting in a measure of intensity versus the position in the nanofilter.

The experimental data presented here used PCR marker dsDNA (New England Biolabs) with 5 fragments at 50, 150, 300, 500, and 766 bp with approximate weight percentages of 30%, 20%, 16%, 13%, and 21% respectively, dyed with YOYO-1 (Molecular Probes) at a dye ratio of 1 dye molecule per 5 base pairs of DNA. PCR marker

at 250 μg/mL was loaded into one of the side reservoirs while buffer was loaded to the other three reservoirs. DNA was loaded and injected into the nanofilter geometry using a standard shifted-T protocol [138].

3.4 Results and Discussion

To calibrate the ratchet, we first measured the electrophoretic mobilities in one of our devices under the constant electric fields $E_1 = 20$ V/cm and $E_2 = 37$ V/cm, as reported in Table 3.1. The elution order was confirmed by integrating deconvolved Gaussian fits to the electropherogram for baseline resolved data and comparing to the relative areas under each peak to the concentrations of the mixture provided by New England Biolabs. Note that the ratchet can operate at many different electric field combinations, which we will explore shortly. Overall, we found that this particular device led to separations as a function of molecular weight for constant electric fields of around 15 V/cm to 40 V/cm. We then needed to select ratchet times t_1 and t_2 that lead to the desired cut-off molecular weight N^* from Eq. (3.1). The values of t_1 and t_2 must be large enough

Table 3.1: Calibration data and net velocities for the ratchet experiments in Figs. 3.2 and 3.3. The predicted values are computed from Eq. (3.1) and the experimental values are computed from the electropherograms from the experiment. The calibration data were acquired on the same day as the separation. For the ratchet, the times are $t_1 =$ 30 s and $t_2 = 7$ s.

Molecular Size (bp)	Calibration Velocity (μm/s)		Net Velocity (μm/s)		
	20 V/cm	37V/cm	Eq. (3.1)	Fig. 3.2	Fig. 3.3
50	14.1	28.6	6.03	4.57	5.48
150	7.45	26.7	0.99	2.66	2.30
300	5.46	24.1	-0.14	1.11	0.28
500	3.25	23.8	-1.86	-0.64	-1.18
766	2.11	22.9	-2.61	-1.80	-2.15

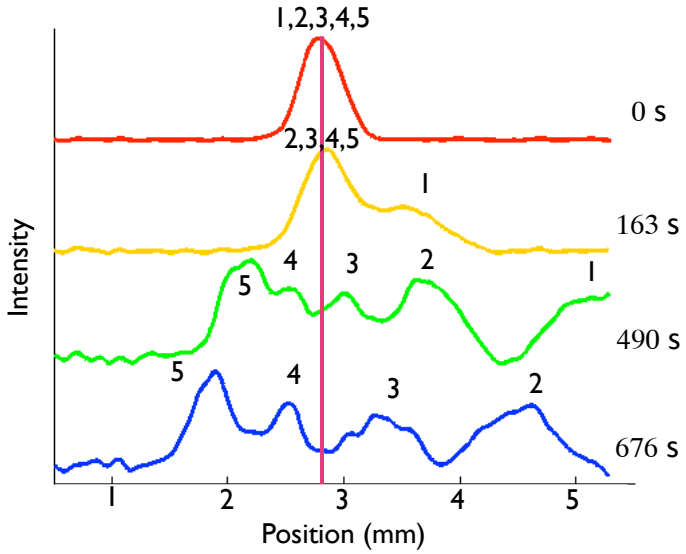

Figure 3.2: Ratchet nanofiltration using the calibration data in Table 3.1. The DNA were injected at 80 V/cm. The forward field $E_1 = 20$ V/cm was applied for $t_1 = 30$ s and the reverse field $E_2 = 37$ V/cm was applied for $t_2 = 7$ s. The numbers above the peaks represent the different sized DNA in the mixture to identify peaks; 1, 2, 3, 4, and 5 represent the 50, 150, 300, 500, and 766 bp fragments respectively.

that the DNA molecules are able to travel across several slit-well periods during each cycle of the ratchet. This is not a very difficult criterion to satisfy, making the pulse times very useful degrees of freedom in the ratchet design. For these first experiments, we arbitrarily chose $t_1 = 30$ s and calculated v_{net} as a function of t_2 for each DNA size according to Eq. (3.1), using the measured $v_i(N, E_i)$ values in Table 3.1. For $t_2 = 7$ s, the predictions in Table 3.1 suggest that 150 bp $< N^* <$ 300 bp, whereupon the two smaller DNA peaks should move towards the exit and the three larger DNA peaks should move back towards the entrance.

Immediately after calibration, we ran the device in ratchet mode using the parameters discussed above and seen in Table 3.1. The initial injection was performed under a strong electric field of 80 V/cm, which leads to no separation and allows us to place

the DNA mixture in the center of the device. We denote the time $t = 0$ as the end of the injection and the start of the ratcheting procedure. The result is seen in Fig. 3.2, the application of the temporal asymmetry ratchet lead to bi-directional motion of the DNA thus creating a non-clogging filter. As seen in Table 3.1 the resulting velocities are reasonably close to the predictions as well.

Using the same ratcheting parameters as in Fig. 3.2, we demonstrated filtration from a partially separated mixture, as seen in Fig. 3.3. In these experiments, we injected the plug at a lower electric field, 37 V/cm, so that by the time the DNA mixture reached the center of the array the 50 bp fragment had already separated from the rest of the mixture. As seen in Table 3.1, the experimental velocities are still in relatively good agreement with the predictions. This second experiment with the same ratcheting protocol shows that sharp injections are not necessary for ratchet nanofiltration. This attractive feature contrasts with the stringent requirements for conventional analytical separations in the nanofilter geometry [44], where the injection plug width can be a substantial source of band broadening.

In addition to filtration, we were also able to show that a reverse pulse actually enhances the separation when compared to a constant forward electric field. For these experiments, we used a ratchet with $E_1 = 20$ V/cm and $E_2 = 37$ V/cm and times $t_1 = 60$ s and $t_2 = 5$ s. In this case, using the calibration data in Table 3.1, Eq. (3.1) predicts that all the DNA fragments have positive net velocities. Figure 3.4 compares the electropherograms obtained from the ratchet separation (a) to a separation obtained under a constant dc field of 20 V/cm (b). In both cases, the peaks are resolved but the ratchet protocol, which includes the reverse pulses at a strong field, resolved all five species more quickly and used less of the array. As seen in Fig. 3.4, the ratchet achieved easily resolved peaks for all five species after about 200 s using only 3 mm of the 5 mm array. In contrast, the constant field separation required well over 400 s to visibly

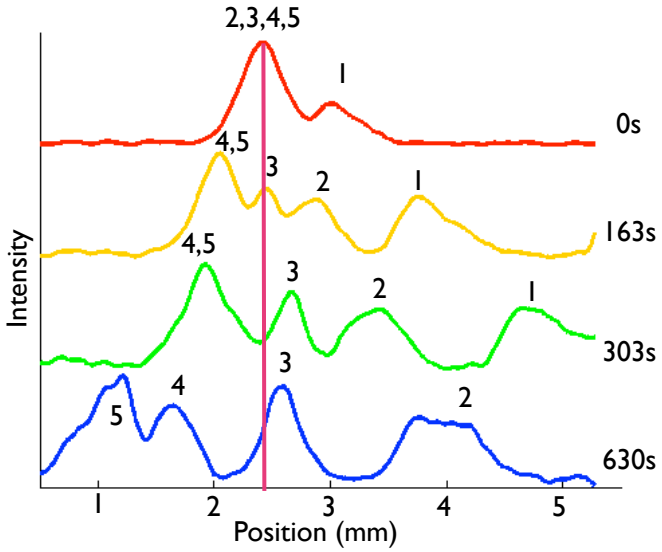

Figure 3.3: Using the ratchet to filter a partially separated plug. The DNA were injected at 37 V/cm, which led to some separation before the plug reached the center of the array. After time t = 0, the forward field $E_1 = 20$ V/cm was applied for $t_1 = 30$ s and the reverse field $E_2 = 37$ V/cm was applied for $t_2 = 7$ s. The numbers above the peaks represent the different sized DNA in the mixture to identify peaks; 1, 2, 3, 4, and 5 represent the 50, 150, 300, 500, and 766 bp fragments respectively.

resolve all five species. This would allow the pulsed field separation to occur in smaller devices, while keeping a similar separation time. Moreover, by the time the 4th and 5th peaks were resolved in the constant field separation, the 1st peak had already left the device and we were not able to see all five peaks within the device.

Note that the enhanced separation time seen in Fig. 3.4a is only visible for the scanning detection mode, where we obtain the fluorescence intensity as a function of position in the device at fixed times. While the ratchet results in faster separations, it takes longer for the all the fragments to reach the end of the device due to the ratcheting mechanism. Using finish line detection scheme with a fixed detection window, the ratchet could be used in a shorter separation array than a DC field separation.

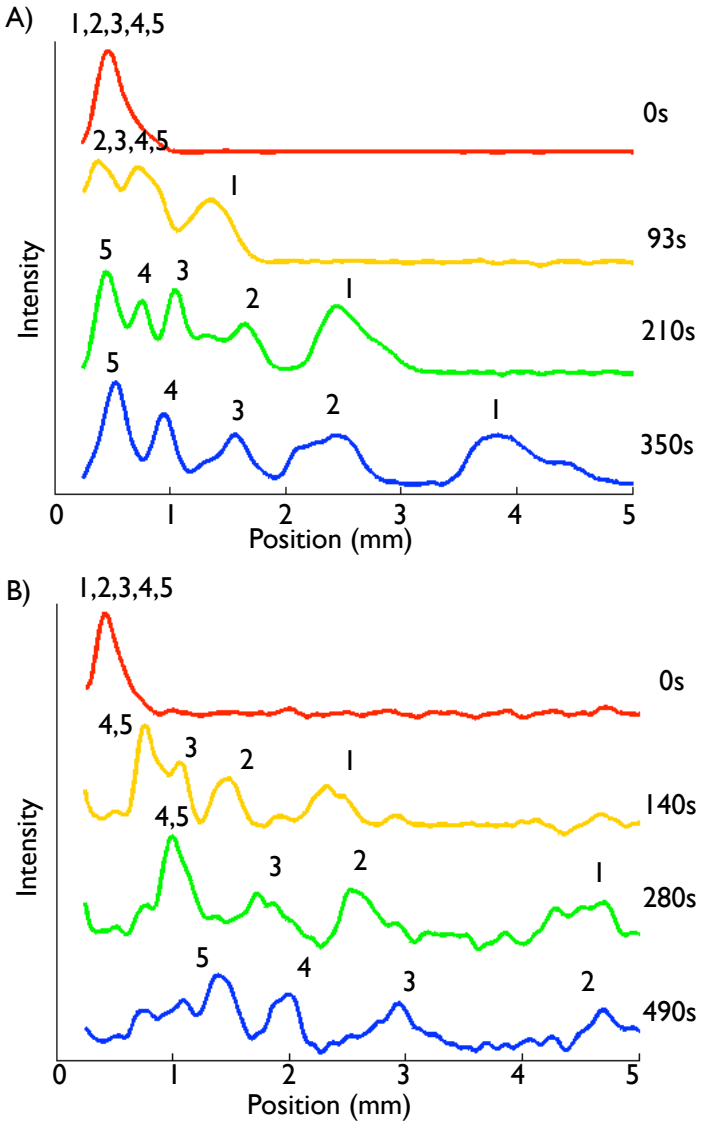

Figure 3.4: Comparison between (A) the ratchet protocol with all species moving forward and (B) a constant field separation with E = 20 V/cm. For the ratchet separation, the forward field E_1 = 20 V/cm was applied for t_1 =60s and the reverse field E_2 = 37V/cm was applied for t_2 =5s. The numbers above the peaks represent the different sized DNA in the mixture to identify peaks; 1, 2, 3, 4, and 5 represent the 50, 150, 300, 500, and 766 bp fragments respectively.

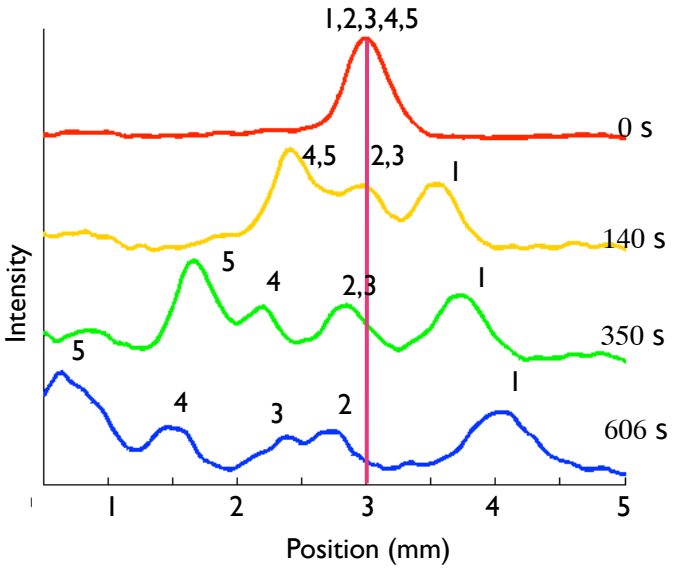

Figure 3.5: Ratchet nanofiltration using the calibration data in Table 3.2. The DNA were injected at 80 V/cm. The forward field $E_1 = 12$ V/cm was applied for $t_1 = 17$ s and the reverse field $E_2 = 25$ V/cm was applied for $t_2 = 6$ s. The numbers above the peaks represent the different sized DNA in the mixture to identify peaks; 1, 2, 3, 4, and 5 represent the 50, 150, 300, 500, and 766 bp fragments respectively

Ideally, we would like to calibrate a given nanofilter device and then use this device for numerous ratchet nanofiltration experiments over several days or even weeks. To test out this desirable approach, we made a new chip and calibrated the velocities in this second nanofilter array. For this chip we found that the optimum electric fields were $E_1 = 12$ V/cm and $E_2 = 25$ V/cm with the times of $t_1 = 17$ s and $t_2 = 6$ s. As seen in Table 3.2, this lead to the prediction that 300 bp $< N^* <$ 500 bp, whereupon the three smaller DNA peaks should move towards the exit and the two larger DNA peaks should move back towards the entrance.

To test the longevity of the calibration we operated the nanofilter using this ratchet protocol and chip on a subsequent day. The initial injection was performed under a strong electric field of 80 V/cm, which leads to no separation, a fairly narrow injection

band, and allows us to place the DNA in the center of the device. We denote the time $t = 0$ as the end of the injection and the start of the racheting procedure. It is clear from Fig. 3.5 that the repetitive application of the temporal asymmetry ratchet indeed leads to filtration, with the 50 bp fragment moving towards the exit of the device and the remaining species being rejected from the nanofilter. The scan after 606 s of the ratchet in Fig. 3.5 shows the 50 bp DNA about to enter the waste reservoir. Unfortunately, as we see in Table 3.2, the theory given by Eq. (3.1) predicts that the 150 bp and 300 bp fragment should also move towards the exit of the device, albeit at a relatively slow speed.

In principle, the calibration data in Table 3.2 should be sufficient to design a temporal asymmetry ratchet with a desired cut-off molecular weight N^*. In practice, although the relative mobilities are reproducible, the absolute mobilities fluctuate from day-to-day due to variations in the surface coating, buffer pH, reservoir pressures, and other uncontrollable experimental parameters [73]. For a ratchet nanofilter, shifts in the absolute mobility can lead to changes in the direction of the net velocity for a given DNA molecule, which then leads to an undesirable shift in the cut-off molecular weight N^*.

Table 3.2: Calibration data and net velocities for the ratchet experiments in Fig. 3.5. The predicted values are computed from Eq. (3.1) and the experimental values are computed from the electropherograms from the experiment. The calibration data were acquired on a different day than the separations

Molecular Size (bp)	Calibration Velocity (μm/s)		Net Velocity (μm/s)	
	12 V/cm	25V/cm	Eq. (3.1)	Fig. 3.5
50	15.0	30.9	3.78	1.11
150	10.6	28.9	0.94	-0.49
300	8.62	25.7	0.24	-1.02
500	6.56	25.7	-1.31	-2.36
766	4.35	25.7	-2.98	-3.92

To circumvent these problems with the absolute mobility fluctuations between experiments, one can calibrate the device immediately before running the ratchet. In this approach, one first quickly obtains the electrophoretic mobilities at E_1 and E_2 from two separation experiments, flushes the test DNA to the outlet, and then immediately initiates the ratchet nanofiltration with a fresh injection. In practice, the calibration procedure can be decoupled from the ratchet nanofiltration by employing two exit reservoirs; the analytes from the calibration step would be eluted to the first exit and the filtered analytes would be eluted to the second exit.

3.5 Conclusions

In the current contribution, we have shown how the slit-well motif can be combined with a temporal asymmetry ratchet to achieve filtration of DNA. The key to the operation of the device [136, 137] is that under a constant, unidirectional electric field, rod-like DNA exhibit a size dependent electrophoretic mobility that is non-linear with respect to the applied electric field [45]. By switching the duration, direction, and magnitude of the applied electric field, we are able to tune the direction of the DNA motion based on the size of the DNA molecule. The asymmetry in the applied electric fields allows operation of the device as a clog-free, tunable filter where only DNA smaller than N^* are eluted. We also showed that a brief backward pulse can enhance conventional analytical separations as a function of molecular weight.

The ratchet experiment described here required the injection of a group of DNA into the nanofilter geometry before applying the temporal asymmetry ratchet. True filter operation could be accomplished by applying the ratchet to the entirety of the loaded DNA sample using a two-reservoir design. In the portion of the microfluidic channel devoid of the slit-well geometry, all DNA sizes move away from the loading reservoir and toward the nanofilter during application of the ratchet. In the slit-well geometry,

DNA with size greater than N^* are rejected from the nanofilter while DNA smaller than N^* pass through the nanofilter. The data presented here shows that the direction of transport in the nanofilter depends on DNA size, and thus the nanofilter geometry can be operated as a true filter.

As a microfluidic device, the throughput of the nanofilter is naturally limited by the small volume of fluid it handles. While the width of the slits is limited by the mechanical stability of the material [139], the process is trivial to parallelize by creating multiple channels separated by thin walls. However, it is unlikely that a ratchet nanofilter will replace gel electrophoresis for purifying larger quantities of DNA. Rather, we envision that this nanofilter geometry can be used as an in-line filtration step in integrated lab-on-a-chip type devices designed to perform multiple manipulation steps on a small (and often precious) sample. It could purify DNA following PCR of a cell lysate, or only allow desired DNA molecular weights through to the rest of the device for further processing [36]. Processes upstream in a device would likely not need large amounts of analyte so the lower throughput of this device would not be an issue. This filter should work in continuous mode, so a concentrator upstream can be used if higher amounts of analyte are needed.

Chapter 4

Tilted Post Arrays

4.1 Introduction

Hexagonal post arrays are one microfluidic method for rapidly separating long DNA, typically tens to hundreds of kilobase pairs (kbp) [4,50]. Agarose gel electrophoresis can only separate these long fragments using pulsed electric fields [13]. Unfortunately, due to the slow migration of long DNA in the net direction of the applied field, pulsed field separations take hours to days to achieve a baseline separation [13]; this time is compared to minutes needed to separate long DNA in post arrays [66,78,79]. Regular arrays of micro- and nano-sized posts, fabricated by semiconductor methods, have been the subject of substantial experimental work [65–75,84,85,87] using a wide variety of materials, post sizes, and post spacing. In addition to microfabricated arrays with perfectly ordered features, results also exist for self-assembled magnetic beads [78–80], which form quasi-hexagonal arrays, microfabricated arrays with intentional disorder [76], and nanowire-based posts [81, 82]. Given the extensive experimental work on DNA electrophoresis in post arrays, let alone the corresponding efforts using computer simulation [50], it would seem that further work in this area would lead to merely incremental

advances in the device performance. In the present contribution, we argue otherwise by exploiting the orientation of the electric field with respect to the lattice vectors of the array [77], i.e., DNA electrophoresis in a "tilted" post array. This previously underutilized design parameter leads to a substantial improvement in separation resolution and time compared to conventional hexagonal post arrays without introducing any complicated nanofabrication methods [66, 84].

Our interest in the orientation of the electric field with respect to the lattice vectors characterizing the two dimensional, crystalline array arises from the deleterious effect of "channeling" during DNA electrophoresis in a post array, a concept first identified in two-dimensional Brownian dynamics simulations by Patel and Shaqfeh [97]. Figure 4.1 illustrates the basic idea behind the channeling effect. When the DNA disengages from a collision with the post, its center-of-mass is slightly to the side of the post. If the electric field is applied along the low porosity lattice vector (Fig. 4.1A) or the high porosity lattice vector (Fig. 4.1C) of a hexagonal array, which are the standard approaches in experiments, the DNA will travel through these channels at its free solution mobility until it collides with another post. When the electric field strength is high, which is desirable for fast separations, the DNA can spend the majority of their time inside the channels. The mobility of the DNA in the array thus approaches the free solution mobility, which is independent of molecular weight, and the separation is lost.

The channeling effect was explored more deeply by Mohan and Doyle [98, 99], using three-dimensional Brownian dynamics simulations, and their simulation results suggested that post arrays with regularly spaced patterns, such as a hexagonal array, would fail to separate long DNA due to the channeling effect. This conclusion was at odds with experimental work demonstrating separations in such arrays [66], and the disagreement between simulation and experiment was ultimately resolved by recognizing that the curved field lines in electrically (and ionically) insulating post arrays break up the

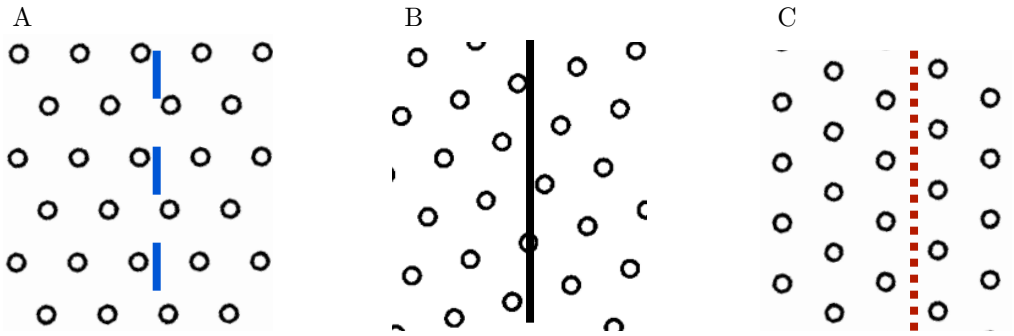

Figure 4.1: Schematic illustration of an electric field applied at (A) 0° tilt, (B) 15° tilt and (C) 30° tilt. The lines illustrate the direction of the applied voltage drop. Only tilt angles between 0° and 30° need to be examined due to the symmetry of hexagonal symmetry, and we have arbitrarily assigned the 0° tilt as the lattice vector corresponding to the low porosity direction.

channeling effect to some extent [72]. The channeling effect described in simulations only dominates when the array is so sparse that the electric field lines are hardly perturbed by the posts [73]. However, since transport across field lines occurs by diffusion, the effects of channeling seem to limit separations in sparse arrays to electric fields in the 10-20 V/cm range [74, 78, 79]. At higher electric fields, the time to diffuse onto a "collision" field line is long compared to convection through the array [73] and the separation fails.

Further improvement in DNA separations in post arrays thus requires a way to remove the channeling effect. One approach to break up the channels is tilting the array, as in Fig. 4.1B, such that the macroscopic voltage drop is no longer coincident with the lattice vectors of the array. Brownian dynamics simulations [77] indicate that tilted arrays should preserve the cyclic rope-over-pulley mechanism [85, 90, 140] underlying the separation without producing the dispersive, multi-post collisions that can occur at higher post densities. Indeed, these simulations [77] indicate that tilting the post array increases the collision probability while leaving the hold-up time unchanged, so

the speed difference between different sized DNA molecules increases upon tilting the array without greatly affecting the dispersion [77]. The model used for these simulations has been well parameterized with post array experiments and has been shown to match single molecule experiments in normal hexagonal post arrays very well [75].

To date, Brownian dynamics simulations [77] are the only evidence supporting the efficacy of tilted post arrays compared to their untilted counterparts. In the present contribution, we test these simulation results by experiments in a post array with a 15° tilt, as illustrated in Fig. 4.1B. Our results confirm that a tilted post array results in an improved separation when compared to the standard hexagonal post array, but we do observe some differences between the optimistic predictions of the Brownian dynamics simulations and our experimental results.

4.2 Materials and methods

We created the tilted post array, consisting of 1 μm diameter posts with a 3 μm center-to-center spacing, using projection photolithography on a 4 inch silicon dioxide coated silicon wafer. The oxide layer was grown by placing the silicon wafer in a 1000°C furnace (Tylan) with an oxygen and hydrogen rich environment (36% oxygen, 64% hydrogen) for 1 hour. This resulted in a silicon dioxide layer of about 370 nm, as measured by ellipsometry. SPR 995 CM 0.7 photoresist (Rohm & Haas) was spun on the wafer at 3000 rpm for 30 seconds then exposed on a Cannon i-line projection lithography system (Cannon FPA 2500 i3) at 155 mJ/cm^2 with a -0.2 μm focus offset. Using the photoresist as an etch mask, the silicon dioxide was etched away using reactive ion etching (Surface Technology Systems 320). The exposed silicon was then etched to a depth of about 4 μm, with the oxide layer serving as the etch mask, using a deep reactive ion etching system (Plasma-Therm SLR 770). Through holes were etched for the reservoirs using a KOH wet etch at 90°C, using the photoresist PSB (ProTEK) as the etch mask. The

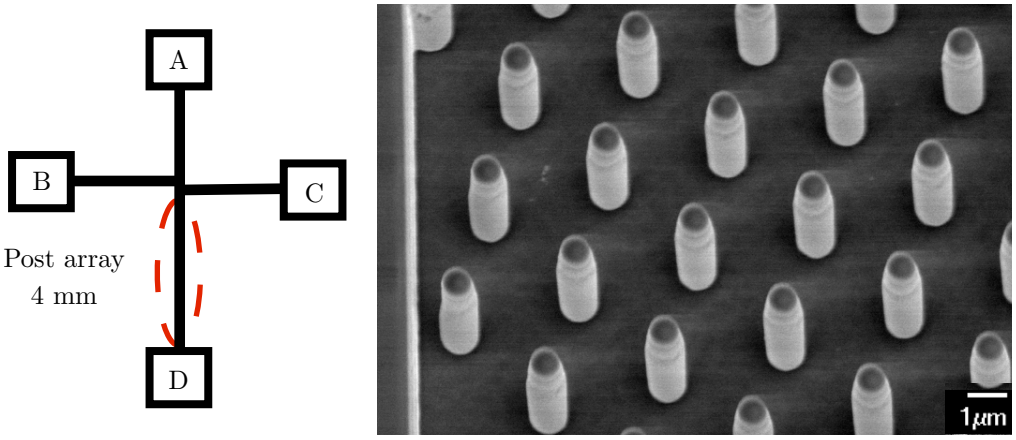

Figure 4.2: A schematic of the overall device and a scanning electron micrograph of the 15° tilted post array separation matrix. The letters in the reservoirs indicate the labeling convention used later. The 4 mm long separation matrix is in the region indicated by the dashed circle.

device was then oxidized for 4 hours at 1100°C in an oxygen rich environment to provide electrical insulation. Finally, the device was sealed with a borosilicate wafer using an anodic bonding process (Karl Suss SB6) and then diced using a wafer saw (Disco), resulting in the final working device in Fig. 4.2.

For the electrophoresis experiments the device was initially filled with ethanol for easy wetting. After initial wetting, the device was soaked overnight in a 1% (w/v) solution of polyvinylpyrrolidone (Sigma) in water. Finally the device was mounted onto the chip holder and filled with a 5x TBE buffer (Sigma) at a pH of 8.1 with 0.07% (w/v) polyvinylpyrrolidone (Sigma) and ascorbic acid (Sigma) and 3% (v/v) β-mercaptoethanol (Sigma). The holder was then placed on an inverted microscope (Leica DMI-4000). Platinum electrodes, inserted into each reservoir, were connected to a high voltage power supply (Labsmith HVS-1500) to control and monitor the potentials in the four reservoirs. Fluorescence intensity data were collected using a photomultiplier tube (Hamamatsu H7422-04), which collected the data though a 40x objective situated at a finish line located 4 mm from the start of the post array. The data were collected

at a rate of 1 kHz. To test the reproducibility of the separation, the experiments were performed over 5 separate days using two different devices; the experiments for days 1 and 2 were performed in one device (chip 1) and the experiment for days 3, 4, and 5 were performed in another device (chip 2).

The DNA used in the experiments was a mixture of λ DNA (New England Biolabs), which is 48.5 kbp, and 20 kbp DNA (Thermo Scientific). The DNA was dyed with YOYO-1 intercalating dye (Life Technologies) at a concentration of 1 dye molecule per 5 bp by staining for 24 hours. The dyed solution was added to the loading reservoir (B in Fig. 4.2). A small plug of DNA was injected into the separation channel using a standard shifted-T injection scheme [138]. If the device was to be used again the next day, the DNA solution in reservoir B was replaced with buffer and the device and holder were wrapped in parafilm so the reservoirs would not dry out. If the device was not going to be used the next day, it was soaked first in 30% hydrogen peroxide to clean out any residue and then the hydrogen peroxide solution was replaced with a 1% solution of polyvinylpyrrolidone (Sigma) in water for storage.

4.3 Results

The natural metric for assessing the quality of the separation is the resolution [141]

$$R = \frac{t_\lambda - t_{20}}{2(\sigma_\lambda + \sigma_{20})}. \tag{4.1}$$

where, for a finish line separation, t_i is the average time for species i to cross the finish line and σ_i^2 is the variance of the peak of species i. The main panel of Figure 4.3 shows representative electropherograms obtained in the 15° tilted post array at 10 V/cm, 30 V/cm and 50 V/cm after 4 mm of separation distance. In all cases, the two peaks are easily resolved; the resolution exceeds 0.7 at 50 V/cm in about 3 minutes, is approximately 1 for 30 V/cm after 5 minutes, and more than 1.5 at 10 V/cm in 15

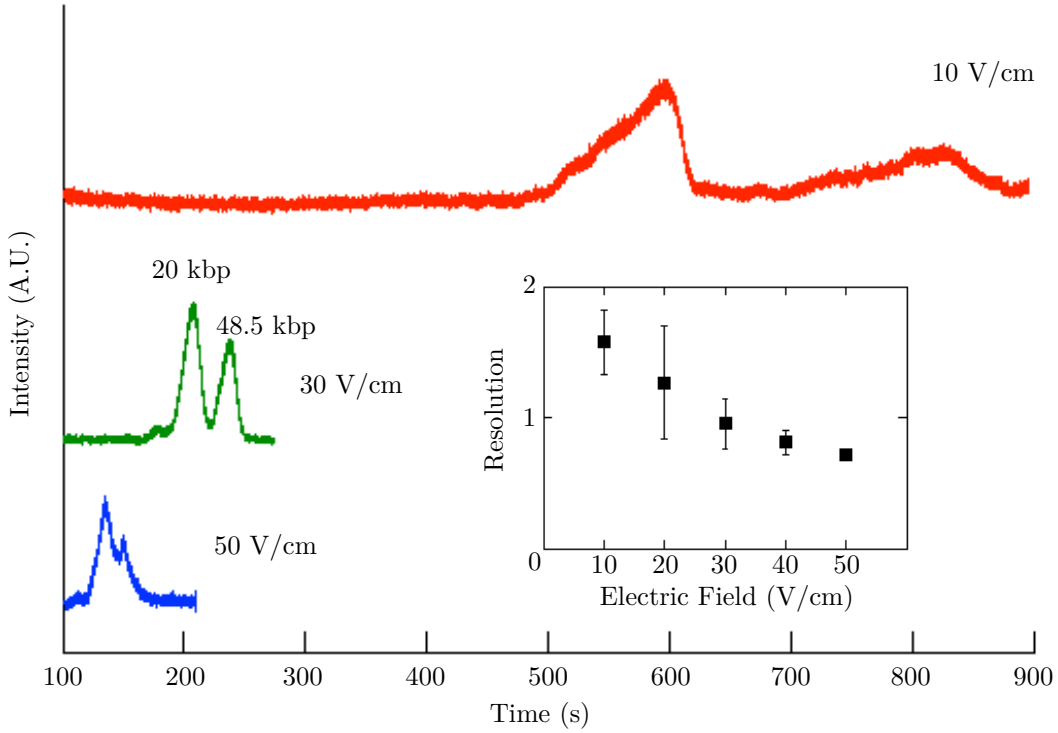

Figure 4.3: Representative electropherograms for 10 V/cm, 30 V/cm and 50 V/cm for 20 kbp and 48.5 kbp DNA with finish line detection at 4 mm inside the array. The peak identities are labeled only for the 30 V/cm electropherogram. The inset presents the resolution as a function of electric field obtained over multiple devices and multiple days.

minutes. The inset of Fig. 4.3 shows the resolution data as a function of electric field obtained over multiple devices and multiple days for electric fields between 10 V/cm and 50 V/cm in 10 V/cm intervals.

In addition to the separation resolution, reproducibility of the separation is also a figure of merit. Figure 4.4 provides a scatter plot of the resolution as a function of the time t_λ for the slower moving peak to reach the detector. The plot contains the data for all of the experiments performed in the tilted array. Interestingly, we found that the separations performed at the higher electric fields led to more reproducible separation

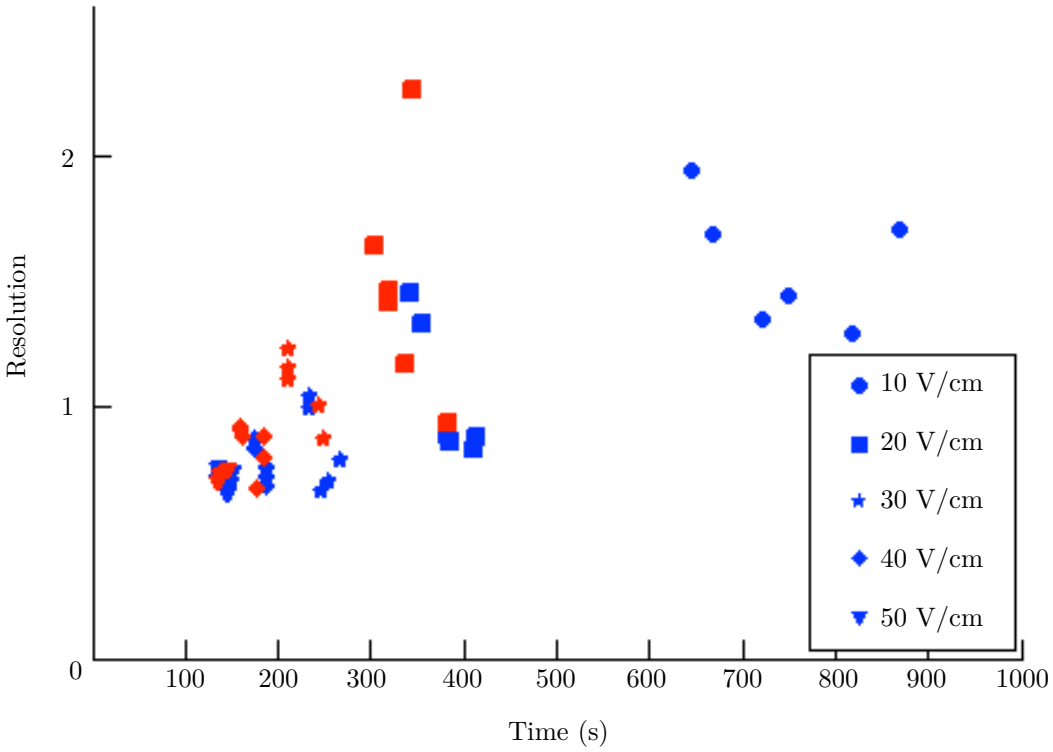

Figure 4.4: Scatter plot of the resolution and time required for the slower λ-DNA peak to reach the detector. The data were collected over 5 days and in two different devices. The red shows the data collected using chip 1 and the blue shows the data collected using chip 2.

resolution and elution time.

We also performed experiments up to 80 V/cm in the devices, but we were not able to fit the peaks for electric fields exceeding 50 V/cm. At electric fields around 130 V/cm the oxide layer suffers electrical break down [43], so our upper bound of 80 V/cm is a conservative estimate to avoid destroying the device. While we did not observe any measurable separation resolution above 50 V/cm, this result does not necessarily preclude the possibility of separating DNA at these higher electric fields in a longer device. However, the separation must eventually fail at a sufficiently high electric field

because the hold-up time of the rope-over-pulley collision is inversely proportional to the electric field strength, E [50, 85, 94]. If we denote $t_h \sim E^{-1}$ as the holdup time and $t_c \sim E^0$ as the time between collisions, the total time for a collisions-translation cycle is $t_c + t_h$. The distance traveled between collisions is $x = \mu_0 E t_c$, where μ_0 is the free solution mobility. This very simplified model leads to the in-array mobility μ of the form [72]

$$\frac{\mu}{\mu_0} = \left(1 + \frac{t_h}{t_c}\right)^{-1} \tag{4.2}$$

Since the quantity $t_h/t_c \to 0$ as the electric field increases, the separation must eventually be lost at a high enough electric field.

4.4 Discussion

4.4.1 Comparison with other post array separations

The separation resolutions and times in Fig. 4.3 compare favorably with prior results using the same post diameter and center-to-center spacing, but the 0° tilt orientation in Fig. 4.1A [74]. Explicitly, the latter experiments [74] used a 12.5 mm separation channel to obtain a separation resolution of 1.22 after 20 minutes at 10 V/cm. Indeed, our results compare favorably to all of the post array separations we could identify that used a similar range of DNA to our 20 kbp and 48.5 kbp mixture. The most closely related separations in the literature are the first experiments performed in a magnetic bead array [78], which required 800 seconds to get a resolution of 1.0 when separating 33.5 kbp and 48.5 kbp. Note that subsequent experiments in the magnetic bead array system [79] improved on the overall separation quality but did not revisit these particular molecular weights.

It is useful to consider how the tilted array compares with other strategies for removing the channeling effect. One idea is to make a random arrangement of posts to

break up the ordering due to the channels [97,98] while maintaining a pattern that can still be produced using typical microfabrication [76]. If the array is sufficiently dilute, then this strategy can increase the frequency of collisions compared to an ordered array of the same density [98]. Unfortunately, once the array density increases to that used for successful separations in micropost arrays (e.g., the post size and center-to-center distance used in our experiments), the DNA will often engage with multiple posts in the denser regions of the system, leading to increased band broadening [76] due to the wide variance in holdup times for such long-lived collisions [93,142]. As a result, it is not surprising that there are no experimental data available for separations in micropatterned, disordered arrays.

A second strategy involves reducing the size of the channels between posts by moving from micron-spaced posts to nano-spaced posts, with a somewhat less dramatic decrease in the post diameter. Increasing the post density requires sophisticated nanopatterning methods [66,68–70,84], which are available for prototyping and somewhat more challenging to implement for mass production. Note that this strategy cannot be extended down to an arbitrarily small gap between the posts; as the post density increases, the transport mechanism will switch eventually from the cyclic rope-over-pulley model [85,90,140] to biased reptation in a tight (artificial) gel [23]. After the cross-over point, the separation will no longer take place as the strong field in a tight gel leads to biased reptation with orientation.

In many cases, such nanopost arrays have been used to separate quite different sizes of DNA at very high rates. For example, the nanopost array of Chan *et al.* [67] obtained a resolution of 0.8 in 121 seconds between 21 kbp DNA and 165 kbp DNA, where the latter molecule is much larger than λ-DNA. Similarly, Yasui *et al.* [143] reported a remarkable 12 second separation of λ-DNA and 1 kbp DNA in a nanopost array, but in this case the smaller DNA contour length is only a few Kuhn lengths. The separations

of binary mixtures of very widely different molecular weights can arise by spanning different migration regimes [50], which makes comparing these very high quality results to separations of narrower molecular weight regimes more challenging. Indeed, referring back to the pioneering work on nanopost arrays [66], it seems from the relative mobility plots (Fig. 5 of Ref. [66]) that the molecular weights we studied here would not be effectively separated in a nanopost array.

It is also interesting to compare our results to the so-called "nanofence" array [87]. The latter device uses a lamellar configuration consisting of two offset rows of small posts (500 nm diameter) that are closely spaced (700 nm center-to-center distance) with a large gap (20 μm) between each of the fences. The operating principle behind the nanofence is that the DNA is forced to collide in each fence, since the spacing between the posts is commensurate with the radius of gyration of the DNA, but the DNA have sufficient time to relax between subsequent collisions. The nanofence thus represents a different way to break up the channels inside an array while preserving the rope-over-pulley separation mechanism. Experiments show that the open region between fences leads to more efficient collisions with the posts than in a hexagonal array [87]. Moreover, Brownian dynamics simulations [144] indicate that lamellar configurations are superior to (untilted) hexagonal arrays of similar post density, and the experimental data [87] are in accord with the simulation result. For the XhoI digest, the nanofence array achieved a resolution of 0.91 in 400 seconds for the 33.5 kbp and 48.5 kbp peaks, which is comparable to the separation in our tilted array of the 20 kbp and 48.5 kbp DNA. The correspondence between the separation resolution in a tilted array and the nanofence array serves to reinforce the general principle that breaking up the channels in the device, while maintaining good collision statistics, is the key to improving separations in post arrays.

Finally, while separation resolution is clearly an important figure of merit, there are

some challenges when comparing resolutions reported in different publications for different devices. The separation resolution arises from a number of factors [141], in particular the width of the injection band, that are independent of the separation mechanism inside the array. For example, recent experiments [145] showed that the separation resolution in a post array is markedly improved using sample-stacking at the inlet to sharpen the initial band. This injection method should, in principle, also improve the separation resolution of our experiments as well. Thus, while separation resolution is clearly the metric of choice for comparing different experiments, making an "apples-to-apples" comparison is not always straightforward. These differences should be kept in mind with respect to our discussion here, especially for the comparison between results from different labs.

4.4.2 Comparison with Brownian dynamics simulations

The key simulation data [77] suggesting that tilted post arrays would lead to improved separations were obtained using different molecular weights (λ and T4 DNA, 169 kbp) with tilt angles at 10° increments from 0° (Fig. 4.1A) to 30° (Fig. 4.1C). Extensive simulation data were obtained for the low porosity, untilted array (0°) and a tilt angle of 20° for a range of electric fields, using a large number of DNA per ensemble and long travel distances to obtain good statistics. Two key results emerged from this study [77]. First, while the separation in the untilted array degraded as the electric field increases, separations should still be obtained at relatively high electric fields in the tilted array. This prediction is already realized in the experimental data in Fig. 4.3, where we observe separations in the tilted array up to 50 V/cm while untilted arrays usually lose resolution in the 10-20 V/cm range [74, 78, 79]. Second, the time to achieve a resolution $R = 1$ in a tilted array should decrease almost exponentially as a function of the electric field, albeit with a relatively small prefactor. This particular mode of analysis, namely fixing

the desired separation resolution and then computing the required time/length for the separation, allows us to remove artifacts due to the finite length of the device; the separation is usually faster but lower resolution as the electric field increases for a device of fixed length, which is what we saw in Fig. 4.3. The idea behind rescaling to a fixed resolution is to evaluate the most important figure of merit (time for the separation) in the context of the constraints imposed by fabrication (the length of the device).

We should also note that the simulation prediction of superior performance in a tilted array [77] motivated us to use a smaller molecular weight difference in our experiments than the simulations, which provides a stringent test of the device performance, while at the same time avoiding some of the challenges of loading very large DNA without breakage [146] (and thus band broadening due to small differences in molecular weight in the sheared DNA). While we have easily separated the 20 kbp and 48.5 kbp molecular weights over a range of electric fields, the particular dependence of the separation performance as a function of field is not readily apparent from the data presented thus far.

In order to test this second prediction from the Brownian dynamics simulations, we need to first recognize that the simulation data correspond to trajectories of individual molecules, and the resolution is thus obtained in the "snapshot" mode at a fixed time using the average velocity and effective diffusion coefficients obtained from these trajectories. In order to compare our finish line resolution data in a 4 mm device to the snapshot data obtained from the simulations as a function of time we need to make two assumptions. For a snapshot detection [4, 141], the separation resolution can be expressed in the alternate form

$$R = \frac{\Delta\mu}{\langle\mu\rangle}\sqrt{\frac{N}{16}} \tag{4.3}$$

where $\Delta\mu$ is the difference between the mobility of the two species, $\langle\mu\rangle$ is the average of their mobilities, and N is the number of theoretical plates. Since the number of

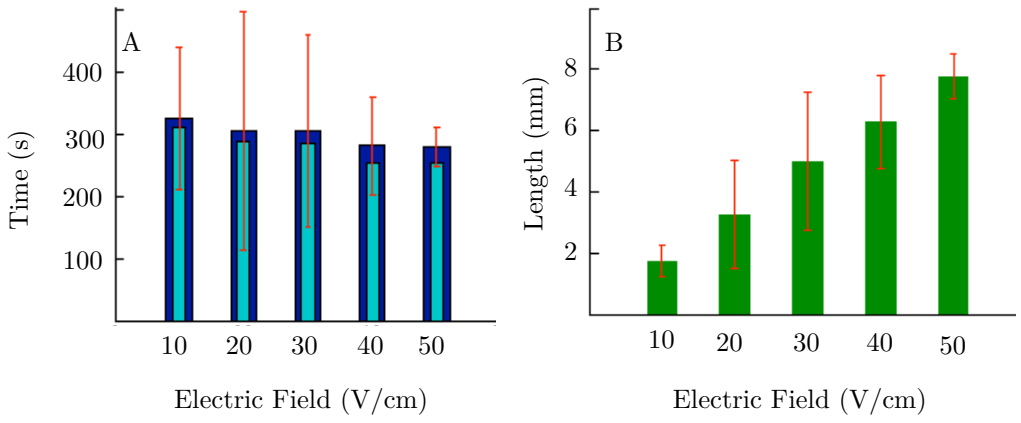

Figure 4.5: Estimates for the time (A) and array length (B) needed to reach a resolution $R = 1$. The projections to $R = 1$ were made for each data point in Fig. 4.3 and the error bars correspond to the standard deviation of this population of estimates. The sub-bars in (A) are estimates that do not include the contribution to the variance due to the injection, corresponding more closely with the simulation methodology. The error bars are excluded from these second estimates for clarity, but they are similar to the error bars for the dark bars.

plates is linear in the length L of the device, we have $R \sim \sqrt{L}$. Moreover, we also know that the elution time is proportional to the size of the device, $t \sim L$. As a result, we can rescale our data in Fig. 4.4 to estimate both the device size and the corresponding time required to reach $R = 1$ if we assume that the snapshot and finish line detection are equivalent. While these scaling relationships are only rigorously true for snapshot detection, they are a reasonable approximation for finish line detection, especially when the residence time in the detector is small [4, 141].

With the latter assumptions in mind, let us now consider the time and device size estimates for achieving a unit resolution in Fig. 4.5. The magnitudes of these quantities for our experiments are larger than the typical simulation values [77] of $t \approx 60$ seconds and $L \approx 1$ mm. The quantitative disagreement is entirely expected; the simulations correspond to an easier separation (molecular weight ratio of 4 versus a ratio of 2 in

the experiments) and a "perfect" separation apparatus with delta function injection and zero detector width. Nevertheless, it is satisfying to see that simulations predict the correct order of magnitude for t and L in the experiments, even if the systems are somewhat different. This concordance further underscores the quality of the simulation model, as evidenced in previous work [75].

While we expect that the device should continue to reach unity resolution at a reasonable length even up to 50 V/cm, we did not observe the exponential decay in the required time as a function of electric field that was seen in simulations [77]. Rather, to within the experimental error, the time required to reach $R = 1$ should be approximately 300 seconds. This is clearly much improved over the untilted post array, which requires around 10 to 15 minutes to reach the same resolution for this range of molecular weights [74].

We might suspect that the deviation between the simulation predictions and our experiments may be attributed, at least in part, to the methodology used in the calculations. Explicitly, the resolution calculations from the simulation only consider the transport inside the array, neglecting contributions due to injection, the finite width of the detector, and other experimentally relevant factors [141]. In our analysis, we assume that the resolution from our experiment simply scales up like $t^{1/2}$ to the longer array, which includes the initial peak width due to the injection. As a result, we are likely underestimating the performance of a rescaled device when the residence time is small, i.e., for the larger electric fields.

To provide a somewhat more realistic comparison with the simulations, let us denote by σ_e^2 the variance at the end of the finish line experiment for a given electric field, converted from the time domain to the space domain using the mean velocity [4]. It is common practice to assume that the variances are additive [141], so

$$\sigma_e^2 = \sigma_d^2 + \sigma_i^2 \tag{4.4}$$

where $\sigma_d^2 = 2D^*t$ is the contribution due to the effective diffusivity of strength D^* at the time t of the elution of the peak and σ_i^2 is the band width caused by the finite injection, which we measured in each experiment directly before the DNA entered the array. We can then can use Eq. (4.4) to estimate the effective diffusion coefficient, D^*. We can then estimate the variance of the scaled-up system as

$$\sigma_s^2 = 2D^*t_s + \sigma_i^2 \tag{4.5}$$

where t_s is the time required to reach a resolution $R = 1$ for the scaled-up channel length. Note that σ_i^2, the contribution due to injection, and D^*, the rate of band broadening due to transport inside the array, are unchanged by increasing the channel length.

The light-blue bars in Fig. 4.5A show the result of this slightly more realistic analysis. The decrease in separation time as a function of electric field is somewhat more pronounced that our original analysis (dark-blue bars in Fig. 4.5A), but the effect due to injection is not substantial. This is not unexpected. Tight injection bands, along with dissipation of Joule heat, were the major driving force behind microfluidic electrophoresis systems in the first place [147]. As a a result, we conclude that the time to reach a resolution of $R = 1$ is indeed independent of electric field, at least to within experimental error.

There are other possible reasons for the disagreement between simulations and experiments. For example, the simulation results correspond to single molecule trajectories, which are used to extract a mean velocity and effective diffusion coefficient for the ensemble, whereas the experiments can involve complicated interactions between the DNA molecules since the suspension is not infinitely dilute. There are also interactions due to roughness of the walls and the posts, as well as electroosmotic flow in the channel, that are not included in the simulation model. The impact of these effects on the band broadening would be larger at higher electric fields [148], which could be keeping the time to reach $R = 1$ from decreasing as the electric field is increased.

Although the time to reach resolution of unity is about the same for all electric fields, we saw in Fig. 4.4 that running the device at higher electric fields does seem to increase the reproducibility of the separation. However, larger electric fields require longer separation channels to reach high resolution in the tilted post array. For integrated lab-on-a-chip devices with many operations, space is at a premium. Wafers can be up to 300 mm, but that needs to be for the entire device and machines to process 300 mm wafers are not readily available outside semiconductor manufacture facilities. A more standard wafer size for academic research is 100 mm. Even if the device only performs the separation, as opposed to some integrated lab-on-a-chip functionality, we have found that 25 mm is roughly the upper limit for the separation channel since we need to (i) keep the reservoir spacing far enough for pipetting (and avoiding electrical short circuits) and (ii) have the entire pattern far enough away from the edge of the wafer to get sharp walls during photolithography. One option for increasing the channel length is to use serpentine channels [149, 150], thereby keeping the pattern far from the walls while increasing the length of the channel. We suspect that the increase in band broadening in serpentine channels is not worth the increased length they provide. Thus, one must consider these opposing effects for increasing the electric field when designing a separation device using the tilted post array.

4.4.3 Comparison with other tilted systems

Our tilted array strategy, which relies on periodic collisions with the posts and strong deformation of the DNA, differs qualitatively from related work using driving forces at an angle with respect to the lattice vectors of a periodic array. Two notable examples from previous work from the Austin group at Princeton include pulsed field electrophoresis in post arrays [34] and the DNA prism [103], both of which involved alternating electric fields between 0° and 135° to effect either a separation by the switchback mechanism

[34, 151] or a continuous separation [103]. In both cases, the DNA remain in a highly extended state, stretched between the posts, rather than recoiling and then extending again in a DNA-post collision.

Our tilted array strategy also differs from tilted Brownian ratchets [106,112,115,116]. Although the latter devices apply a continuous field at an angle with respect to the lattice vectors of the array, the obstacles in the device are larger than the radius of gyration of the DNA. As a result, DNA in the tilted Brownian ratchet leads to no deformation of the DNA and a qualitatively different separation mechanism.

The deformation of the DNA also makes DNA electrophoresis in a tilted array qualitatively different than separations of colloidal particles [152] and cells [153] in tilted post arrays. In the latter cases, the analytes tend to move at an angle with respect to the driving force, a method known as deterministic lateral displacement [117]. Since the DNA loses memory of its previous transport upon collision with a post [75], it is not deflected by the post and thus does not exhibit deterministic lateral displacement. Rather, the separation proceeds in a manner similar to the separation in a conventional post array, with the DNA all moving in the direction of the applied voltage drop.

4.5 Conclusion

We presented results for the separation of 20 kbp DNA and λ DNA in a 4 mm long separation channel using a 15° tilted post array. We were able to achieve measurable separation resolutions in this system for electric fields up to 50 V/cm. This compares favorably with untilted post arrays, which require separation lengths that are typically 15 mm or larger and lose the separation around 20 V/cm [74, 78, 79]. However we did not see the exponential decrease in the time required to achieve a resolution of unity as predicted by simulations [77]. Rather, with some reasonable assumptions, we estimate that the separation time will be independent of the electric field strength. We also

observed that the DNA separation is more reproducible at higher fields, which could be useful in designing a device to achieve a desired separation.

The prototype tilted post arrays we studied here are promising, and there are two obvious routes for improving the separation resolution. First, we suspect that the resolution would increase if we maintained the same post density but used smaller posts. Ou *et al.* previously showed that thinner posts work very well in improving separations in an untilted array [74], and there is no reason to expect that the case will be different for an untilted array. Second, improved injection schemes such as sample stacking [145] could reduce the width of the injection band and thus further increase the resolution. By implementing these improvements into the tilted post array, it may be possible to achieve rapid base line separations that could be very useful in an integrated lab-on-a-chip device.

Chapter 5

Towards a PnP Separation Device

The goal of this project was to create a continuous separation device, specifically the DNA prism [103], using a new technique called proximity field nano-patterning (PnP) [154–156] for the separation matrix. PnP allows for the creation of a large defect free regular array of three dimensional features. It also has a low consumable cost as the entire device is made in negative photoresist. The initial proof of concept goal was to create a batch separation device to show the PnP features would separate DNA. The channel and separation matrix was to be made in SU-8, an epoxy-based photoresist that cross-links when exposed to UV light. The channel geometry was a shifted-T [138], a standard shape used for batch separations, with a 100 μm offset. The entire device was designed to be the size of a standard microscope slide, 1 in. by 3 in. We have tried several different channel geometries, but in most recent design the channel is about 100 μm wide and about 10 μm deep. I was working on this project for the majority of my time here. Ultimately we were unable to achieve a separation in the batch separation device. What follows is a record of the motivation, methods attempted, and the unresolved issues encountered during the project.

5.1 Introduction

Many groups are investigating microfabricated devices for DNA separation due to the advantages the devices provide over the currently used technology. Microfabricated devices require less buffer, can be used to separate longer DNA fragments faster, are easily integrated into larger lab-on-a-chip devices, and provide well-defined separation structures. Further, they are more reproducible than gels and they lend themselves to separation mechanism studies [34, 42, 52, 65, 72, 157–162]. While prior work has lead to great improvements in separation times, most of the devices only separate long DNA. Also, very few of these devices have been commercialized and those that have can be very expensive, large initial investment for the machine and around $200 per disposable chip. This leaves the routine separation of smaller DNA fragments to the old technology, agarose gels. Another issue limiting the use of microfabricated devices for routine separations is that most microfabricated devices made are essentially two-dimensional. The fabrication of deep post arrays is difficult because of the large aspect ratios needed to create the deep and narrow posts. Two-dimensional devices are good for mechanism studies since all the DNA molecules remain in the focal plane of the high magnification objectives used for observing DNA molecules. However, for routine separations, the higher throughput of a three-dimensional device would be more effective. Work has been done to make three-dimensional separation devices using colloidal self assembly [107, 120, 163–165] and these devices have been shown to separate DNA, but they have a large density of defects and cracks that could effect the separation efficiency and reproducibility.

PnP can create three-dimensional features over a large area with little to no defects [156]. Also, after the initial investments of a phase mask and a light source, the fabrication is cheap and lends itself to producing disposable separation devices. PnP was developed and initially used as a microfluidic mixer [154, 166]. The microfluidic

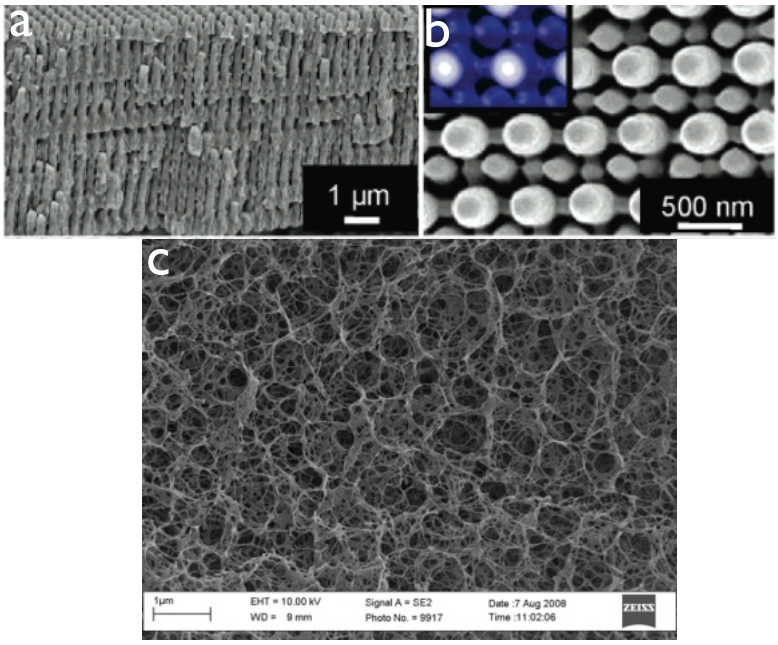

Figure 5.1: a) and b) An SEM image of the PnP created pattern taken from reference [156] for a phase mask with 375 nm diameter posts, 566 nm pitch, and 420 nm post height. a) A side view of the features showing the three-dimensional nature of the features. b) A top view of the features with the theoretically predicted shape inset in blue. c) An SEM image of a dried agarose gel. Image taken from the National Physical Laboratory website http://www.npl.co.uk/advanced-materials/materials-areas/biomaterials/characterisation-of-tissue-scaffold.

mixer requires a much smaller matrix array than a separation, which will be a challenge to overcome. PnP creates a regular three-dimensional structure that has pore sizes comparable to the pore sizes found in agarose gels, as seen in Fig. 5.1 c. PnP works by shining light through an elastomeric phase mask. The phase mask is a series of cylindrical posts that form conformal contact with the SU-8 and change the light's phase as the light passes through it, creating a complex diffraction pattern, shown in Fig. 5.2. This diffraction pattern produces a repeating self-imaging effect of the phase mask in the SU-8, known as the Talbot effect, where the periodic surface feature appears

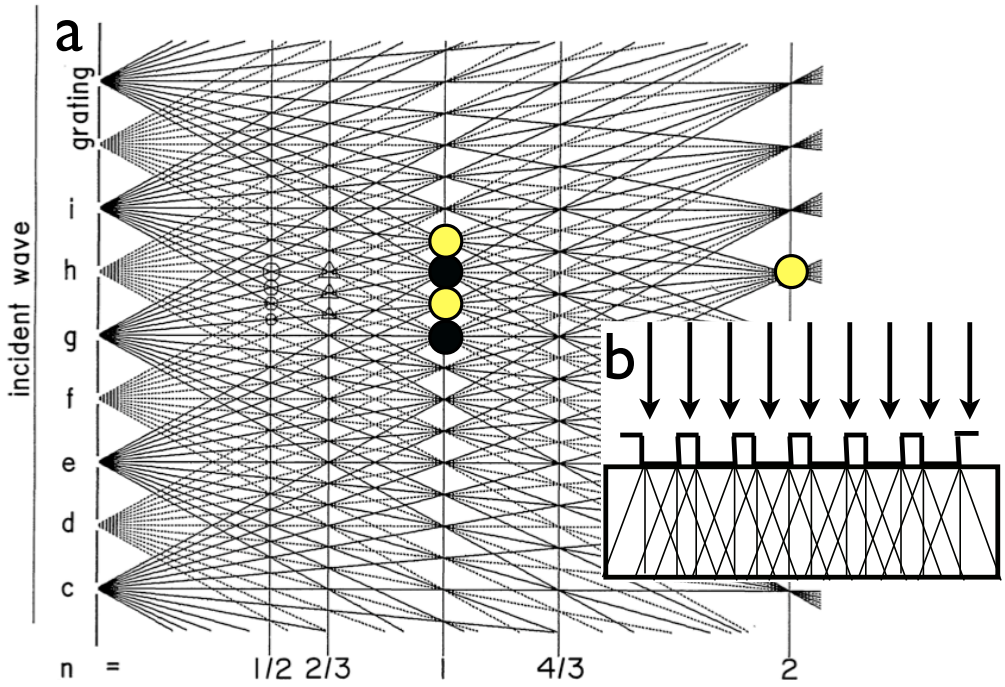

Figure 5.2: a) Calculated fringe pattern from a periodic aperture. The black dots represent complete destructive interference and the yellow dots represent constructive interference. The self-image occurs when n is even and the reverse image occurs when n is odd, where n is a lumped parameter that depends on the properties of the light and the phase mask. Taken from reference [168]. b) A schematic of the phase mask and how the light interacts with it. The array of rectangles represents the phase mask in contact with the SU-8, image not to scale.

at regular known distances from the surface on which the light initially shines. These distances depend on the properties of the light and the phase mask [167,168]. Since the SU-8 begins to cross-link when exposed to 60 mJ/cm^2 of 350 nm to 360 nm light, we get features where the light constructively interferes and we get the three-dimensional feature seen in Fig. 5.1 a and b.

PnP has the advantages of being able to create complex three-dimensional structures reproducibly with a low defect density and should be able to create an entire separation device with a low consumables cost. The only consumables needed are glass, SU-8,

and PDMS. A simple cost estimate finds that these components cost about $1 for each device, which is about the same cost to manufacture a gel, but PnP should increase the reproducibility, increase the speed, and reduce the amount of reagent required for each separation. These components are much cheaper when compared to what was needed for the original design for a microfabricated separation device [65], which was an array of silicon dioxide posts on silicon and required expensive fabrication techniques for every device. The economy of scale may lower the cost compared to prototype, but we still believe it would be more expensive than the component cost of our proposed device. A newer type of device uses PDMS to replicate a microfabricated array of posts [52], allowing several chips to be made from a single microfabricated feature, but PDMS has the undesired property of being permeable to water. Also, simple molding techniques can only create two-dimensional features. Using PnP to create the separation matrix allows for a reproducible three-dimensional structure and moves away from using PDMS as a separation matrix material, while keeping the consumable cost of each device relatively low.

5.2 Creating the PnP Features

The first step in creating the separation device was to create the PnP features for ourselves, seen in Fig. 5.1. We had to create a master mold, then the phase mask, and finally pattern the features in SU-8. We decided that the features created using a phase mask with 375 nm diameter posts, 566 nm spacing, and 420 nm post height, from ref. [156], seemed to have the pore sizes we desired. With the facilities available at that time, electron beam (e-beam) lithography (Raith 150) was the only tool that was capable of creating features that small. The desired pattern was a series of holes in the silicon. To create that using an electron beam tool one designates the location of several dots with the desired spacing and changes the dwell time of the electron beam

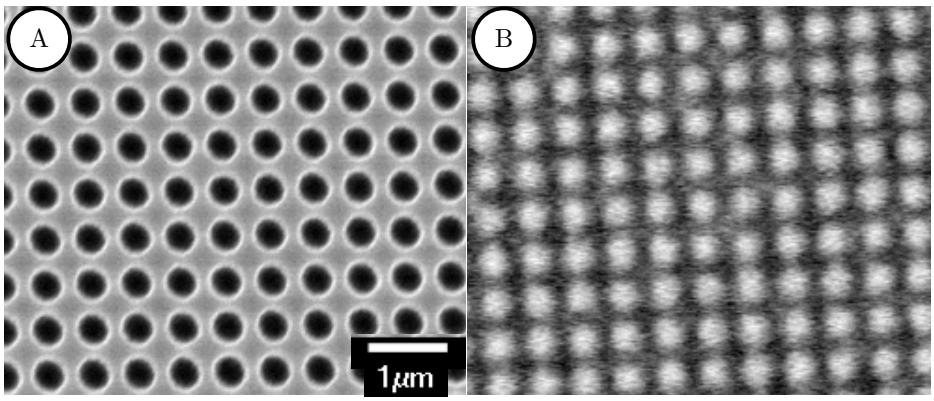

Figure 5.3: (A) The shows the master mold patterned using e-beam lithography and etched into silicon. (B) The shows the features replicated using the h-PDMS/PDMS composite phase mask. The phase mask is blurry because it is a nonconductive material; it is difficult to obtain sharp images of non-conductive material using SEM. The feature sizes are about 400 nm in diameter, with a center to center spacing and 566 nm and a depth of about 420 nm.

to determine the size of the circle. The longer the dwell time the larger the dot. The dwell time is internally calculated using the set beam energy and the desired exposure dose. Initial work done using the e-beam tool was to perform dose tests to determine the dose that would give the best circles that were close to the size we desired. Eventually, using an acceleration voltage of 20 KeV, a 20 μm aperture, and a beam dose of 0.3 pAs, we were able to get circles in poly(methyl methacrylate) in anisole (PMMA A4) photoresist that were about 400 nm in diameter and 566 nm center to center spacing, shown in Fig. 5.3A. The entire array was a square about 200 μm long on each side. We then etched the circles into holes about 420 nm deep using reactive ion etching (Surface Technology Systems 320).

Once we had the master we needed to create the phase mask using PDMS replication. Features this size are difficult to replicate using normal PDMS, but there is a similar substance called hard PDMS (h-PDMS) that works well for these geometries [169].

We found that using 1 ml (25-35% methylhydrosiloxane) - dimethylsiloxane copolymer (Gelest) and 3.4 ml (7.0-8.0% vinylmethylsiloxane) - dimethylsiloxane copolymer (Gelest), with 200 μl 2,4,6,8-tetramethyltetravinylcyclotetrasiloxane (Sigma) to modulate the surface and 18 μl platinum- divinyltetramethyldisiloxane complex in xylene (Gelest) as a catalyst, worked well to replicate the features. H-PDMS is very brittle after it has cured and very difficult to peel away from the features without breaking. By adding normal PDMS on top of the h-PDMS after it has partially cured and baking it all together results in a mask that is flexible and easy to handle while still replicating the small features [154]. To achieve this we spun the h-PDMS onto the master at 1000 rpm for 1 min, then spun at 500 rpm for 30 mins. This resulted in a very smooth thin partially cross-linked h-PDMS layer. PMDS was then added on top of this and was placed in an oven at 65-75°C, typically overnight. We found that the temperature was not important, so we allowed other users to change the temperature of the oven if they needed. After the phase mask had cured we took it out of the oven and carefully peeled the phase mask off of the features given the final working mask, shown in Fig. 5.3B.

We had created a phase mask, so it was time to create the PnP features. Our first attempt to create features used a contact aligner (Karl Suss) in flood exposure mode with the phase mask placed on top of the SU-8. The procedure was as follows:

1. Spin SU-8 2010 (Microchem) at 3500 rpm for 30 sec.
2. Soft bake at 95°C for 3 minutes.
3. Expose the SU-8 with 355 nm light.
4. Post exposure bake at 95°C for 4 minutes.
5. Develop in propylene glycol monomethyl ether acetate (PM acetate) for 30 minutes.

Using the manufacturer-recommended exposure energy, we initially tried a 13.8 s exposure, shown in Fig. 5.4A. The result was a series of bumps; the features were overexposed. We systematically lowered the exposure time and found that the lower the exposure the better the features looked, but we could still not get the features we desired. For example, the 3 second exposure is shown in Fig. 5.4B. We decided we needed a better quality light source than a UV lamp. We purchased a 355 nm laser (Teem Photonics) and, by using a hand-driven stage, we were able to pattern the PnP features in SU-8, shown in Fig. 5.4C.

We also found that the SU-8 would sometimes delaminate during the developing step. After consulting members of the group and staff at the university cleanroom we developed a new procedure that helped alleviate the delamination issues:

1. Spin SU-8 2002, a thinner formulation of SU-8, at 500 rpm for 30 seconds, then at 3500 rpm for 60 seconds.
2. Soft bake at 65°C for 2 minutes then at 95°C for 5 minutes.
3. Flood expose until fully cured, 30 seconds is usually enough but longer is not bad.
4. Hard bake at 200°C for 5 minutes.
5. Let this cool to room temperature.
6. Spin SU-8 2010 at 500 rpm for 30 seconds then at 3500 rpm for 60 seconds.
7. Soft bake at 65°C for 10 minutes followed by 95°C for 15 minutes.
8. Expose the SU-8 with the phase mask.
9. Post exposure bake for 7 minutes at 75°C.
10. Develop in PM acetate for 2-24 hours.

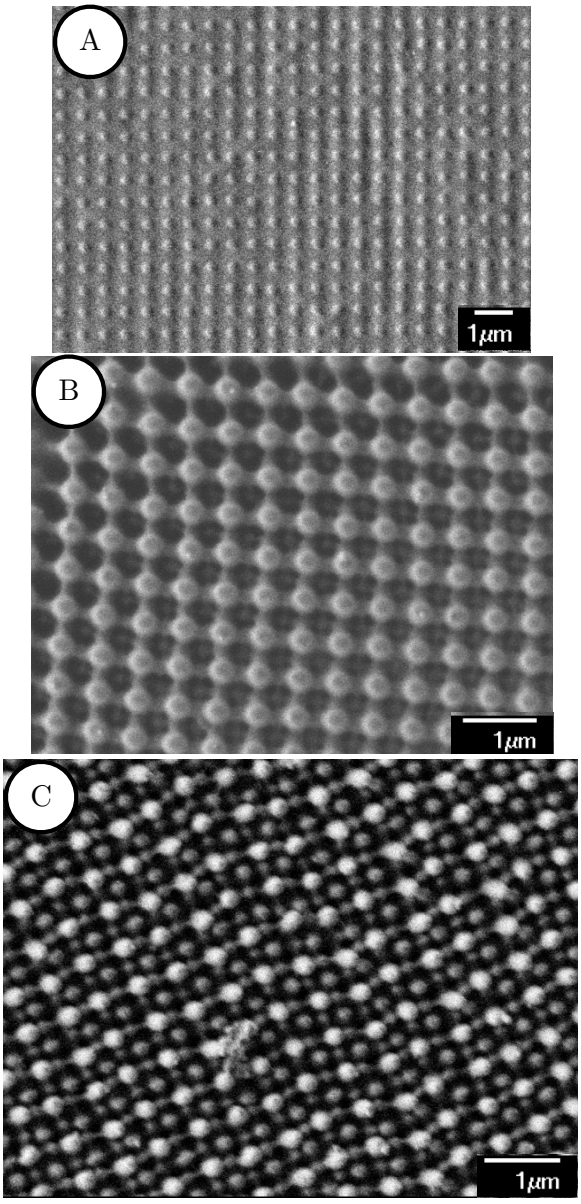

Figure 5.4: (A) The first attempt at creating the PnP features using a contact aligner with a 13.8 second exposure. It is basically a solid block of of SU-8 with dots. (B) After systematically reducing the exposure time, these are the best features using the contact aligner. There is evidence the pattern is 3-dimensional, but this is only true in the corner. (C) The desired features. These were the result of using a 355 nm laser at a fixed position and a hand turned translation stage to drive the chip through the laser spot. The stage is moved at its maximum velocity but this does not permit an accurate measurement of the exposure time. The defect in the center is debris.

11. Rinse the chip with isopropyl alcohol after developing.

12. Dry with filtered air.

With the exception of the post exposure bake parameters and the develop times, this is the procedure used throughout the remainder of this chaper. We had created a robust protocol for creating PnP features in SU-8, although replicating the exact features with a hand driven translation stage was difficult. We next needed to integrate these features into a separation channel.

5.3 The Integrated Separation Device

We had managed to create the PnP features in SU-8. It was a big step, but this was just reproducing the work performed by others [154–156]. We needed to integrate the features into a separation device and show that these features do in fact separate DNA. The first challenge would be to make a large array of features; 200 μm was not long enough for a DNA separation device. We would then have to seal the device and fill it with a buffer solution and load in DNA. Finally, we would have to apply an electric field to the device and separate the DNA.

5.3.1 Large array of features

The master made using e-beam lithography was 200 μm long. This was not going to be enough to separate DNA. We needed at least 2 mm, ten times what we had, and even that was short. Our first idea was to keep using the e-beam tool. The master was 200 μm long because that was the largest write field the e-beam tool was capable of, while still getting features as small as we wanted. There was a routine in the machine for stitching several write fields together and it was quoted to have a very accurate stage, which should translate into accurate stitching. However, we found there to be

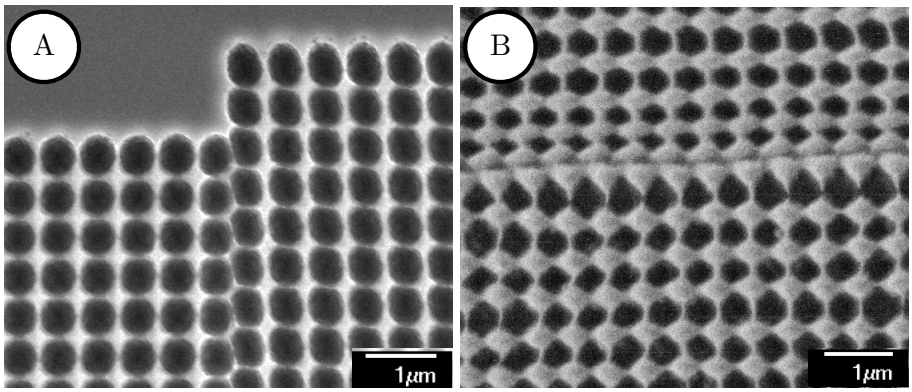

Figure 5.5: (A) The master mold when attempting to stitch several write fields together to make a larger array. This shows the stitching error of the e-beam. (B) The resulting PnP features due to the stitching error. This could possibly be a clog in the channel, which is unacceptable for a separation channel.

significant stitching error when trying to stitch 5 write fields together into a 1 mm long array. This is shown in Fig. 5.5A. We also found this stitching error resulted in a block when creating the pattern in SU-8, shown in Fig. 5.5B. We are not sure this went all the way through the array, but another tool had recently been installed in the cleanroom that seemed to be a better solution to the problem of creating a larger array.

A projection lithography system (Canon FPA 2500 i3) was added to the cleanroom. Projection lithography uses a series of lenses to shrink a pattern on an amplitude mask down. For the system we used, there is a 5× reduction and it is specified to make features down to 400 nm. It also allows for a square pattern as large as 20 mm, although practical limitations puts it usually under 10 mm for our array of circles. The features we wanted to make were slightly smaller than machine specifications, but we decided to attempt the pattern anyways. It quickly became clear this would not work, shown in Fig. 5.6A and B, and we decided to redesign the size of the master. Our next design, which had been shown to give PnP features [156], had a circle diameter of 570 nm with a 1140 nm center to center spacing and a depth of 420 nm. Also, the entire array was a square

that was about 6.5 mm. We were quickly able to create these patterns in photoresist with the following procedure:

1. Prebake a clean wafer at 115°C for 1 minute.
2. Expose the wafer to hexamethyldisilazane (HMDS) for 2 minutes to promote adhesion of the photoresist.
3. Spin coat the wafer with SPR 995 CM 0.7 at 4000 rpm for 30 seconds.
4. Clean off the backside of the wafer.
5. Soft bake the wafer for 60 seconds at 105°C.
6. Expose using projection lithography, with an intensity of 165 mJ/cm^2 and a -0.2 μm offset.
7. Post exposure bake the wafer at 115°C for 90 seconds, let cool to room temperature.
8. Develop in CD-26 for 30 seconds.

While we were easily able to pattern the photoresist, etching the pattern into the silicon presented an unexpected challenge. With the e-beam feature a silicon etch using the reactive ion etching system worked well to etch the pattern into the silicon. Following the same procedure with the projection lithography features resulted in very rough side walls of the holes, shown in Fig. 5.6C. This made replicating into h-PDMS impossible; the h-PDMS would not release and get stuck in the holes. This is most likely due to the holes being larger and the side wall more easily bombarded with the plasma particles, resulting in the rough walls. We found that using a deep reactive ion etch system (Plasma-Therm SLR 770), which uses a passivating agent to protect the side

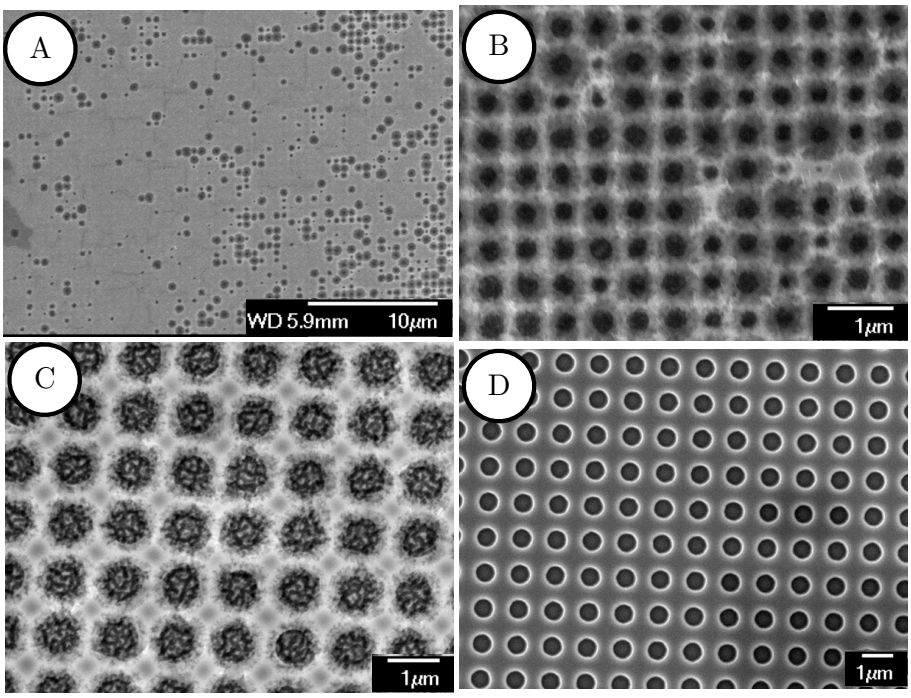

Figure 5.6: (A) and (B) The attempt to make a master mold with 375 nm circles and 566 nm center to center spacing. (A) The edges of the die, where the holes where not exposed properly. (B) The area where the circles where exposed fully still resulted in uneven circle sizes. (C) The master mold with 570 nm circles and 1140 nm center to center spacing. Notice the circles are more consistent. This was etched using reactive ion etching giving rough side walls. This would not allow the h-PDMS to release during replication. (D) The working master mold. This was etched using a continuous etch in a deep reactive ion etching system, which passivates the side wall, giving much smoother side walls.

walls, gave a very smooth etch that was able to be readily replicated using our h-PDMS composite mask, Fig. 5.6D.

We now had a large mask and had a procedure to pattern the features in SU-8. Next we needed to put the features into a separation channel. In order to do this we needed a method for aligning the laser spot and to accurately control the time the spot is on the SU-8, the exposure time. To this end, we built a laser exposure system that had an aperture to set the beam size, a computer controlled translation stage, and a

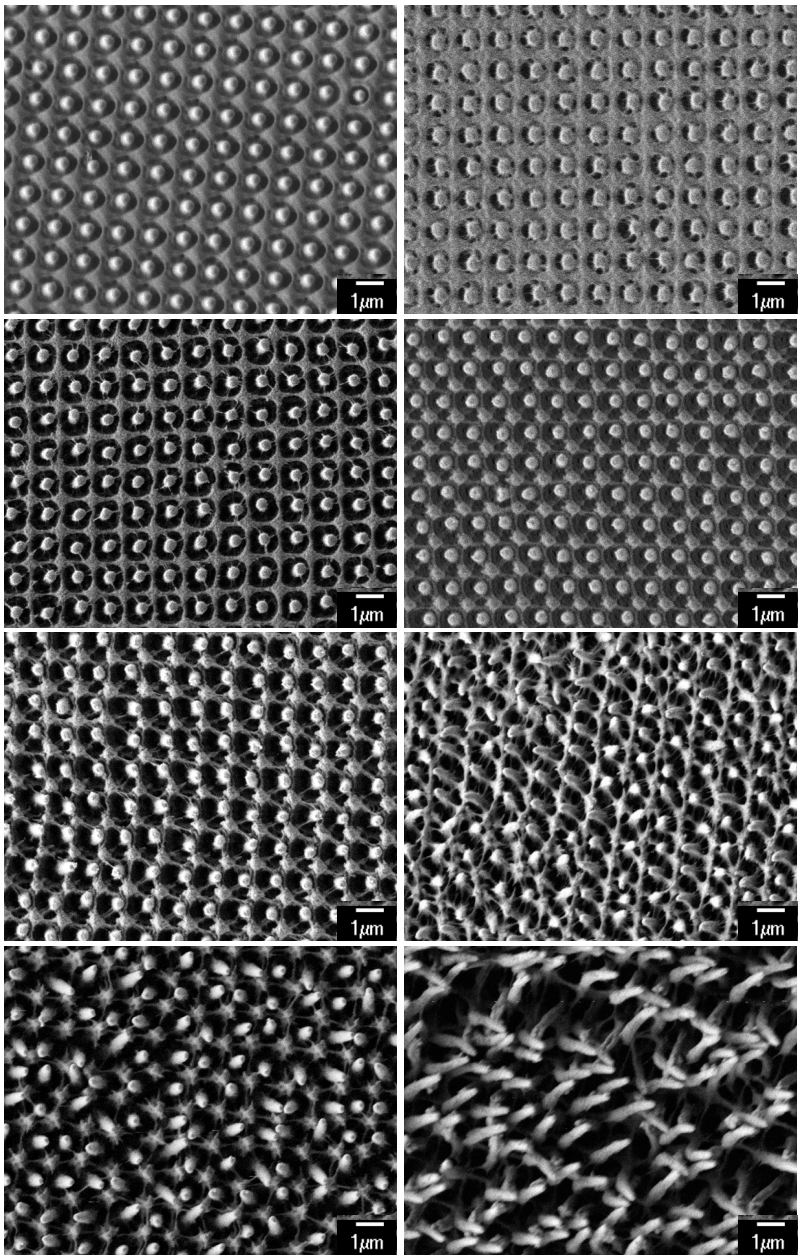

Figure 5.7: Ability to tune the pore size of the PnP features through the exposure time. All of these images were created with the same size photo mask. At long exposure time one get small pores, to a point where there are no pores. At very short exposure times the pores get very large and structures begin to collapse, giving a more random array of features. The actual exposure time, in our case the exposure speed, can vary largely for different phase masks.

computer controlled shutter. Using a custom Labview program, this system allowed us to set a beam size and use the speed of the stage to set the exposure time. The shutter allowed us to shut off the beam when it reached the edge of the mask as to not clog the channel around the features. Using this setup we were able to integrate the features into a separation channel. The procedure is very similar to just patterning the feature into bulk SU-8. The differences are, first, the channel is patterned using a contact aligner and amplitude mask. This is then baked at 95°C for 4 mins. This gives a "shadow" of the channel and allows for easy alignment. The SU-8 is then exposed with the laser through the phase mask, which is then baked and developed as described above. While testing different exposure speeds for integration, we also saw that the pore sizes are tunable with exposure time, as shown in Fig. 5.7. This effect was seen consistently, but the exposure speeds would widely vary between different phase masks.

We now had PnP features integrated into a separation channel. All that was left to do was to seal, wet, and run the device. However, this is where everything started to go wrong.

5.3.2 Sealing and wetting

While we were working to create the larger features and integrating them into the separation channel, we were also testing different sealing and wetting methods using an empty SU-8 device. Our initial method was to treat both the SU-8 channel and a flat slab of PDMS with an air plasma (Harrick Plasma), followed by heating the device at 70°C for 10 minutes. This method was used by another group to seal a PnP device used to make a microfluidic mixer [154]. We then filled the channel with 2.2x TBE buffer and attempted to put DNA into the device and inject it into the empty channel. We found that, while the device seemed to seal well, the DNA would leak out of the channel during the loading and injection. This leaking was unacceptable so we tried a

new sealing method.

Next we attempted using a compound called Norland's Optical Adhesive (NOA-81) from Norland products. This has been shown to be able to seal devices by partially cross-linking the NOA-81 and using it as an adhesive to seal glass to a channel [170]. The procedure is to spin the NOA-81 onto a glass slide or coverslip, then cover it with PDMS. Expose the NOA-81 through the PDMS using UV light. The oxygen permeance of the PDMS does not allow it to fully cross-link, leaving the NOA-81 sticky on that side. Finally one then sticks this to the channel to be sealed and exposes again to complete the seal. While we found this procedure to work, it required very careful hands and often the seal would fail due to dust, air bubbles, or mishandling. We also found that once the device was sealed we were unable to wet the channel. Between the difficultly of the procedure and the device not wetting well, we decided to try a new method.

The next two sealing methods were quickly abandoned. The first method was to funtionalize the PDMS with amine groups, which would react with the non-cross-linked epoxy groups in the SU-8 when heated [171]. By evaporating a 0.5 % (v/v) 3-aminopropyltrimethoxysilane in toluene onto the PDMS, the PDMS is functionalized with the silane groups sticking to the PDMS and the amine groups sticking out. This is then placed onto the SU-8 and heated at 80°C for 30 mins to create a very strong bond. However, we were unable to wet the device after it was sealed. The second method was to seal with SU-8, creating an all SU-8 device. By only partially soft baking the SU-8 it remains sticky. Tuomikoski and Franssila were able to create a seal by applying pressure on a hot plate [172]. We were unable to replicate this result and were also doubtful we would be able to wet the device, as we had previous problems with the wettability of SU-8.

Finally, we found a sealing method that seemed to solve all the problems we were encountering. It was simple, reproducible (although it did leak a little sometimes), and

led to spontaneous wetting of the channel. Treating the SU-8 with sulfuric acid caused the SU-8 to become more hydrophilic [173]. This effect may have seemed subtle, but it allowed for air plasma treated PDMS to seal to the SU-8 and it allowed for spontaneous wetting of the channel. This was even true once the features had been integrated into the device. The procedure was to soak the SU-8 channel in 1.0 M sulfuric acid for 5 mins at room temperature. We found that higher concentration sulfuric acid reacted with the SU-8, turning it brown. Longer times delaminated the SU-8 from the glass slide. Higher temperature caused the delamination to happen faster. It was reported that higher temperature and longer time results in the SU-8 being more hydrophilic [173], but we found that it destroyed the device. The SU-8 channel was then rinsed and bonded to an air plasma treated slab of PDMS. This was put into an oven at 75°C for 5 minutes. We found that any longer in the oven and device would not spontaneously wet and the seal was not strong enough for pumping. With this new sealing method it seemed we had completed our objective of creating a PnP separation device. However, as we started running DNA through the device we noticed something was wrong.

5.3.3 The gap

Thinking we had created a PnP DNA separation device, we began to attempt separations in these devices. However, the DNA would not separate. The DNA actually traveled faster in the separation array than in the empty channel, shown in Fig. 5.8. As the pores sizes in the PnP features were a similar size to agarose gels, we would expect either Ogston sieving or biased reputation like movement through the array depending on the size of the DNA. Both of these would result in the DNA being slowed down by the array, which is not what we observed. Our hypothesis was that there was a gap between the top of the array and the PDMS roof. This is not an uncommon problem when integrating delicate holographic features in a microfluidic channel [166, 173, 174],

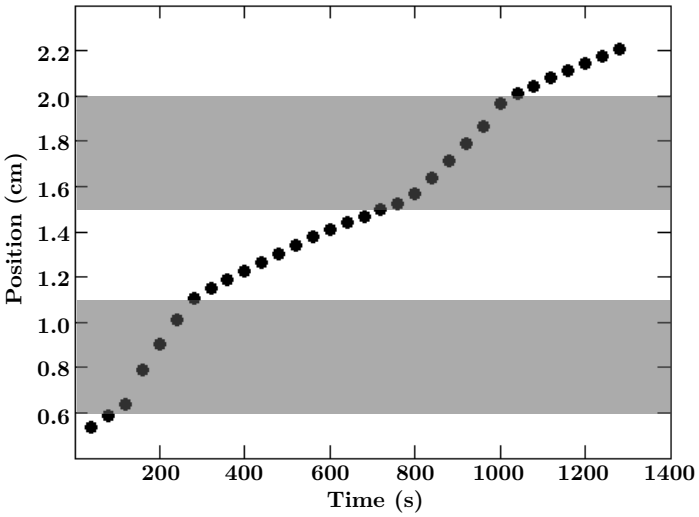

Figure 5.8: Plot of the center-of-mass postiion of a DNA plug as a function of time in the device. The faster velocities occur from 0.6 cm to 1.1 cm and again from 1.5 cm to 2.0 cm. These two locations correspond to the PnP arrays.

but we had partially taken this into account by, first, lowering the post exposure bake temp from 95°C to 75°C and, second, using a large channel allowing the PDMS to bow into the channel covering any remaining gap. However, this was not sufficient as we found the height of the array to be 3 μm lower than the side wall, which we measured by profilometer. This gap was too large.

The first thing we changed was the rinsing procedure after developing. We first tried super critical drying, a common procedure to reduce collapse of delicate structures, which we thought may be a part of the issue. We found there to be a small improvement, but not significant compared to extra effort required. We then attempted rinsing with isopropyl alcohol followed by rinsing with ethanol, then drying with filtered air. We found this gave a very similar result to super critical drying, but this still only reduced the gap to about 2 to 2.5 μm, which was still too large.

We next turned our efforts to the post exposure bake, knowing that elevated temperatures does cause the SU-8 to shrink. However, we found that changing the temperature

of the second post exposure bake, the one after exposing the features with the laser, did not change the size of the gap. We then lowered the temperature of the first post exposure bake, the one after defining the channel structure, and found the gap to be reduced. Carefully examining our procedure, we decided to eliminate the first post exposure bake and lower the temperature of the second post exposure bake. After many experiments, we determined a single post exposure bake at 65°C in a glass pertri dish wrapped in aluminum foil in an oven for 23 minutes gave the best results. As a note of caution, lowering the temperature of the post exposure bake too much, or baking for too short of time, results in partially cross-linked SU-8. This has a white color and can leak. The new procedure for integrating the features into the channel was to expose the channel using a contact aligner and then immediately expose the chip using the laser. Then a post exposure bake at 65°C for 23 minutes and developed for 4 minutes in PM acetate with agitation. We found the long developing times were not necessary with agitation. Finally the device was rinsed with isopropyl alcohol and then ethanol and dried with filtered air. This procedure resulted in a gap that was usually less than 500 nm, which is small enough that the bow from the PDMS covers it up. The resulting features are shown in Fig. 5.9.

We had eliminated the gap. The devices were slower to wet, which we took to be confirmation that the gap was gone in the assembled device. We attempted to separate DNA once again. We found that usually the DNA would not respond as expected to the electric fields, either traveling in the incorrect directions or moving at a different speed than expected. When this was not the case the DNA would not travel as a plug down the empty part of the channel. It usually traveled faster along one wall, causing the plug to tilt. The wall it traveled faster down was not consistent. The plug would also slow down significantly right before the array and then stop either right before the array or right after entering the array. We were unable to explain these observations

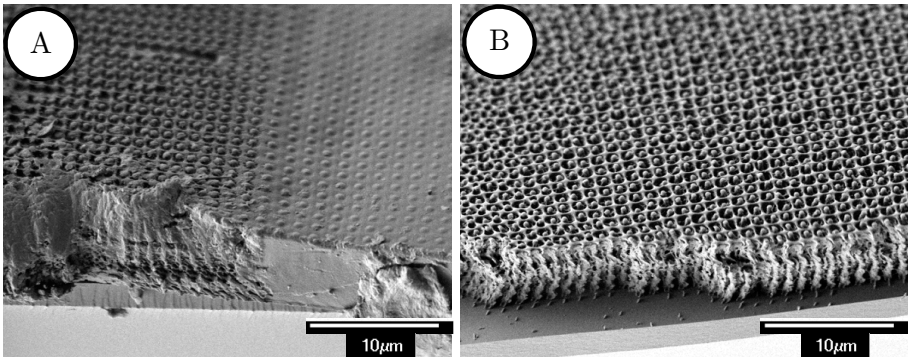

Figure 5.9: (A) Cross section of the PnP feature at the side wall. There is a smooth transition to the PnP features and no noticeable drop in the height. The blocked areas are due to breaking the chip to image the cross section. (B) Cross section in the center of the features showing the pore size is consistent through the entire depth of the device.

and nothing about the behavior was consistent enough to pinpoint a specific problem. We decided to do one last thing to try to treat the SU-8 so that the properties would be more familiar to us.

5.3.4 Atomic layer deposition

Atomic layer deposition (ALD) is a method to coat a substrate one atomic layer at a time, typically with a metal oxide. This means it will get into the small pores of the feature that other deposition techniques would just coat over. We decided to coat the SU-8 in a layer of silicon dioxide. This is the material used for silicon devices, although that is thermally grown silicon dioxide it is still has the same properties. Our group is much more familiar with the properties of silicon dioxide under the conditions we are running the device, 5x TBE buffer and applied electric fields. This previous experience with the material would make troubleshooting easier.

However, ALD is a high temperature process. Most recipes call for temperatures exceeding 200°C. With the help of the staff at the university clean room we were able to develop a recipe to deposit silicon dioxide at 150°C, but this still caused the features

to shrink again and the gap returned. We then found a method to thermally stabilize the SU-8, which was reported to allow for temperatures up to 200°C with no effect on the delicate features [174]. The procedure we found to work best was to soak the PnP features in 5% (v/v) N,N'-bis(3-aminopropyl)ethyl-enediamine (BAPEN) in PM acetate for 10 minutes. The BAPEN started to precipitate on the chip leaving globs behind, which made sealing impossible, it can also cause the SU-8 to swell. Soaking the device in isopropyl alcohol for 5 mins seemed to alleviate both those problems. The chip was then rinsed in isopropyl alcohol followed by ethanol and dried with filtered air. This stabilized the devices up to 200°C, as tested in a furnace. This allowed us to perform the ALD without damaging the device. One interesting observation we had, although sporadic and rare, was that sometimes the gap would get smaller. If the array was 500 nm lower than the side wall initially, after the ALD the array would be the same height as the side walls or even taller. We were not able to achieve this consistently or often and we attribute this to the BAPEN swelling the SU-8 during the treatment.

The sealing method once the chip was coated was simple. Air plasma treat both the chip and the flat PDMS for 5 minutes, stick them to together, and wet. This created a seal that was usually strong enough to perform the separation experiments, although it did leak sometimes. With this device we were able to get DNA to travel through the array, but we still did not see separation. A representative electropherogram is shown in Fig. 5.10. However, the electric fields moved the DNA as expected and we were able to achieve good injections into the device. This definitely seemed to be the right direction, but the device was still not separating. Even when using two vastly different sized species, 709 bp and 48500 bp, there was no obvious separation. Also the device would stop working after 2-3 injections. So there were still problems to be worked out, sadly we ran out of time and could not fix those issues.

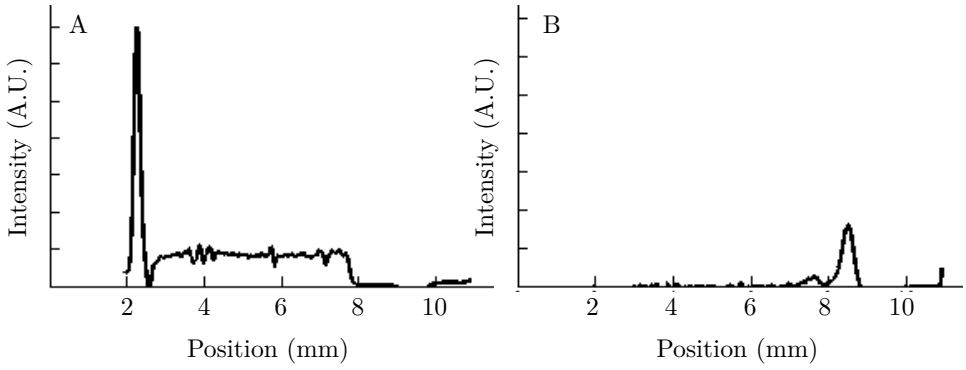

Figure 5.10: Electropherograms from an attempted PnP separation. The DNA used was 709 bp and λ (48500 bp) dyed with TOTO-1 with a 5 to 1 base pair to dye ratio. The experiment was performed at 10 V/cm in a ALD treated PnP separation matrix. The buffer was 5x TBE buffer with 0.07% (w/v) ascorbic acid and polyvinylpyrrolidone and 3% (v/v) β-mercaptoethanol (all from Sigma). A) Both DNA before they enter the separation array, which can be seen by the intensity plateau from 3mm to 8 mm. B) The DNA species after exiting the array which had been bleached by the scanning. There is no sign of separation, just peak spreading.

5.4 Conclusion

Overall, we have created a device with a PnP separation matrix, but we have not been able to show that the device is able to separate DNA. The major issues seem to be a combination of materials issues and problems with sealing the device properly. The ALD treatment of the SU-8 seems to be the best method for creating the device, but we still did not observe separation. There is one major change that I believe will improve the chance for success: using something other than PDMS for sealing the device. PDMS has a known issue of fluid permeance, which could be the reason the DNA being unresponsive after 2-3 injections. The device could be drying out from the center. However, I do not know what could be used. We have tried many different sealing techniques and none were as good as PDMS. In the end, I still believe this is not only possible, but is a good idea. With more time I believe that PnP features can be used to separate DNA.

Chapter 6

Conclusions

DNA is a very important biological molecule and the manipulation of DNA is ubiquitous in biological research. One common manipulation of DNA is to sort it by size. The common techniques for this sorting is agarose gel electrophoresis and it is well established, but does have some deficiencies. It has reproducibility problems due to the randomness of the gels. It is also unable to separate long DNA without the use of pulsed fields and these take a very long time to separate. Performing the separations in microfluidic devices seems to be a solution to most of the issues that arise in gels. They have precisely defined and regular features. They are smaller and can be run at higher fields. They are fast. They also lend themselves to the exciting prospect of lab on a chip technologies, miniaturizing an entire lab down to something that can fit in the palm of your hand to perform complex analyses in the field.

There are many geometries and separation techniques that have been developed for DNA separation in microfluidic devices. One very promising geometry is the slit-well geometry. This can be used for separation of small or large DNA, depending on the size of the slit. This device is a bit difficult to fabricate and is expensive compared to gels, but it features rapid separation and an impressive peak capacity. Another geometry is

the post array, which is one of the earliest microfluidic devices. This geometry is very good at separating long DNA quickly. It is one of the easier geometries to fabricate and can even be made using soft lithography techniques. However, this device seems to have limited peak capacity and limited commercial interest. Finally, a very interesting separation mode is the continuous separation device. These continuous devices were designed using already developed geometries and using the understanding of how these geometries work. They cause different sized DNA to travel at different angles to separate the DNA spatially, typically using a pulsed electric field. There is also the Brownian ratchet that uses a DC field and an array of tilted rectangles to achieve continuous separation.

Despite the slit well and post array geometries being well understood, there are still novel separation modes to be discovered. By using a low frequency asymmetrically pulsed electric field in the slit well geometry, we were able to achieve bi-directional migration of small DNA, presented in chapter 3. This should also work for large DNA with a change in the slit height. The effect was tunable, meaning by changing the frequency of the pulses, we could choose which sized molecules travel forward and which travel backwards. One could easily imagine using this as a filtration step in an integrated microfluidic device. The advantage over a traditional filter is that all the species are mobile, so there is no clogging and after the process the remaining DNA can readily be flushed out with an electric field.

The hexagonal post array has also been studied quite thoroughly, but we were still able to test a novel separation mode and discovered a new design parameter. By rotating the hexagonal post array the channels between the posts are broken up and separation is improved. This is shown in chapter 4. In a normal hexagonal post array, if the posts are too far apart or if the electric field is too high, the DNA will enter the channel between the posts. This significantly lowers the collision probability and as a result the

separation quality. Typically it is difficult to achieve separation at electric fields higher than 15 V/cm. In the tilted post array we were able to achieve separations at 50 V/cm. We were also able to achieve this separation in a 4 mm array. This is much shorter than other arrays, which are typically 10 to 20 mm long.

Continuous separation devices show the greatest promise for larger lab on a chip devices. Continuous processes are convenient when putting many unit operations together into a single pipeline. Batch processes require the entire process to stop and wait while the batch process is being performed. The original DNA prism, an example of a continuous separation device, was an ingenious device. The only problem is that the post array used as the separation matrix can be expensive to make. In chapter 5 we showed our work attempting to create a continuous separation device using PnP as the separation matrix. With PnP, the entire device could be made in photoresist. The process of replicating the array, once the phase mask was made, could be very cheap. However, we were never able to realize this goal as we were plagued by materials issues we were unable to overcome. In the end it was a valuable learning experience, but no fruitful results were produced.

In conclusion, it seems unlikely that microfabricted DNA separation devices will be able to dethrone gels for routine analysis. Gels, while they can take a long time, are easy to make, easy to use, and require very little initial investment. I believe the real benefits from DNA separations in microfluidic devices were the deeper understanding of DNA physics. Researchers were able to uncover a lot of physical phenomena, leading to an understanding of how DNA behaves in different environments. This has led to the development of DNA manipulation devices never even thought of before. One example of this is stretching DNA in nanochannels for DNA barcoding. There are many examples of new DNA manipulation devices and a good place to start is our recent review article [4]. While DNA separation in microfluidic devices did not change the way people separate

DNA in research labs, it still provided many useful insights and new techniques for DNA manipulation. I think researchers will continue to use this information to create unimaginable devices and techniques in the future.

Bibliography

[1] F. Sanger, S. Nicklen, and A. R. Coulson. DNA sequencing with chain-terminating inhibitors. *P. Natl. Acad. Sci. USA*, 74(12):5463–5467, 1977.

[2] M. Rubinstein and R. H. Colby. *Polymer Physics*. Oxford University Press, 2003.

[3] G. S. Manning. Limiting laws and counterion condensation in polyelectrolyte solutions i. colligative properties. *J. Chem. Phys.*, 51(3):924–933, 2003.

[4] K. D. Dorfman, S. B. King, D. W. Olson, J. D. P. Thomas, and D. R. Tree. Beyond gel electrophoresis: Microfluidic separations, fluorescence burst analysis, and DNA stretching. *Chem. Rev.*, 113(4):2584–2667, 2013.

[5] C. Brockman, S. J. Kim, and C. M. Schroeder. Direct observation of single flexible polymers using single stranded dna. *Soft matter*, 7(18):8005–8012, 2011.

[6] F. Latinwo and C. M. Schroeder. Model systems for single molecule polymer dynamics. *Soft matter*, 7(18):7907–7913, 2011.

[7] D. R. Tree, A. Muralidhar, P. S. Doyle, and K. D. Dorfman. Is DNA a good model polymer? *Macromolecules*, 46(20):8369–8382, 2013.

[8] D. Long, J. L. Viovy, and A. Ajdari. Simultaneous action of electric fields and nonelectric forces on a polyelectrolyte: Motion and deformation. *Phys. Rev. Lett.*, 76(20):3858–3861, 1996.

[9] D. Long, J. L. Viovy, and A. Ajdari. Stretching DNA with electric fields revisited. *Biopolymers*, 39(6):755–759, 1996.

[10] G. A. Griess, E. T. Moreno, R. A. Easom, and P. Serwer. The sieving of spheres during agarose gel electrophoresis: quantitation and modeling. *Biopolymers*, 28(8):1475–1484, 1986.

[11] N. Pernodet, M. Maaloum, and B. Tinland. Pore size of agarose gels by atomic force microscopy. *Electrophoresis*, 18(1):55–58, 1997.

[12] G. W. Slater, J. Rousseau, J. Noolandi, C. Turmel, and M. Lalande. Quantitative analysis of the three regimes of DNA electrophoresis in agarose gels. *Biopolymers*, 27(3):509–524, 1988.

[13] J. L. Viovy. Electrophoresis of DNA and other polyelectrolytes: Physical mechanisms. *Rev. Mod. Phys.*, 72(3):813–872, 2000.

[14] A. G. Ogston. The spaces in a uniform random suspension of fibres. *T. Faraday Soc.*, 54:1754–1757, 1958.

[15] D. Rodbard and A. Chrambach. Unified theory for gel electrophoresis and gel filtration. *P. Natl. Acad. Sci. USA*, 65(4):970–977, 1970.

[16] D. Rodbard and A. Chrambach. Estimation of molecular radius, free mobility, and valence using polyacrylamide gel electrophoresis. *Anal. Biochem.*, 40(1):95–134, 1971.

[17] K. A. Ferguson. Starch-gel electrophoresis–application to the classification of pituitary proteins and polypeptides. *Metabolism*, 13(10), 1964.

[18] L. S. Lerman and H. L. Frisch. Why does the electrophoretic mobility of DNA in gels vary with the length of the molecule? *Biopolymers*, 21(5), 1982.

[19] O. J. Lumpkin and B. H. Zimm. Mobility of DNA in gel electrophoresis. *Biopolymers*, 21(11):2315–2316, 1982.

[20] P. G. De Gennes. Reptation of a polymer chain in the presence of fixed obstacles. *J. Chem. Phys.*, 55(2):572–579, 1971.

[21] T. A. J. Duke, J. L. Viovy, and A. N. Semenov. Electrophoretic mobility of DNA in gels. i. new biased reptation theory including fluctuations. *Biopolymers*, 34(2), 1994.

[22] T. A. J. Duke, A. N. Semenov, and J. L. Viovy. Mobility of a reptating polymer. *Phys. Rev. Lett.*, 69(22):3260–3263, 1992.

[23] A. N. Semenov, T. A. J. Duke, and J. L. Viovy. Gel electrophoresis of DNA in moderate fields: The effect of fluctuations. *Phys. Rev. E*, 51(2):1520–1537, 1995.

[24] C. Heller, T. A. J. Duke, and J. L. Viovy. Electrophoretic mobility of DNA in gels. ii. systematic experimental study in agarose gels. *Biopolymers*, 34(2), 1994.

[25] J. Yan, N. Best, J. Z. Zhang, H. J. Ren, J. Hou, and N. J. Dovichi. The limiting mobility of DNA sequencing fragments for both cross-linked and noncross-linked polymers in capillary electrophoresis: DNA sequencing at 1200 v/cm. *Electrophoresis*, 17:1037–1045, 1996.

[26] G. T. Barkema, J. F. Marko, and B. Widom. Electrophoresis of charged polymers: Simulation and scaling in a lattice model of reptation. *Phys. Rev. E*, 49(6):5303–5309, 1994.

[27] A. Baumgartner and M. Muthukumar. A trapped polymer chain in random porous media. *J. Chem. Phys.*, 87:3082, 1987.

[28] M. Muthukumar and A. Baumgartner. Effects of entropic barriers on polymer dynamics. *Macromolecules*, 22:1937, 1989.

[29] M. Muthukumar and A. Baumgartner. Diffusion of a polymer chain in random-media. *Macromolecules*, 22:1941, 1989.

[30] G. W. Slater and S. Y. Wu. Reptation, entropic trapping, percolation, and rouse dynamics of polymers in "random" environments. *Phys. Rev. Lett.*, 75(1):164, 1995.

[31] D. C. Schwartz and C. R. Cantor. Separation of yeast chromosome-sized DNAs by pulsed field gradient gel electrophoresis. *Cell*, 37(1):67–75, 1984.

[32] G .F. Carle and M. V. Olson. Separation of chromosomal DNA molecules from yeast by orthogonal-field-alternation gel electrophoresis. *Nucleic Acids Res.*, 12(14):5647–5664, 1984.

[33] C. L. Smith and C. R. Cantor. Purification, specific fragmentation, and separation of large dna molecules. *Method. Enzymol.*, 155:449–467, 1986.

[34] O. Bakajin, T. A. J. Duke, J. O. Tegenfeldt, C. F. Chou, S. S. Chan, R. H. Austin, and E. C. Coxs. Separation of 100-kilobase DNA molecules in 10 seconds. *Anal. Chem.*, 73(24):6053–6056, 2001.

[35] R. E. Burton, E. J. White, T. R. Foss, K. M. Phillips, R. H. Meltzer, N. Kojanian, L. W. Kwok, A. Lim, N. L. Pellerin, N. V. Mamaeva, and R. Gilmanshin. A microfluidic chip-compatible bioassay based on single-molecule detection with high sensitivity and multiplexing. *Lab Chip*, 10:843–851, 2010.

[36] R. H. Meltzer, J. R. Krogmeier, L. W. Kwok, R. Allen, B. Crane, J. W. Griffis, L. Knaian, N. Kojanian, G. Malkin, M. K. Nahas, V. Papkov, S. Shaikh, K. Vyavahare, Q. Zhong, Y. Zhou, J. W. Larson, and R. Gilmanshin. A lab-on-chip for biothreat detection using single-molecule DNA mapping. *Lab Chip*, 11:863–873, 2011.

[37] C. J. O. R. Morris. Gel filtration and gel electrophoresis. *Protides of the Biological Fluids*, 14:543, 1966.

[38] J. Wang, A. D. Gonzalez, and V. M. Ugaz. Tailoring bulk transport in hydrogels through control of polydispersity in the nanoscale pore size distribution. *Adv. Mater.*, 20:4482, 2008.

[39] Nan Shi and Victor Ugaz. Tailoring the nanoporous architecture of hydrogels to exploit entropic trapping. *Phys. Rev. Lett.*, 105:108101, 2010.

[40] J. Han, S. W. Turner, and H. G. Craighead. Entropic trapping and escape of long DNA molecules at submicron size constriction. *Phys. Rev. Lett.*, 83:1688–1691, 1999.

[41] J. Han and H. G. Craighead. Entropic trapping and sieving of long DNA molecules in a nanofluidic channel. *J. Vac. Sci. Technol. A*, 17:2142–2147, 1999.

[42] J. Han and H. G. Craighead. Separation of long DNA molecules in a microfabricated entropic trap array. *Science*, 288:1026–1029, 2000.

[43] J. Han and H. G. Craighead. Characterization and optimization of an entropic trap for DNA separation. *Anal. Chem.*, 74:394–401, 2002.

[44] J. Fu, P. Mao, and J. Han. Nanofilter array chip for fast gel-free biomolecule separation. *Appl. Phys. Lett.*, 87(26):263902, 2005.

[45] J. Fu, J. Yoo, and J. Han. Molecular sieving in periodic free-energy landscapes created by patterned nanofilter arrays. *Phys. Rev. Lett.*, 97:18103, 2006.

[46] H. Bow, J. Fu, and J. Han. Decreasing effective nanofluidic filter size by modulating electrical double layers: Separation enhancement in microfabricated nanofluidic filters. *Electrophoresis*, 29(23):4646–4651, 2008.

[47] E. A. Strychalski, H. W. Lau, and L. A. Archer. Nonequilibrium separation of short DNA using nanoslit arrays. *J. Appl. Phys.*, 106:024915–024915, 2009.

[48] T Yasui, N Kaji, R Ogawa, S. Hashioka, M Tokeshi, Y. Horiike, and Y. Baba. DNA separation in nanowall array chips. *Anal. Chem.*, 83:6635, 2011.

[49] M. B. Mikkelsen, W. Reisner, H. Flyvbjerg, and A. Kristensen. Pressure-driven DNA in nanogroove arrays: Complex dynamics leads to length-and topology-dependent separation. *Nano Lett.*, 2011.

[50] K. D. Dorfman. DNA electrophoresis in microfabricated devices. *Rev. Mod. Phys.*, 82(4):2903, 2010.

[51] T. T. Duong, G. Kim, R. Ros, M. Streek, F. Schmid, J. Brugger, D. Anselmetti, and A. Ros. Size-dependent free solution DNA electrophoresis in structured microfluidic systems. *Microelectron. Eng.*, 67:905–912, 2000.

[52] K. Inatomi, S. Izuo, S. Lee, H. Ohji, and S. Shiono. Electrophoresis of DNA in micro-pillars fabricated in polydimethylsiloxane. *Microelectron. Eng.*, 70:13–18, 2003.

[53] S. F. Hsieh, C. P. Chang, Y. J. Juang, and H. H. Wei. Stretching DNA with electric fields beneath submicron interfacial constriction created by a closely fitting microdroplet in a microchannel. *Appl. Phys. Lett.*, 93:084103, 2008.

[54] S. F. Hsieh and H. H. Wei. Entropic trap, surface-mediated combing, and assembly of DNA molecules within submicrometer interfacial confinement. *Phys. Rev. E*, 79:021901, 2009.

[55] J. C. Giddings, E. Kucera, C. P. Russell, and M. N. Myers. Statistical theory for the equilibrium distribution of rigid molecules in inert porous networks. Exclusion chromatography. *J. Phys. Chem.*, 72(13):4397–4408, 1968.

[56] N. Laachi, C. Declet, C. Matson, and K. D. Dorfman. Nonequilibrium transport of rigid macromolecules in periodically constricted geometries. *Phys. Rev. Lett.*, 98(9):098106, 2007.

[57] G. W. Slater and H. L. Guo. An exactly solvable Ogston model of gel electrophoresis: I. The role of the symmetry and randomness of the gel structure. *Electrophoresis*, 17:977, 1996.

[58] G. W. Slater and H. L. Guo. An exactly solvable Ogston model of gel electrophoresis II. Sieving through periodic gels. *Electrophoresis*, 17:1407, 1996.

[59] G. W. Slater and J. R. Treurniet. Exactly solvable Ogston model of gel electrophoresis: III. Percolation and sieving through two-dimensional gels. *J. Chromatogr. A*, 772:39, 1997.

[60] J. Boileau and G. W. Slater. An exactly solvable Ogston model of gel electrophoresis. VI. Towards a theory for macromolecules. *Electrophoresis*, 22:673, 2001.

[61] J. F. Mercier and G. W. Slater. An exactly solvable Ogston model of gel electrophoresis. VII. Diffusion and mobility of hard spherical particles in three-dimensional gels. *Macromolecules*, 34:3437, 2001.

[62] M. G. Gauthier and G. W. Slater. Exactly solvable Ogston model of gel electrophoresis. IX. Generalizing the lattice model to treat high field intensities. *J. Chem. Phys.*, 117:6745, 2002.

[63] M. G. Gauthier, G. W. Slater, and K. D. Dorfman. Exact lattice calculations of dispersion coefficients in the presence of external fields and obstacles. *Eur. Phys. J. E*, 15:71, 2004.

[64] J. F. Mercier, F. Tessier, and G. W. Slater. An exactly solvable Ogston model of gel electrophoresis: VIII. Nonconducting gel fibers, curved field lines, and the Nernst-Einstein relation. *Electrophoresis*, 22:2631, 2001.

[65] W. D. Volkmuth and R. H. Austin. DNA electrophoresis in microlithographic arrays. *Nature*, 358, 1992.

[66] N. Kaji, Y. Tezuka, Y. Takamura, M. Ueda, T. Nishimoto, H. Nakanishi, Y. Horiike, and Y. Baba. Separation of long DNA molecules by quartz nanopillar chips under a direct current electric field. *Anal. Chem.*, 76(1):15–22, 2004.

[67] Y. C. Chan, Y. K. Lee, and Y. Zohar. High-throughput design and fabrication of an integrated microsystem with high aspect-ratio sub-micron pillar arrays for free-solution micro capillary electrophoresis. *J. Micromech. Microeng.*, 16(4):699, 2006.

[68] R. Ogawa, H. Ogawa, A. Oki, S. Hashioka, and Y. Horiike. Fabrication of nanopillar chips by a plasma etching technique for fast DNA separation. *Thin Solid Films*, 515(12):5167–5171, 2007.

[69] R. Ogawa, N. Kaji, S. Hashioka, Y. Baba, and Y. Horiike. Fabrication and characterization of quartz nanopillars for DNA separation by size. *Jpn. J. of Appl. Phys.*, 46:2771–2774, 2007.

[70] N. Kaji, A. Oki, R. Ogawa, Y. Takamura, T. Nishimoto, H. Nakanishi, Y. Horiike, M. Tokeshi, and Y. Baba. Influences of electroosmotic flows in nanopillar chips on DNA separation: Experimental results and numerical simulations. *Isr. J. Chem.*, 47(2):161–169, 2007.

[71] Y. C. Chan, Y. Zohar, and Y. K. Lee. Effects of embedded sub-micron pillar arrays in microfluidic channels on large DNA electrophoresis. *Electrophoresis*, 30(18):3242–3249, 2009.

[72] J. Ou, J. Cho, D. W. Olson, and K. D. Dorfman. DNA electrophoresis in a sparse ordered post array. *Phys. Rev. E*, 79(6):61904, 2009.

[73] J. Ou, S. J. Carpenter, and K. D. Dorfman. Onset of channeling during DNA electrophoresis in a sparse ordered post array. *Biomicrofluidics*, 4:013203, 2010.

[74] J. Ou, M. N. Joswiak, S. J. Carpenter, and K. D. Dorfman. Plasma thinned nanopost arrays for DNA electrophoresis. *J. Vac. Sci. Technol. A*, 29(1):011025–011025, 2011.

[75] D. W. Olson, J. Ou, M. Tian, and K. D. Dorfman. Continuous-time random walk models of DNA electrophoresis in a post array: Part I. Evaluation of existing models. *Electrophoresis*, 32(5):573–580, 2011.

[76] D. W. Olson and K. D. Dorfman. Experimental study of the effect of disorder on DNA dynamics in post arrays during electrophoresis. *Phys. Rev. E*, 86(4):041909, 2012.

[77] Z. Chen and K. D. Dorfman. Tilted hexagonal post arrays: DNA electrophoresis in anisotropic media. *Electrophoresis*, 35(2-3):405–411, 2014.

[78] P. S. Doyle, J. Bibette, A. Bancaud, and J. L. Viovy. Self-assembled magnetic matrices for DNA separation chips. *Science*, 295(5563):2237–2237, 2002.

[79] N. Minc, C. Fütterer, K. D. Dorfman, A. Bancaud, C. Gosse, C. Goubault, and J. L. Viovy. Quantitative microfluidic separation of DNA in self-assembled magnetic matrixes. *Anal. Chem.*, 76(13):3770–3776, 2004.

[80] N. Minc, P. Bokov, K. B. Zeldovich, C. Futterer, J. L. Viovy, and K. D. Dorfman. Motion of single long DNA molecules through arrays of magnetic columns. *Electrophoresis*, 26(2), 2005.

[81] N. Araki, E. S. Aydil, and K. D. Dorfman. Collision of a long DNA molecule with an isolated nanowire. *Electrophoresis*, 31(22):3675–3680, 2010.

[82] T. Yasui, S. Rahong, K. Motoyama, T. Yanagida, Q. Wu, N. Kaji, M. Kanai, K. Doi, K. Nagashima, M. Tokeshi, M. Taniguchi, S. Kawano, T. Kawai, and Y. Baba. DNA manipulation and separation in sublithographic-scale nanowire array. *ACS nano*, 7(4):3029–3035, 2013.

[83] M. Baba, T. Sano, N. Iguchi, K. Iida, T. Sakamoto, and H. Kawaura. DNA size separation using artificially nanostructured matrix. *Appl. Phys. Lett.*, 83(7):1468–1470, 2003.

[84] J. Shi, A. P. Fang, L. Malaquin, A. Pepin, D. Decanini, J. L. Viovy, and Y. Z. Chen. Highly parallel mix-and-match fabrication of nanopillar arrays integrated in microfluidic channels for long DNA molecule separation. *Appl. Phys. Lett.*, 91(15):153114, 2007.

[85] W. D. Volkmuth, T. A. J. Duke, M. C. Wu, R. H. Austin, and A. Szabo. DNA electrodiffusion in a 2d array of posts. *Phys. Rev. Lett.*, 72(13):2117–2120, 1994.

[86] M. N. Joswiak, J. Ou, and K. D. Dorfman. Statistical properties of the electrophoretic collision of a long DNA molecule with a small obstacle. *Electrophoresis*, 33(6):1013–1020, 2012.

[87] S. G. Park, D. W. Olson, and K. D. Dorfman. DNA electrophoresis in a nanofence array. *Lab Chip*, 12(8):1463–1470, 2012.

[88] J. M. Kim and P. S. Doyle. Brownian dynamics simulations of a DNA molecule colliding with a small cylindrical post. *Macromolecules*, 40(25):9151–9163, 2007.

[89] G. C. Randall and P. S. Doyle. Electrophoretic collision of a DNA molecule with an insulating post. *Phys. Rev. Lett.*, 93(5):058102, 2004.

[90] E. M. Sevick and D. R. M. Williams. Collision of a field-driven polymer with a post: Electrophoresis in microlithographic arrays. *Phys. Rev. Lett.*, 76(14):2595, 1996.

[91] G. C. Randall and P. S. Doyle. DNA deformation in electric fields: DNA driven past a cylindrical obstruction. *Macromolecules*, 38(6):2410–2418, 2005.

[92] G. C. Randall and P. S. Doyle. Collision of a DNA polymer with a small obstacle. *Macromolecules*, 39(22):7734–7745, 2006.

[93] E. M. Sevick and D. R. M. Williams. Long-lived states in electrophoresis: Collision of a polymer chain with two or more obstacles. *Europhys. Lett.*, 56(4):529, 2001.

[94] G. I. Nixon and G. W. Slater. DNA electrophoretic collisions with single obstacles. *Phys. Rev. E*, 50(6):5033, 1994.

[95] N. Laachi, J. Cho, and K. D. Dorfman. DNA unhooking from a single post as a deterministic process: Insights from translocation modeling. *Phys. Rev. E*, 79(3):031928, 2009.

[96] P. M. Saville and E. M. Sevick. Collision of a field-driven polymer with a finite-sized obstacle: A brownian dynamics simulation. *Macromolecules*, 32(3):892–899, 1999.

[97] P. D. Patel and E. S. G. Shaqfeh. A computational study of DNA separations in sparse disordered and periodic arrays of posts. *J. Chem. Phys.*, 118(6):2941–2951, 2003.

[98] A. Mohan and P. S. Doyle. Effect of disorder on DNA electrophoresis in a microfluidic array of obstacles. *Phys. Rev. E*, 76(4):040903, 2007.

[99] A. Mohan and P. S. Doyle. Stochastic modeling and simulation of DNA electrophoretic separation in a microfluidic obstacle array. *Macromolecules*, 40(24):8794–8806, 2007.

[100] H. Scher and M. Lax. Stochastic transport in a disordered solid. I. Theory. *Phys. Rev. B*, 7(10):4491, 1973.

[101] K. D. Dorfman. DNA electrophoresis in microfluidic post arrays under moderate electric fields. *Phys. Rev. E*, 73(6):061922, 2006.

[102] D. W. Olson, S. Dutta, N. Laachi, M. Tian, and K. D. Dorfman. Continuous-time random walk models of DNA electrophoresis in a post array: Part II. Mobility and sources of band broadening. *Electrophoresis*, 32(5):581–587, 2011.

[103] L. R. Huang, J. O. Tegenfeldt, J. J. Kraeft, J. C. Sturm, R. H. Austin, and E. C. Cox. A DNA prism for high-speed continuous fractionation of large DNA molecules. *Nat. Biotechnol.*, 20:1048–1051, 2002.

[104] S. K. Mohanty, D. Kim, and D. J. Beebe. Do-it-yourself microelectrophoresis chips with integrated sample recovery. *Electrophoresis*, 27:3772, 2006.

[105] K. Sun, Z. Li, K. Ueno, S. Juodkazis, S. Noji, and H. Misawa. Electrophoretic chip for high-fidelity fractionation of double-stranded DNA. *Electrophoresis*, 28:1572, 2007.

[106] L. R. Huang, E. C. Cox, R. H. Austin, and J. C. Sturm. Tilted brownian ratchet for DNA analysis. *Anal. Chem.*, 75:6963–6967, 2003.

[107] Y. Zeng, M. He, and D. J. Harrison. Microfluidic self-patterning of large-scale crystalline nanoarrays for high-throughput continuous DNA fractionation. *Angew. Chem. Int. Edit.*, 120:6488–6491, 2008.

[108] J. Fu, R. B. Schoch, A. L. Stevens, S. R. Tannenbaum, and J. Han. A patterned anisotropic nanofluidic sieving structure for continuous-flow separation of DNA and proteins. *Nat. Nanotechnol.*, 2:121–128, 2007.

[109] P. Mao and J. Han. Massively-parallel ultra-high-aspect-ratio nanochannels as mesoporous membranes. *Lab Chip*, 9(4):586–591, 2009.

[110] A. Van Oudenaarden and S. G. Boxer. Brownian ratchets: molecular separations in lipid bilayers supported on patterned arrays. *Science*, 285(5430):1046–1048, 1999.

[111] J. S. Bader, R. W. Hammond, S. A. Henck, M. W. Deem, G. A. McDermott, J. M. Bustillo, J. W. Simpson, G. T. Mulhern, and J. M. Rothberg. DNA transport by a micromachined brownian ratchet device. *P. Natl. Acad. Sci. USA*, 96(23):13165, 1999.

[112] C. F. Chou, O. Bakajin, S. W. P. Turner, T. A. J. Duke, S. S. Chan, E. C. Cox, H. G. Craighead, and R. H. Austin. Sorting by diffusion: An asymmetric obstacle course for continuous molecular separation. *P. Natl. Acad. Sci. USA*, 96:13762, 1999.

[113] R. W. Hammond, J. S. Bader, S. A. Henck, M. W. Deem, G. A. McDermott, J. M. Bustillo, and J. M. Rothberg. Differential transport of DNA by a rectified brownian motion device. *Electrophoresis*, 21(1):74–80, 2000.

[114] J. S. Bader, M. W. Deem, R. W. Hammond, S. A. Henck, J. W. Simpson, and J. M. Rothberg. A brownian-ratchet dna pump with applications to single-nucleotide polymorphism genotyping. *Appl. Phys. A-Mater.*, 75(2):275–278, 2002.

[115] M. Cabodi, Y. Z. Chen, S. W. P. Turner, H. G. Craighead, and R. H. Austin. Continuous separation of biomolecules by the laterally asymmetric diffusion array with out-of-plane sample injection. *Electrophoresis*, 23:3496–3503, 2002.

[116] L. R. Huang, P. Silberzan, J. O. Tegenfeldt, E. C. Cox, J. C. Sturm, R. H. Austin, and H. G. Craighead. Role of molecular size in ratchet fractionation. *Phys. Rev. Lett.*, 89:178301, 2002.

[117] L. R. Huang, E. C. Cox, R. H. Austin, and J. C. Sturm. Continuous particle separation through deterministic lateral displacement. *Science*, 304:987–990, 2004.

[118] T. A. J. Duke, R. H. Austin, E. C. Cox, and S. S. Chan. Pulsed-field electrophoresis in microlithographic arrays. *Electrophoresis*, 17(6):1075–1079, 1996.

[119] L. R. Huang, J. O. Tegenfeldt, J. J. Kraeft, J. C. Sturm, R. H. Austin, and E. C. Cox. Generation of large-area tunable uniform electric fields in microfluidic arrays for rapid DNA separation. In *Electron Devices Meeting, 2001. IEDM Technical Digest. International*, pages 16–3. IEEE, 2001.

[120] Y. Zeng and D. J. Harrison. Self-assembled colloidal arrays as three-dimensional nanofluidic sieves for separation of biomolecules on microchips. *Anal. Chem.*, 79(6):2289–2295, 2007.

[121] N. Nazemifard, S. Bhattacharjee, J. H. Masliyah, and D. J. Harrison. DNA dynamics in nanoscale confinement under asymmetric pulsed field electrophoresis. *Angew. Chem. Int. Edit.*, 49:3326, 2010.

[122] N. Nazemifard, L. Wang, W. Ye, S. Bhattacharjee, J. H. Masliyah, and D. J. Harrison. A systematic evaluation of the role of crystalline order in nanoporous materials on DNA separation. *Lab Chip*, 12:146, 2012.

[123] Z. Chen and K. D. Dorfman. Relationship between frequency and deflection angle in the DNA prism. *Phys. Rev. E*, 87(1):012723, 2013.

[124] J. Fu, P. Mao, and J. Han. Continuous-flow bioseparation using microfabricated anisotropic nanofluidic sieving structures. *Nat. Protoc.*, 4:1681–1698, 2009.

[125] K. J. Morton, K. Loutherback, D. W. Inglis, O. K. Tsui, J. C. Sturm, S. Y. Chou, and R. H. Austin. Hydrodynamic metamaterials: Microfabricated arrays

to steer, refract, and focus streams of biomaterials. *Proc. Natl. Acad. Sci. U.S.A.*, 105:7434, 2008.

[126] K. J. Morton, K. Loutherback, D. W. Inglis, O. K. Tsui, J. C. Sturm, S. Y. Chou, and R. H. Austin. Crossing microfluidic streamlines to lyse, label and wash cells. *Lab Chip*, 8:1448, 2008.

[127] J. P. Beech and J. O. Tegenfeldt. Tuneable separation in elastomeric microfluidic devices. *Lab Chip*, 8:657, 2008.

[128] P Reimann. Brownian motors: Noisy transport far from equilibrium. *Phys. Rep.*, 361:57, 2002.

[129] R. D. Astumian. Thermodynamics and kinetics of a Brownian motor. *Science*, 276:917, 1997.

[130] T. A. J. Duke and R. H. Austin. Microfabricated sieve for the continuous sorting of macromolecules. *Phys. Rev. Lett.*, 80:1552–1555, 1998.

[131] D. Ertas. Lateral separation of macromolecules and polyelectrolytes in microlithographic arrays. *Phys. Rev. Lett.*, 80:1548–1551, 1998.

[132] R. H. Austin, N. Darnton, R. Huang, J. Sturm, O. Bakajin, and T. Duke. Ratchets: the problems with boundary conditions in insulating fluids. *Appl. Phys. A*, 75:279, 2002.

[133] Z. Li and G. Drazer. Separation of suspended particles by arrays of obstacles in microfluidic devices. *Phys. Rev. Lett.*, 98:050602, 2007.

[134] Z. R. Li, G. R. Liu, Y. Z. Chen, J. S. Wang, H. Bow, Y. Cheng, and J. Han. Continuum transport model of ogston sieving in patterned nanofilter arrays for separation of rod-like biomolecules. *Electrophoresis*, 29(2):329–339, 2008.

[135] Z. R. Li, G. R. Liu, J. Han, Y. Cheng, Y. Z. Chen, J. S. Wang, and N. G. Hadjiconstantinou. Analytical description of ogston-regime biomolecule separation using nanofilters and nanopores. *Phys. Rev. E*, 80(4):041911, 2009.

[136] G. W. Slater, H. L. Guo, and G. I. Nixon. Bidirectional transport of polyelectrolytes using self-modulating entropic ratchets. *Phys. Rev. Lett.*, 78(6):1170, 1997.

[137] F. Tessier and G. W. Slater. Strategies for the separation of polyelectrolytes based on non-linear dynamics and entropic ratchets in a simple microfluidic device. *Appl. Phys. A-Mater.*, 75(2):285–291, 2002.

[138] S. C. Jacobson, R. Hergenroder, L. B. Koutny, R. J. Warmack, and J. M. Ramsey. Effects of injection schemes and column geometry on the performance of microchip electrophoresis devices. *Anal. Chem.*, 66(7):1107–1113, 1994.

[139] P. Mao and J. Han. Fabrication and characterization of 20 nm planar nanofluidic channels by glass–glass and glass–silicon bonding. *Lab Chip*, 5(8):837–844, 2005.

[140] N. Minc, J.-L. Viovy, and K. D. Dorfman. Non-markovian transport of DNA in microfluidic post arrays. *Phys. Rev. Lett.*, 94:198105, 2005.

[141] J. C. Giddings. *Unified Separation Science*. John Wiley Sons, Inc., 1991.

[142] J. Cho and K. D. Dorfman. Brownian dynamics simulations of electrophoretic DNA separations in a sparse ordered post array. *J. Chromatogr. A*, 1217:5522–5528, 2010.

[143] T. Yasui, N. Kaji, R. Ogawa, S. Hashioka, M. Tokeshi, Y. Horiike, and Y. Baba. DNA separation by square patterned nanopillar chips. In J.-L. Viovy, P. Tabeling, S. Descroix, and L. Malaquin, editors, *Proceedings of the 11th International*

Conference on Miniaturized Systems for Chemistry and Life Sciences, pages 1207–1209, Paris, France, October 7-11 2007.

[144] Z. Chen and K. D. Dorfman. Comparison of microfabricated hexagonal and lamellar post arrays for DNA electrophoresis. *Electrophoresis*, 35:654–661, 2014.

[145] T. Yasui, N. Kaji, Y. Okamoto, M. Tokeshi, Y. Horiike, and Y. Baba. Nanopillar array chip integrated with on-line stacking for fast DNA separation with high sensitivity and high resolution. *Microfluid. Nanofluid.*, 14:961–967, 2013.

[146] R. T. Kovacic, L. Comai, and A. J. Bendich. Protection of megabase DNA from shearing. *Nucleic Acids Res.*, 23:3999–4000, 1995.

[147] D. J. Harrison, A. Manz, Z. Fan, H. Ludi, and H. M. Widmer. Capillary electrophoresis and sample injection systems integrated on a planar glass chip. *Anal. Chem.*, 64:1926–1932, 1992.

[148] L. Mitnik, C. Heller, J. Prost, and J. L. Viovy. Segregation in DNA solutions induced by electric fields. *Science*, 267(5195):219–222, 1995.

[149] C. T. Culbertson, S. C. Jacobson, and J. M. Ramsey. Dispersion sources for compact geometries on microchips. *Anal. Chem.*, 70(18):3781–3789, 1998.

[150] J. I. Molho, A. E. Herr, B. P. Mosier, J. G. Santiago, T. W. Kenny, R. A. Brennen, G. B. Gordon, and B. Mohammadi. Optimization of turn geometries for microchip electrophoresis. *Anal. Chem.*, 73(6):1350–1360, 2001.

[151] E. M. Southern, R. Anand, W. R. A. Brown, and D. S. Fletcher. A model for the separation of large DNA molecules by crossed field gel electrophoresis. *Nucleic Acids Res.*, 15:5925–5943, 1987.

[152] M. Balvin, E. Sohn, T. Iracki, G. Drazer, and J. Frechette. Directional locking and the role of irreversible interactions in deterministic hydrodynamics separations in microfluidic devices. *Phys. Rev. Lett.*, 103:078301, 2009.

[153] J. P. Gleghorn, J. P. Smith, and B. J. Kirby. Transport and collision dynamics in periodic asymmetric obstacle arrays: rational design of micro fluidic rare cell immunocapture devices. *Phys. Rev. E*, 88:032136, 2013.

[154] S. Jeon, J. U. Park, R. Cirelli, S. Yang, C. E. Heitzman, P. V. Braun, P. J. A. Kenis, and J. A. Rogers. Fabricating complex three-dimensional nanostructures with high-resolution conformable phase masks. *P. Natl. Acad. Sci. USA*, 101(34):12428–12433, 2004.

[155] S. Jeon, E. Menard, J. U. Park, J. Maria, M. Meitl, J. Zaumseil, and J. A. Rogers. Three-dimensional nanofabrication with rubber stamps and conformable photomasks. *Adv. Mater.*, 16(15):1369–1373, 2004.

[156] D. J. Shir, S. Jeon, H. Liao, M. Highland, D. G. Cahill, M. F. Su, I. F. El-Kady, C. G. Christodoulou, G. R. Bogart, A. V. Hamza, and J. A. Rogers. Three-dimensional nanofabrication with elastomeric phase masks. *J. Phys. Chem. B*, 111(45):12945, 2007.

[157] C. H. Ahn, J. W. Choi, G. Beaucage, J. Nevin, J. B. Lee, A. Puntambekar, and R. J. Y. Lee. Disposable smart lab on a chip for point-of-care clinical diagnostics. *Pr. Inst. Electr. Elect.*, 92(1):154–173, 2004.

[158] H. G. Craighead. Future lab-on-a-chip technologies for interrogating individual molecules. *Nature*, 442:387–393, 2006.

[159] J. D. Cross, E. A. Strychalski, and H. G. Craighead. Size-dependent DNA mobility in nanochannels. *J. Appl. Phys.*, 102:024701, 2007.

[160] P. S. Dittrich and A. Manz. Lab-on-a-chip: microfluidics in drug discovery. *Nat. Rev. Drug Discov.*, 5(3):210–218, 2006.

[161] B. M. Paegel, R. G. Blazej, and R. A. Mathies. Microfluidic devices for DNA sequencing: sample preparation and electrophoretic analysis. *Curr. Opin. Biotech.*, 14(1):42–50, 2003.

[162] G. M. Whitesides. The origins and the future of microfluidics. *Nature*, 442:368–373, 2006.

[163] L. Meistermann and B. Tinland. DNA electrophoresis in a monodisperse porous medium. *Phys. Rev. E*, 62(3):4014–4017, 2000.

[164] H. Zhang and M. J. Wirth. Electromigration of single molecules of DNA in a crystalline array of 300-nm silica colloids. *Anal. Chem.*, 77(5):1237–1242, 2005.

[165] Y. Zeng and D. J. Harrison. Confinement effects on electromigration of long DNA molecules in an ordered cavity array. *Electrophoresis*, 27:3747–52, 2006.

[166] S. Jeon, V. Malyarchuk, J. O. White, and J. A. Rogers. Optically fabricated three dimensional nanofluidic mixers for microfluidic devices. *Nano Lett.*, 5(7):1351–1356, 2005.

[167] J. W. Goodman. *Introduction to Fourier Optics*. Roberts Company, 3rd edition, 2005.

[168] P. Latimer and R. F. Crouse. Talbot effect reinterpreted. *Appl. Optics*, 31(1):80–89, 1992.

[169] H. Schmid and B. Michel. Siloxane polymers for high-resolution, high-accuracy soft lithography. *Macromolecules*, 33(8):3042–3049, 2000.

[170] D. Bartolo, G. Degré, P. Nghe, and V. Studer. Microfluidic stickers. *Lab Chip*, 8(2):274–279, 2008.

[171] Z. Zhang, P. Zhao, and G. Xiao. The fabrication of polymer microfluidic devices using a solid-to-solid interfacial polyaddition. *Polymer*, 50(23):5358–5361, 2009.

[172] S. Tuomikoski and S. Franssila. Wafer-level bonding of MEMS structures with SU-8 epoxy photoresist. *Phys. Scripta*, 2004(T114):223, 2004.

[173] S. G. Park, S. K. Lee, J. H. Moon, and S. M. Yang. Holographic fabrication of three-dimensional nanostructures for microfluidic passive mixing. *Lab Chip*, 9(21):3144–3150, 2009.

[174] R. G. Denning, C. F. Blanford, H. Urban, H. Bharaj, D. N. Sharp, and A. J. Turberfield. The control of shrinkage and thermal instability in SU-8 photoresists for holographic lithography. *Adv. Funct. Mater.*, 21(9):1593–1601, 2011.